University of Szeged

Faculty of Pharmacy

Institute of Pharmaceutical Technology and Regulatory Affairs

EVALUATION OF DRUG-MATRIX INTERACTIONS IN DIRECTLY COMPRESSED DRUG DELIVERY SYSTEMS AND MODELLING OF DRUG-RELEASE RATE

Ph.D. Thesis

Ernő Máté Benkő
Pharm. D.

Supervisors:

Dr. Tamás Sovány

Prof. Dr. Ildikó Csóka

Szeged

2022

LIST OF PUBLICATIONS AND CONFERENCE PROCEEDINGS

List of publications

I. T. Sovány, A. Csüllög, **E. Benkő**, G. Regdon, and K. Pintye-Hódi, 'Comparison of the properties of implantable matrices prepared from degradable and non-degradable polymers for bisphosphonate delivery', *International Journal of Pharmaceutics*, vol. 533, no. 2, pp. 364-372, Nov. 2017, doi: 10.1016/j.ijpharm.2017.07.023.

Q1 IF.: 4.09 (2017)

II. **E. Benkő**, I.G. Ilič, K. Kristó, G. Regdon Jr., I. Csóka, K. Pintye-Hódi, S. Srčič, T. Sovány. 'Predicting Drug Release Rate of Implantable Matrices and Better Understanding of the Underlying Mechanisms through Experimental Design and Artificial Neural Network-Based Modelling', *Pharmaceutics*, vol. 14, no. 2, pp. 228, Jan. 2022, doi: 10.3390/pharmaceutics14020228.

Q1 IF.: 6.29 (2021)

List of conference proceedings

Oral presentations

I. **E. Benkő**, API – polimer interaction studies in solid matrix systems, XIII. Clauder Ottó Emlékverseny, 22-23 November 2018, Budapest, Hungary

II. **E. Benkő**, API – excipient interaction studies within solid dosage forms, II. Ph.D. symposium on University of Szeged - Medical and Pharmaceutical Sciences, 30 November 2018, Szeged, Hungary

III. **E. Benkő**, T. Sovány, I. Csóka, API – excipient interactions in non-biodegradable solid matrix systems, I. Symposium of Young Researchers on Pharmaceutical Technology, Biotechnology and Regulatory Science, 31 January 2019, Szeged, Hungary

IV. **E. Benkő**, T. Sovány, I. Csóka, API – excipient interactions in solid matrix systems, II. Symposium of Young Researchers on Pharmaceutical Technology, Biotechnology and Regulatory Science, 23-24 January 2020, Szeged, Hungary

V. **E. Benkő**, T. Sovány, I. Csóka, API – excipient interaction and compressibility studies in solid matrix systems, Medical Conference for Ph.D. Students and Experts of Clinical Sciences, 17 October 2020, Online event, Hungary

VI. **E. Benkő**, I.G. Ilič, G. Regdon Jr., I. Csóka, K. Pintye-Hódi, S. Srčič, T. Sovány, Investigation of drug-matrix interaction in directly compressed matrices, III. Symposium of Young Researchers on Pharmaceutical Technology, Biotechnology and Regulatory Science, 20-22 January 2021, Szeged, Hungary,

Poster presentations

VII. **E. Benkő**, G. Regdon jr., T. Sovány, API - excipient interaction studies in solid matrix systems, 12th Central European Symposium on Pharmaceutical Technology and Regulatory Affairs, 20-22 September 2018, Szeged, Hungary

VIII. **Benkő E.** , Ilič I.G., ifj. Regdon G., Srčič S., Sovány T., Mátrixtablettákon belüli fizikai kémiai kölcsönhatások hatóanyag-felszabadulásra gyakorolt befolyásának vizsgálata; Gyógyszertechnológiai és Ipari Gyógyszerészeti Konferencia 2019, 26-28 September 2019, Siófok, Hungary

TABLE OF CONTENTS

LIST OF ABBREVIATIONS

ACE	Aceclofenac
adjR^2	Adjusted goodness of fit
ANN	Artificial neural network
API	Active pharmaceutical ingredient
CHIT	Chitosan
CQA	Critical Quality Attributes
DIS	Diclofenac sodium
DoE	Design of experiments
EE	Eudragit E100
EL	Eudragit L100-55
FT-IR	Fourier-transform infrared
GI	Gastrointestinal
HATR	Horizontal Attenuated Total Reflectance
MS	Mean square
NIR	Near infrared
PAR	Paracetamol
PVC	Polyvinyl chloride
QbD	Quality by Design
RIS	Risedronate sodium
RMSE	Root mean square error

1 INTRODUCTION

Individual differences among patients have considerable importance in the effectiveness of the therapy of different chronic diseases. Co-morbidities, genetical differences or various life-events may cause changes in important physiological parameters affecting the absorption, elimination or effectiveness of drugs and influence treatment efficacy. Personalized medicine is a recently emerging trend (1,2) meant to overcome these difficulties. Therefore, pharmaceutical industry faces a new challenge on providing solid dosage forms, which as still the most favourable medicines, with tailorable properties.

Tailored release of drugs has even higher importance in the long-term therapy of chronic diseases, when ensuring a stable plasma level is a key question regarding to the treatment effectiveness. Patient compliance is advised if medicines needed to be administered multiple times throughout long therapies but may be problematic in case of psychiatric or neurodegenerative diseases, or if the administration interval is long, such in case of osteoporosis. Implantable drug delivery devices may provide controlled release for months (3,4), which may be very advantageous in those cases, especially if the active pharmaceutical ingredient (API) has poor bioavailability in the gastrointestinal (GI) tract, such as the antiosteoporotic bisphosphonates.

The present work aims the better understanding of the mechanism and kinetics of drug release from directly compressed, biodegradable and non-degradable implantable matrices designed for bisphosphonate delivery, in order to utilize a novel approach on the use of drug-polymer interactions in the tailoring of sustained-release solid delivery matrices.

The use of the principles of Quality by Design (QbD) nowadays is essential in applied drug development but its tools such as Design of Experiments (DoE) or artificial neural networks (ANNs) may be well utilized also in fundamental research. In present work they were used to reveal the role of drug-polymer interactions on the Critical Quality Attributes (CQA), such as diametral breaking hardness, porosity and drug dissolution rate of implantable matrices. Therefor a line of chemically similar drugs with increasing acidic strength were formulated in accordance with a mixed 2 and 3 level full factorial DoE. The presence of solid-state drug-polymer interactions based on the formation of H-bonds were confirmed by FT-IR spectroscopy, while their effect on dissolution was estimated by an ANN based predictive model.

2 AIMS

2.1 Primary aim

The primary aim of present research work was the development of a directly compressed polymer-based implantable monolithic matrix system for the delivery of risedronate sodium by the comparison of the potential of biodegradable (chitosan) and non-degradable (PVC) polymers for such purposes, based on the evaluation of mechanical properties, mechanism and rate of the drug release. The desired QTPP consisted affordable tablet hardness, sustained drug liberation for minimum 3, but preferable for 6 months, without considerable initial burst release of the drug. Biodegradable nature of the applied matrix is also preferred mainly from the aspect of patient compliance, although environmental sustainability of the polymer is also convincing.

2.2 Secondary aims of the research

During the implementation of the primary objective an unexpected occurrence of in-situ formed chemical interactions were observed, which required the revision of the results of the original risk assessment and the better understanding and detailed investigation of that phenomenon, which became the secondary objective of the study. The modified objective was to confirm the hypothesis, that the strength of drug-excipient interactions may be predicted based on acidic strength of the drugs, and the gathered data may help to achieve tailored drug-release from implantable drug delivery systems, which have emerging interest in pharmaceutical sciences, to ensure safe and long-term therapy of patients with chronic diseases. For this fundamental investigation we applied a QbD approach, therefore introduced several model API with varying acidic strength but similar chemical structures and more matrix forming polymers as well.

The main points of the present dissertation are the following:

1. Applicability determination of polymers as solid matrix system forming agents – polymer comparison and release rate, mechanism evaluation.
2. Confirmation the hypothesis, that the strength of drug-excipient interactions may be predicted based on acidic strength of the drugs.
3. A consequential objective of the present work is to compare the effectiveness of various modelling approaches to enable generalized prediction of drug dissolution rates from different matrices. Our hypothesis is that kinetic-based modelling allows for a simplified network structure and faster generalization.

3 LITERATURE SURVEY

3.1 Osteoporosis

Osteoporosis is a major systemic skeletal disease, which can be characterised with the decrement of bone mass and micro-architectural deterioration of bone tissue. These symptoms can cause bone fragility and consequent increase in fracture risk (5). Fractures of the spine or the hip can lead to prolonged hospitalisation and even the survival is not guaranteed compared to smaller fractures like the fracture of a wrist. A 2013 data shows approximately 2 million reported cases in the EU correlated to osteoporosis, causing a ~ €37 billion deficit in the region. The advancement of the past 50 years is unquestionable but the therapeutic effectiveness still could be improved, preferably through the improvement of the bioavailability of the currently used drugs.

3.2 Bisphosphonates

Bisphosphonates are widely used drugs for osteoporosis treatment but have very poor (approx. 0.4-0.7% of iv.) oral bioavailability, which requires the use of relative high doses of according to a once-a-week dosing regimen. Nevertheless, their use is associated with severe side effects, such as irritation and necrosis of the gastrointestinal mucosa (6). Some experimental results suggest the effect of bisphosphonates on gastric mucosa is based on the modification of the hydrophobicity of the phospholipid bilayer surfaces. The strength of this effect was different amongst the investigated bisphosphonates and risedronate exhibited the lowest effect (7). This result was in accordance with the findings of Thomson et al. (8), who confirmed that risedronate exhibits considerably higher safety over alendronate from the aspect of mucosal irritation applied in the regularly used 5 or 10 mg doses in daily oral administration. Based on these results, the use of risedronate may be generally considered as safe also in alternative routes.

In addition, numerous investigations confirm that the long-term local delivery of bisphosphonates has a great advantage in bone regeneration after injuries (9) or implantation of hip or femoral neck prosthesis (10,11). In these studies, the drug was mixed into the bone cement (11), the hydroxyapatite coating of the titanium implant (10) or into the modified chitosan coating of a commercial bone platelet (9), which ensured the targeted local delivery of the drug to the injured bone parts. Under these conditions a 4 μg daily dose may be enough to ensure successful bone remodelling under a 2-month treatment period, without any sign of adverse reactions or cytotoxic effect. The lack of cytotoxicity in the case of extended release

local delivery suggests that the adverse reactions related to the irritative effect of bisphonates are dose dependent and the use of controlled release implants may help to overcome the limitations and risks of oral, intravenous or intramuscular injection use, offering a good way for the systemic delivery of these drugs in osteoporosis, where localized therapy cannot be used due to the generalized nature of the disease (12).

However, this and the age and concurrent comorbidities of patients require the introduction of novel strategies in therapy with the application of implantable matrix tablets made from biocompatible polymers and tailored properties. The development of suitable devices delivering antiosteoporotic agents requires a screening on the applicable polymers, regarding their biocompatibility and their effectivity on tailoring properties of a complex pharmaceutical system.

3.3 Tailorable implantable drug delivery systems

There are numerous considerations to make during the selection of the most suitable implantable delivery systems, such as targeting of passive (degradable or non-degradable reservoir or monolithic matrix systems, micro- or nanospheres) or active (osmotic or programmable pump systems) release for delivery of drugs (13,14). Although the use of pump systems may ensure a better control on drug release, the production of reservoir or monolithic systems is easier and cheaper, therefore they are currently of greater interest from the industrial aspect. The use of degradable (chitosan, polylactide (PLA), poly(lactide-co-glycolide) (PLGA) or poly(thiourethane) or non-degradable (polyvinylchloride (PVC), poly(dimethyl siloxane), polyurethanes (PU), polyethylene (PE), poly(ethylene-co-vinyl-acetate) (PEVA), poly(methyl methacrylate (PMMA)) polymers is also a key question of implantable delivery. Degradable devices have the advantage that the removal of the device after the complete release of the drug is not necessary, but their major drawback that the release rate is concurrently determined by diffusion, erosion and the degradation rate of the polymers. In comparison, the release from non-degradable matrices is completely diffusion determined (15–17) and so better controllable. According to these considerations we aimed the development of a passive delivery system, with a secondary aim of the detailed understanding and comparison of the mechanism of drug liberation from different polymers, which is inevitable to appropriate modelling and for the QbD-based development of tailored matrices.

3.4 Liberation from matrix systems

To be able to model drug dissolution from matrix systems it was essential to extend our knowledge about polymer dissolution (18) properties as polymers are the major matrix forming agents. Some early study therefore focused on the intense study of polymer behaviour. The properties of glassy polymer solutions were studied (19) and some new principles were established such as that diffusivity of the solute and the viscous behaviour of the polymer itself are critical during polymer solution process. In addition of the well-known Fickian diffusion, where the drug liberation is diffusion driven, a new case II diffusion model and even a super case II model were introduced, where the relaxation of the polymer was also taken into account. A preceding study presented more details about the influence of viscosity and particle size (20) of polymers. The higher viscosity grade will cause slower release, and higher particle size will conclude to faster drug liberation due to a slower formation of a deterrent gel layer.

Parallelly with the investigations of polymer behaviour, mathematical models were established for the description of drug release from polymer matrix systems. A comprehensive study (21) summarises the drug liberation procedure and pharmaceutical application of several mathematical models such as zero order, first order, Hixon-Crowell, Weibull, Higuchi, Hopfenberg, and Korsmeyer-Peppas model, as well as other possible variations and parameters. Zero order kinetic can be applied to not disaggregating dosage forms with slow release rate. These systems can be osmotic pumps, coated matrix tablets, modified transdermal systems, etc. The first order kinetic was used mostly to describe absorption and elimination but also can be used for describing dissolution from porous matrices containing water soluble drug. Here the quantity of liberated amount of drug is decreasing by each unit of time. The Hixon-Crowell model is applicable in cases when the diminishing of the drug particle surface is taken into consideration. The Weibull model is just an empirical approach focusing on a log-log assumption between dissolved drug quantity and time. It can be used for coated systems however because of its empirical nature several modifications were applied on this model. The Higuchi model is completely based on a Fickian diffusion and can be applied on semisolid or solid matrices and transdermal systems. In the Hopfenberg model the erosion of the surface is also considered. The Korsmeyer-Peppas model is applicable for matrices showing multiple dissolution profiles consecutively. A following model (22) takes into consideration the formation of a barrier gel layer in addition to previous mechanisms and also the diffusion through this layer. Kaunisto et al. introduced (23) a mechanistic ‘finite element method’ model

applicable for dissolutions from axially symmetric tablets. Later the author published a summary about various advanced mechanistic and even empirical models (24).

Consequently, it can be declared that the drug liberation from porous matrices is complex process, influenced by numerous parameters, and the most important ones are solubility, matrix porosity (25), swelling (26) and gel formation (22) of polymers (Fig. 1), both in case of nanosystems and in solid matrix tablets, which are one of the most popular systems for controlled delivery of drugs. The gel properties are influenced by the particle size (20,25) or molecular weight of polymers (27) and generally determines the drug transport within the matrix, which could be diffusion-driven (26), relaxation-driven (19), external mass-transport-driven or anomalous (23). Especially the anomalous transport mechanism presupposes the presence of interparticle interactions within the system (23,27).

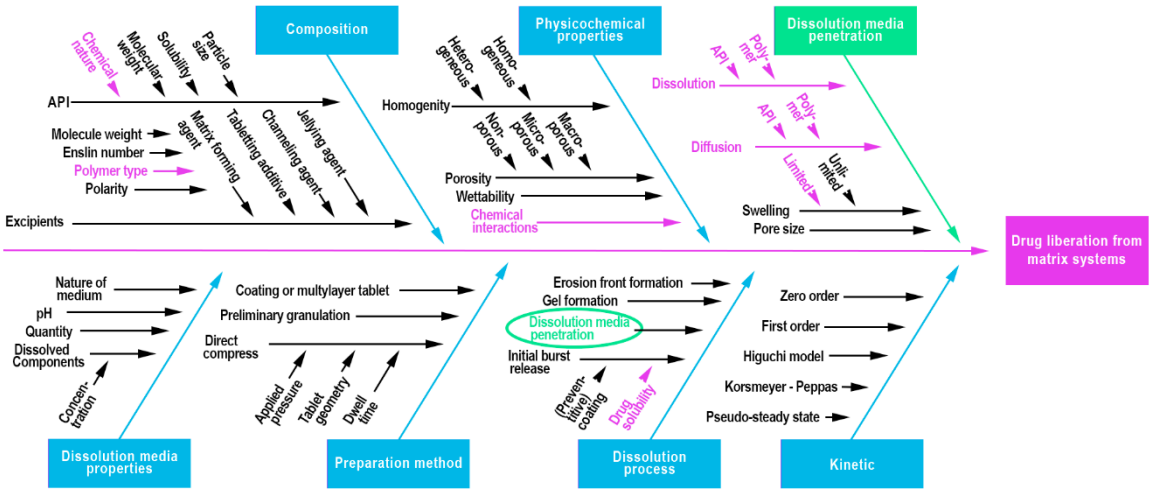

Figure 1. Ishikawa diagram about the factors influencing drug liberation from a solid matrix system

3.5 Summary on polymers

Polymers represent a prominent place in our current pharmaceutical design, and in the past few decades achieved key role in the development of controlled release drug delivery systems (28). Within this category, sustained release system has the aim to achieve an effective, therapeutic tissue (blood) concentration of the active pharmaceutical ingredient (API) for an extended period of time. In form of hard and soft tissue implants, controlled drug-release systems may ensure effective therapy up to 12 months.

PVC is a widely used polymer for fabrication of medical and drug delivery devices, and was maybe first polymer used for compression of non-degradable, “inert” polymer matrices,

despite of the various compressibility depending of the grade used (29). Due to its chemical inertness, the drug release is determined by the physical parameters (e.g. pore size and volume distribution) of the matrix, and is not affected by drug-polymer interactions. In contrast, the free amino side chains of chitosan are highly capable to form various physico-chemical interactions (e.g hydrogen bonds or polyelectrolyte complexes) with drugs or polymers, which may significantly influence the drug release rate from chitosan matrices (30–32). A research work describes the feasibility of extended release matrices made of a Chitosan-Sodium-alginate polymer mixture (33) and a formulation which's liberation property follows the Korsmeyer-Peppas equation (34) is introduced. The formation of polyelectrolyte complexes is common in chitosan nanoparticles or films, where the free amino groups of the chitosan are undergoing protonation during the dissolution in diluted acids (31,35), but not evident in the case of matrix tablets, where the chitosan is in mostly deprotonated form during preparation (36,37). Under these circumstances the formation of polyelectrolyte complexes may be expected only in the GI tract, if the deprotonation of the jellified chitosan in the small intestine is slower as the dissociation of the drug (33,38,39). Therefore, in present study where the dissolution medium is slightly alkaline, the formation of drug-polymer interactions is unexpected (40).

In case of non-degradable systems Eudragits may be mentioned as possible interaction-forming co-matrix-forming excipients, the high versatility of this excipient family enables the reach divers release kinetics. Claeys et al (41) reported immediate release of the model drugs where modified polymethacrylates (Eudragit E PO derivates) where used as matrix former. Gandhi et al. introduced an acyclovir loaded matrix nanosystem with enhanced oral bioavailability and sustained drug release (42). As an excipient Eudragit RL PO was used and nanoprecipitation technique was applied. The resulted dissolution profile fits the Higuchi model. Ramyadevi and Rajan prepared also acyclovir containing nanoparticles but with the use of polyvinyl pyrrolidone, ethyl cellulose and Eudragit RS PO (43). The resulted product has pH dependent release characteristics possessing an initial burst effect followed by a sustained slow release. Another nanomatrix system based on Eudragit S100 and Sylysia 350 mixture were tested as a promising system for oral delivery of cyclosporine A (44). In comparison to a marketed referent product the above-mentioned matrix seemed superior in terms of a moderate, prolonged release and the lack of an initial burst effect. As can be seen above, Eudragit E100 (EE) and Eudragit L100-55 (EL) are well-known compounds for peroral administration, but several reports (45–51) also present them as excipients in parenteral drug delivery. Although their use in human parenteral therapy has not been accepted yet, scientists reached promising results in in vivo mice models using these materials. Recently micro- and nanoparticles were

manufactured then administered into the peritoneal cavity, skeletal muscle, and even to the venous system. During an intramuscular nanoparticle development (47), safety tests were conducted. Damage to the liver and the skeletal muscle of administration was investigated through the 6-week experiment. Tissue samples from the liver were as in the control group, the skeletal muscle showed inflammation in the first week, which decreased by the second week, and at the end of the experiment it became similar to the control group as well. In the case of intravenous microparticulate administration (48) only local inflammation was observed. Overall, the use of these materials as implantable excipients is considerable, especially because quaternerised Eudragit can facilitate paracellular API permeation at pH 7.4, which highlights the benefits of Eudragit copolymers.

Despite the literature survey above, during our research the formation of chemical interactions were identified affecting the drug liberation property of the matrices (see Results and discussion part). Novel achievements require the reconsideration of the traditional thinking about inert excipients and turns the investigation and utilization of drug-excipient interactions into the focus of the development of tailored drug delivery systems. Therefore, we focused our attention on further investigations about the chemical interactions.

3.6 Quality by Design approach and Artificial Neural Networks

As mentioned above drug liberation from a matrix system is a highly complex process with many influencing factors (Fig 1). In order for a systematic investigation a comprehensive approach was required. Quality by Design (QbD) represents a holistic and systemic way of approach towards improvements, and its application is highly recommended by the authorities from the very first step of any pharmaceutical developments. Therefore, a QbD based approach was used to investigate the effect of critical material attributes on the mechanical properties of the matrices, the strength of the interaction, and the drug release rate. Design of Experiments (DoE) was used to reveal basic relationships within and in between matrices. However, the rigid structure of the system is considerable limitation from the aspect of further improvement of model quality with the results of routine productions. In order to achieve better predictability and minimise distortion artificial neural networks (ANN) were used for the prediction of drug dissolution. ANNs are capable of processing multiple parameters in a considerable time, fine tuning their network is also possible therefore ANNs appear as a promising solution towards the concept of tailored medicine design and personalised treatment. ANNs are commonly used types of machine learning/deep learning methods, which mimic the signal transduction and learning mechanism of the human brain. ANNs can self-accommodate to the learning

environment, and therefore are widely applied for modelling of difficult nonlinear problems in a wide range of applications, including pharmaceutics. Previous studies (52,53) have demonstrated that ANNs are excellent tools for modelling the mechanical properties of tablets, whereas Galata et al. has successfully used ANNs to model drug release from hydrophilic, sustained-release matrix systems (54) by point-to-point modelling of drug release. Nevertheless, the question how the developed network may be used for the modelling of general problems remained open. A secondary objective of the present study was to reveal if the tested material attributes will enable a generalized prediction of drug dissolution and furthermore to compare the efficiency of point-to-point modelling with another method where kinetic parameters (shape parameters of the dissolution curve) served as output variables.

4 MATERIALS AND METHODS

4.1 Materials

Risedronate sodium (RIS) was kindly gifted by TEVA Pharmaceuticals Plc. (Debrecen, Hungary). Aceclofenac (Ace) was a kind gift from ExtractumPharma Ltd. (Budapest, Hungary), while diclofenac sodium (DiS), paracetamol (Par), polyvinyl chloride (MW: 60-150) (PVC) and the lubricant calcium stearate were kindly gifted by Gedeon Richter Plc. (Budapest, Hungary). Magnesium stearate was supplied by Faci SPA (Genova, Italy). A powder form of Eudragit E100, Eudragit EPO (EE) and Eudragit L100-55 (EL) was supplied by Evonik Industries AG (Essen, Germany). The biodegradable, chitosan (MW: 400-600 kDa, average viscosity: 1000 cP, deacetylation degree: 80%) (CHIT) was purchased from Heppe Medical Chitosan GmbH (Halle an der Saale, Germany). The chemical structures of the compounds may be seen in Figure 2 and the main physico-chemical properties of raw materials are summarised in Table 1.

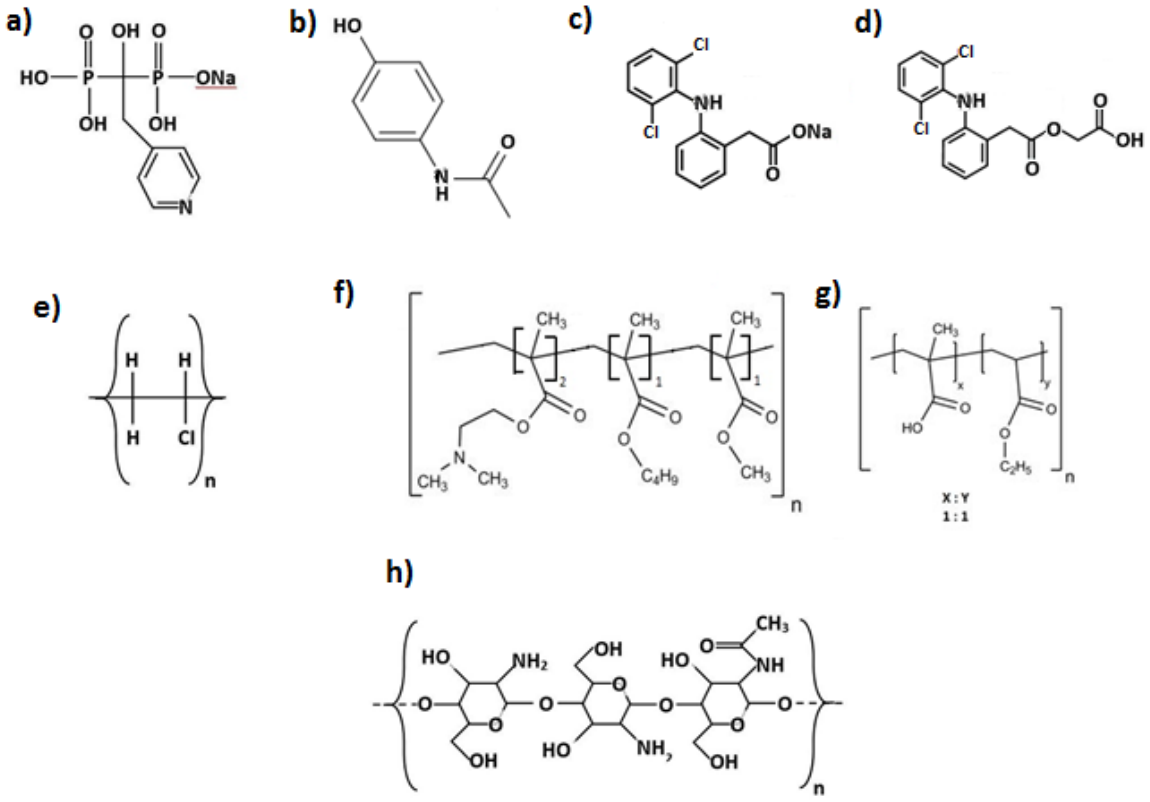

Figure 2: Chemical structures of RIS (a), PAR (b) DIS (c), Ace (d), PVC (e), EE (f), EL (g), CHIT (h)

Table 1. Physicochemical properties of raw materials

	RIS	PAR	DiS	ACE	EE	EL	PVC	CHIT
Solubility (water)	10,4 mg/ml	14g/l	15.9 mg/l	Not soluble	<10 µg/ml (> pH 5)	< 0,03 mg/ml (> pH 6)	<10 µg/ml	Not soluble
logP	-0.75	0.34	3.10	4.16	-	-	-	-
pKa	0.68	9.46	4.00	3.44	-	-	-	-
H^+ acceptor	3	3	3	4	3/n*	3/n*	-	variing
H^+ donor	3	1	1	2	1/n*	1/n*	-	variing
Rotatable bonds	8	3	3	5	-	-	-	2

*x/n: represents the number of H+ acceptor/donor groups per monomer

** predicted value by ChemAxon via https://foodb.ca/compounds/FDB019541 (available on 22.06.2020.)

4.2 Methods

4.2.1 Preformulation studies

During the research and development of the bisphosphonate carrier system preformulation studies were conducted on RiS, Chit and PVC to obtain the most important physical parameters of raw materials.

The flow properties (flow time, angle of repose, bulk density) of the powders were studied with a Pharmatest PTG-1 (Pharmatest GmbH, Germany) powder rheological tester.

The plasticity of materials and mixtures was determined with a computer-connected Korsch EK0 eccentric tablet press (E. Korsch Machienenfabrik, Berlin, Germany), instrumented with strain gauges on both punches and a displacement transducer (Micropulse, BTL5-A11-M0050-P-532, Balluff, Germany) on the upper punch. The strain gauges were calibrated with a Wazau HM-HN-30kN-D cell (Kaliber Ltd., Budapest, Hungary). The transducer distance accuracy was checked by using five measuring pieces of accurately known thickness (1.0, 2.0, 5.0, 7.5 and 10.0 mm) under zero load (Mitutoyo, Tokyo, Japan). The

materials were filled into the die and compressed manually (to ensure similar conditions for the well- and poorly compressible materials) in the compression force range from 1 to 30 kN. The plasticity was calculated from the results of force displacement measurements with the Stamm-Mathis equation (Eq. 1):

$$Pl = E2 / (E2 + E3) *100 \quad (1)$$

where E2 and E3 are the given areas of the force-displacement curve (55).

A DataPhysics OCA 20 (DataPhysics Instruments GmbH, Fielderstadt, Germany) optical contact angle tester was used for the determination of the surface free energies and wettability of the materials using sessile drop method. This method is based on the measurement of the equilibrium contact angle, which is determined by the surface energy of the solid, and the surface tension of the liquid and vapor phases, as described by the Young-equation (Eq. 2):

$$\gamma_{SV} - \gamma_{SL} - \gamma \cos \theta = 0 \quad (2)$$

where θ is the equilibrium contact angle, γ is the surface tension between the given phases, *S* is solid, *L* is liquid and *V* is vapor. The disperse and polar components of the solid surface energy γ_{SV} were calculated with the Wu equations (Eqs. 3 and 4) with the consideration of the surface tensions of polar and nonpolar test liquids (water and diiodomethane). The liquids were dropped onto the surface of solid comprimates 13 mm in diameter, prepared with a Specac hydraulic press (Specac Inc, Orpington, UK) at a pressure of 4 tons.

$$(1+\cos \theta)\gamma_1 = ((\gamma_1^d\gamma_s^d)/(\gamma_1^d + \gamma_s^d) +((\gamma_1^p\gamma_s^p)/(\gamma_1^p + \gamma_s^p)) \quad (3)$$

$$(1+\cos \theta)\gamma_2 = ((\gamma_2^d\gamma_s^d)/(\gamma_2^d + \gamma_s^d) +((\gamma_2^p\gamma_s^p)/(\gamma_2^p + \gamma_s^p)) \quad (4)$$

where γ_d is the disperse and γ_p is the polar component of the liquid surface tension, γ_1 is the surface tension of the first, and γ_2 is the surface tension of the second test liquid, and γ_s is the surface free energy of the solid material.

4.2.2 Tablet preparation

Tablet preparation based on a factorial design. The results of the design experiments were evaluated with the help of Statistica for Windows v12 software package (Statsoft Inc., Tulsa, OK, USA).

The general equation of the response surface was the following (Eq. 5):

$$y=b_0+b_1x_1+b_2x_2+b_3x_3+b_{33}x_3^2+b_{12}x_1x_2+b_{13}x_1x_3+b_{133}x_1x_3^2+b_{23}x_2x_3+b_{233}x_2x_3^2 \quad (5)$$

where b_0 is the average of the results of the given parameter and the other *b* coefficients show the change in the value of the optimization parameter if the value of the given factor increased from the 0 to the +1 level. The unnecessary determinants were deleted from the full equation during the evaluation to avoid overdetermination and improve the model fitting. The optimal number of determinants was selected on the basis of the maximization of the adjusted goodness of fit ($adjR^2$) and the minimization of the mean square of residuals (MS residual).

4.2.2.1 Matrices for bisphosphonate delivery

The composition of the bisphosphonate carrying matrix tablets were according to a mixed 2 and 3 level full factorial design, where the effect of the polymer (biodegradable/non-biodegradable) as a 2 level, qualitative, the amount of the API (10% or 40%) as 2 level, quantitative and the applied compression force (1, 3 or 5 tons equal with 58, 174 or 290 MPa compression pressure, respectively) as a 3 level, quantitative factor was studied.

The composition of tablets for bisphosphonate delivery is displayed in Table 2. The drug and the polymer were homogenized with a Turbula mixer (Willy A. Bachofen Maschienenfabrik, Switzerland) for 8 min +2 min after the addition of the lubricant. The homogenous powder mixture was compressed with the Specac hydraulic tablet press (Specac Inc, Orpington, UK), applying 13 mm in diameter flat punches, manual filling and compression. The mass of the tablets was 0.35 g.

The general QTTP was high drug load, preferably more than 40%, which later may enable the decreasing of the device size, appropriate mechanical hardness ensuring proper handling and implantation procedure (min. 50 N, with an optimal range of 80-120 N), and sustained drug

release for at least 3 months, without considerable burst release (less than 10%-of drug content liberated within the first 24 hrs.

Table 2: Bisphosphonate containing matrix compositions

Materials	Biodegradable		Non-biodegradable	
	CA-1 (%)	CA-2 (%)	CA-3 (%)	CA-4 (%)
RIS	10	40	10	40
PVC	-	-	89	59
CHIT	89	59	-	-
Ca-stearate	1	1	1	1

4.2.2.2 Matrices for the investigation of the role of chemical interactions

The preparation of tablets for the investigation of API-excipient interactions also based on a mixed 2- and 3-level factorial design, where the nature of excipients was studied as 2-level, while the acidic strength of API, the weight ratio of excipients and the applied compression force as 3-level factors. The detailed experimental plan is shown in Table 3 where the primary excipient is PVC.

Table 3. DoE plan for the interaction-investigatory matrices

Compression pressure (MPa) (x_1)		Primary/Secondary exc. ratio (%/%) (x_2)		API (x_3)		Secondary exc. type (x_4)	
Level	Value	Level	Value	Level	Value	Level	Value
-1	75	-1	25/75	-1	PAR	-1	EE
						+1	EL
				0	DIS	-1	EE
						+1	EL
				+1	ACE	-1	EE
						+1	EL
		0	50/50	-1	PAR	-1	EE
						+1	EL
				0	DIS	-1	EE
						+1	EL
				+1	ACE	-1	EE
						+1	EL
		+1	75/25	-1	PAR	-1	EE
						+1	EL
				0	DIS	-1	EE
						+1	EL
				+1	ACE	-1	EE
						+1	EL
0	225	-1	25/75	-1	PAR	-1	EE
						+1	EL
				0	DIS	-1	EE
						+1	EL

				+1	ACE	-1	EE
						+1	EL
		0	50/50	-1	PAR	-1	EE
						+1	EL
				0	DIS	-1	EE
						+1	EL
				+1	ACE	-1	EE
						+1	EL
		+1	75/25	-1	PAR	-1	EE
						+1	EL
				0	DIS	-1	EE
						+1	EL
				+1	ACE	-1	EE
						+1	EL
+1	375	-1	25/75	-1	PAR	-1	EE
						+1	EL
				0	DIS	-1	EE
						+1	EL
				+1	ACE	-1	EE
						+1	EL
		0	50/50	-1	PAR	-1	EE
						+1	EL
				0	DIS	-1	EE
						+1	EL
				+1	ACE	-1	EE
						+1	EL
		+1	75/20	-1	PAR	-1	EE
						+1	EL
				0	DIS	-1	EE
						+1	EL
				+1	ACE	-1	EE
						+1	EL

Powder mixing was made with a Paul Schatz principle based 1,5L mixer (Inversina, BioEngineering, Wald, Switzerland) at 45 rpm for 8 minutes and then for extra 2 minutes with addition of 1% magnesium stearate as lubricant. The mixtures were compressed with an instrumented Kilian SP 300 hydraulic press (IMA Kilian GmbH & Co., KG, Cologne, Germany) using 7 mm diameter punches with bevelled edge. The mass of the tablets here was 0.15 g. The mixtures were loaded into the die manually then compressed in a semi-automatic 'jogging' mode with the application of 2.9, 8.7, or 14.4 kN compression force (75, 225 and 375 MPa compression pressure, respectively)

4.2.3 Tablet testing

4.2.3.1 Physical properties

The physical characterisation of tablets was made with a Kraemer UTS tablet tester (Kraemer Elektronik GmbH, Germany). Mass, hardness, thickness, and diameter were measured. The true density of matrices (ρ_{true}) was determined with a helium gas pycnometer (AccuPyc 1330, Micromeritics, Norcross, GA, USA), while apparent density (ρ_{app}) was calculated from their mass and physical dimensions. Then porosity (ε) was obtained according to the following equation (Eq. 6):

$$\varepsilon=1-(\rho_{app}/\rho_{true}) \quad (6)$$

4.2.3.2 Physico-chemical characterization

For the specific identification and characterization of interactions FT-IR spectra were acquired. ZeSe HATR accessory was used, and measurements were taken on 4 cm^{-1} resolution, 128 scan numbers, with CO_2 and H_2O correction. Spectral data was evaluated with SpectraGryph software v1.2.10 (Dr. F. Menges, Berchtesgaden, Germany).

4.2.3.3 Dissolution tests

There are several methods described in the literature for the testing of dissolution from implantable devices. According to the most commonly used methods, the implants are soaked into the dissolution medium in a watertight container without any agitation (56,57) or applying shaking water bath for continuous mixing of the dissolution liquid (58–61). Nevertheless, Fuchs et al. (62) have performed a comparative study on various testing methods and have described that despite the results obtained with shaking bath are good for comparison of different samples, give not so good correlation with in-vivo data as flow–through cell dissolution, due to the different shear rates. In the lack of flow-through tester, a special apparatus was developed for the testing of the dissolution rate of risedronate sodium from the implantable matrix tablets, mimicking the shear rates obtained with flow-through cells. The tablets were placed into Erlenmeyer flasks containing 50 ml of pH 7.4 phosphate buffered saline (PBS) solution ensuring sink condition for the drug during the whole dissolution study. The continuous closed-loop flow of the dissolution medium was ensured with an Alitea-XV (Alitea, Sweden) peristaltic pump using 2 ml/min flow rate. The dissolution medium was periodically renewed

to maintain the concentration gradient, considering a time-dependent manner. Therefore, 5 ml, 5 ml, 10 ml and 20 ml samples were taken and replaced with fresh medium after 1, 2, 4 and 8 hours respectively. After 24, 48, 72 and 168 hours the full amount of the dissolution medium was renewed regarding to the bisphosphonate drug delivery system.

In case of the matrices prepared for the chemical interaction studies a modified strategy was needed due to the vast number of samples. Only a 24-hour dissolution tests were conducted for all compositions to obtain the most important kinetic parameters, and only few samples were selected afterwards for a one-week study in which the lowest release rates were observed. Therefore, in the 24-hour-long experiments 2.5 ml, 5 ml, 5 ml, 5 ml, 10 ml, 20 ml samples were taken and replaced with fresh medium after 15 min, 30 min, 1 h, 2 h, 4 h, 8 h, respectively, while the last samples were taken after 24 h. In case of the one-week study 5 ml, 5 ml, 10 ml, 20 ml, 35 ml, 35 ml, 35 ml volume was sampled and refreshed as above after 1 h, 2 h, 4 h, 8 h, 24 h, 48 h, 72 h, respectively, while the last samples were taken after 168 h. From each composition three parallel measurements were taken. Quantitative analysis was made with a ThermoGenesys UV-spectrometer at a wavelength of 262 nm for RiS, 274 nm for Ace, 276 nm for DIS and 244 nm in the case of PAR. The dissolution process was evaluated according to the Korsmeyer Peppas equation (Eq. 7.).

$$M_t/M_0=kt^n \tag{7}$$

where M_0 is the initial drug amount in the matrix, M_t is the drug amount at the given time, k is the dissolution rate constant, and n is the shape parameter regarding the diffusion mechanism.

4.2.3.4 Compressibility studies

During the API-excipient interaction studies a more detailed method the Kawakita and Walker method was applied to investigate the compression properties of materials (63).

$$P/C = [P/a + 1/ab] \tag{8}$$

Equation was proposed by Kawakita and Lüdde in 1971, where P is the applied pressure, C is the volume reduction calculated according to Eq. 9, where V is the volume of the powder bed at the applied pressure.

$$C = [(V_0 - V)/V_0] \quad (9)$$

where V_0 is the initial volume of the powder bed, and V is the current volume of the powder after compaction. This equation gives data mostly about the rearrangement phase of compression.

The deformation phase of compression was evaluated by using the equations developed by Walker (Eqs. 10. and 11).

$$log\ P = -LV + C_1 \quad (10)$$

$$100V = -W\ log\ P + C \quad (11)$$

where P is the applied pressure, V is the relative volume calculated from V'/V_0, i.e., the ratio of the volume at the applied pressure and the initial volume of the powder bed, C and C_1 are constants. Coefficient L is the pressing modulus and W shows the percentage volume reduction as the pressure changes on a logarithmic scale.

4.2.4 Design of Experiments and Artificial Neural Networks

DoE analysis and ANN modeling was performed with Statistica v.13.5.0.17 (Tibco Software Inc., Palo Alto, CA, USA). Compression pressure (x_1), amount of excipient (x_2), API (x_3) and excipient used (x_4) were examined as independent factors, while hardness (y_1), porosity (y_2) and release rate (y_3) were used as optimization parameters in the DoE analysis.

One of the objectives of the present study was to compare the effectiveness of various modeling approaches to enable generalized prediction of drug dissolution rates from different matrices. In kinetic-based modelling, the release rate and release exponent were used as the output of the ANN model, while in point-to-point modeling the dissolved amount of drug at the various sampling times was applied according to Galata et al. (54), which included 7 data points. Our hypothesis is that kinetic-based modelling allows for a simplified network structure and faster generalization. To clarify the importance of different input parameters for predictive accuracy, 3 different parameter combinations were used to train the ANNs for both kinetic

based and point-to-point modelling. A list of inputs used in the different training approaches is provided in Table 4, while a detailed data set for training, testing, and validating ANNs is provided in Table S1 in Annex 3.

Table 4. Input variables of the various ANN training approaches.

Modelling type	Approach 1	Approach 2	Approach 3	Approach 4	Approach 5	Approach 6
	Kinetic based	Kinetic based	Kinetic based	Point-to-point	Point-to-point	Point-to-point
Input variable						
Drug	x			x		
Drug solubility (mg/ml)		x	x		x	x
Drug pKa		x	x		x	x
Excipient	x			x		
Excipient solubility (mg/ml)		x	x		x	x
Excipient pKa		x	x		x	x
Excipient amount (%)	x	x	x	x	x	x
Compression pressure (MPa)	x	x	x	x	x	x
Hardness			x			x
Porosity			x			x
Peak Shift	x	x	x	x	x	x

Feed-forward, back-propagation Multilayer Perceptron networks were developed in all cases. The networks were trained with BFGS algorithm. The number of hidden neurons was gradually increased in a dynamic system depending on the number of input and output neurons: $I+O-3 \leq n \leq I+O+1$, where I is the number of inputs O is the number outputs and n is number of hidden neurons., so hidden neuron number was varied from 4-8, 6-10, 8-12, 9-13, 11-15, 13-17 in case of approach 1-6, respectively.

A multistart method including 10.000 networks was applied using the Automated Neural Networks module of Statistica with each hidden neuron number, and training approach to screen the best performing network with different initialization patterns, and activation functions for hidden and output neurons. The training was stopped, when the root mean square error (RMSE) of test dataset reached its minimum. The 5 best preforming networks from each multistart run were retained for further analysis.

The prediction performance of the networks was evaluated based on network perfection, which is the mean R^2 of the observed vs. predicted data of each output neurons, and on the RMSE of predictions on the validation subset.

5 RESULTS AND DISCUSSION

5.1 Matrices for bisphosphonate delivery

5.1.1 Preformulation studies

The results of the powder rheological test revealed that in accordance with the expectations, the micronized risedronate sodium exhibited no measurable flow properties, which may be due to its high surface area and moderately high surface free energy (Table 5). The rheological properties of chitosan platelets confirmed the poor flow properties and extremely low bulk density despite their considerably big size, low surface free energy and low polarity, which was expected based on literature data and may cause problems during tablet preparation (64,65). The PVC has similar surface properties and smaller but more regular particles than chitosan, which resulted in moderate flow properties, bulk density and, in accordance with the value of the angle of repose, excellent arrangement profile.

The result of the deformability tests also reveals considerable differences amongst the 3 materials. The ratio of the plastic/elastic properties (plasticity) of the materials is in negative correlation with the applied compression force. In Table 5 the theoretical maximum (extrapolated to 0 force) of the plasticity and the size of the decrease when the compression force is increased with one kN are displayed.

It can be seen that PVC basically deforms plastically but this value highly depends on the compression force. Chitosan and risedronate sodium exhibit higher elasticity but their behaviour is less dependent on compression force.

Table 5. Results of the preformulation tests

	PVC	CHIT	RIS
Flow time (s)	71.5 (±0.76)	344.7 (±13.75)	n.m.
Angle of repose (°)	25.1 (±1.10)	48.7 (±1.76)	n.m.
Bulk density (g/ml)	0.541 (±0.0166)	0.072 (±0.003)	n.m.
γ (J/m^2)	54.75 (±0.53)	52.16 (±0.71)	76.26 (±0.48)
γ^d (J/m^2)	39.14 (±0.27)	40.49 (±1.15)	41.46 (±0.26)
γ^p (J/m^2)	15.61 (±0.45)	11.12 (±0.70)	34.80 (±0.41)
Polarity (%)	28.51	21.32	45.63
Plasticity (%)	97.76	81.28	84.81
Increase of elasticity (%/kN)	1.1344	0.6671	0.1765

The differences in the rheological and mechanical properties of the raw materials are clearly visible when comparing the mechanical properties of the different samples.

5.1.2 Physical parameters

In case of the RIS containing matrices the response surface of the best fitting model regarding diametric tablet hardness, as one the CQAs, can be described with the following equation (Eq. 12):

$$y=70.71+\mathbf{42.37x_1}+\mathbf{14.76x_3}+\mathbf{5.57x_3^2}-\mathbf{12.72x_1x_2}+2.56x_1x_3+3.52x_2x_3 \quad (12)$$

where the significant factors are highlighted in boldface. The value of the MS residual was 38.93, R^2 was 0.9935 and the adjR^2 value was 0.9867, indicating the excellent fit of the applied model. The predefined acceptance range for this parameter was min 50 N, with an optimal range of 80-120 N.

It can be seen that the hardness of the tablets mostly depends on the properties of the matrix former polymers, and the amount of the API plays a negligible role in this aspect. However, the strong interaction of the type of the polymer indicates that the two polymers behave differently (Fig. 3). The mixing of plastic PVC with the elastic API considerably decreases the hardness of tablets, especially at small compression forces. At high compression forces the difference is negligible due the compression force dependence of the behaviour of PVC. In contrast, the increasing amount of API improves the hardness of chitosan-based tablets both at low and high compression forces due to its higher surface free energy, and less compression force dependency of its plastic-elastic behaviour.

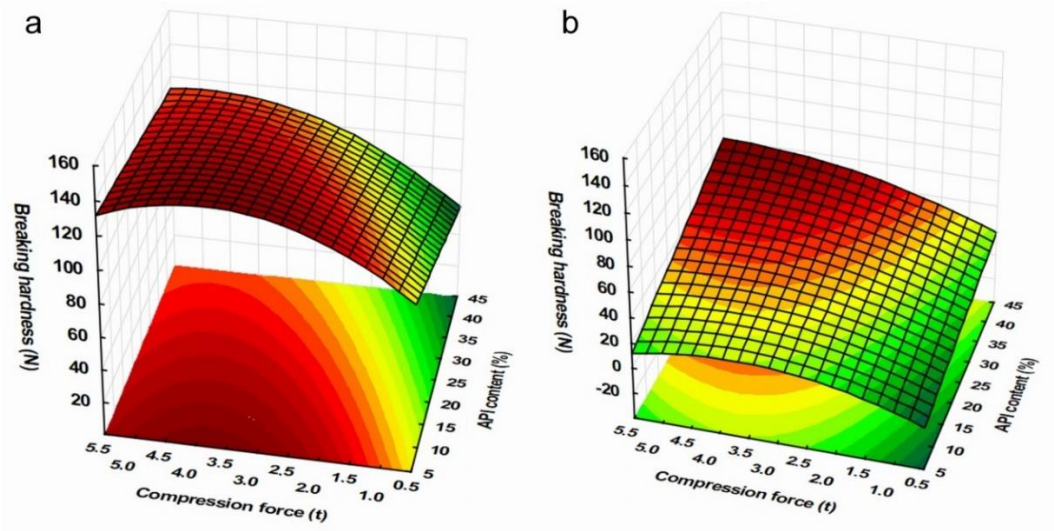

Figure 3: Breaking hardness of RIS containing PVC (a) and chitosan (b) tablets

In general, in the case of PVC-containing matrices, the target acceptance range is available for any API content above 3t compression force, while for chitosan-based matrices, a compression force is greater than 3t and an API content exceeding 30% must be used.

In case of porosity there was no predefined acceptance range, the parameter was analysed as one of the main determinants of drug release rate. The high elastic recovery of compositions resulted in increasing porosity (Fig. 4) and accelerated drug release rate (Fig. 5) at high compression forces.

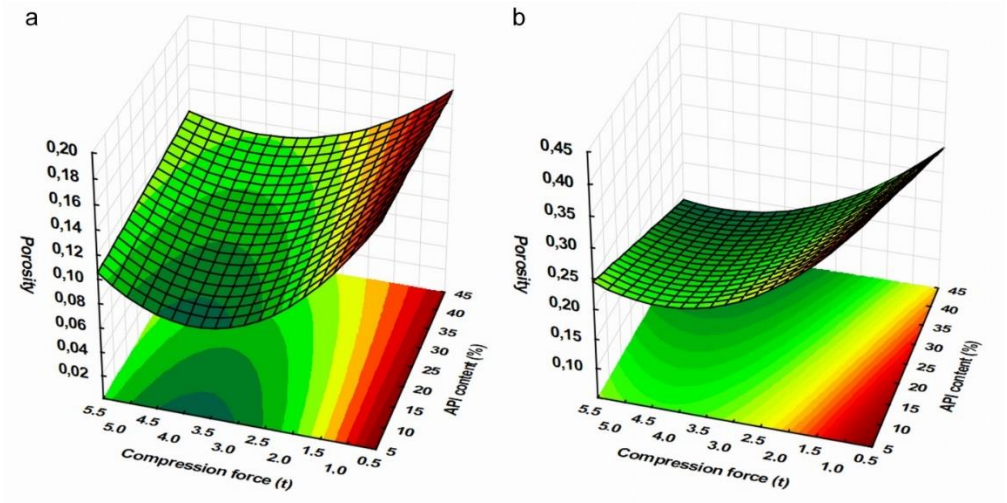

Figure 4. Porosity of RIS containing PVC (a) and chitosan (b) tablets

The change in the porosity of the systems can be described with Eq. 13.

$$y=0.175-\mathbf{0.057x_1-0.016x_2-0.047x_3-0.019x_3^2+0.023x_1x_2+0.021\ x_1x_3} \quad (13)$$

The MS residual value of the model is 0.0002, R^2=0.9856 and adjR^2=0.9682. As expected, the porosity of the tablets exhibits a negative exponential correlation with tablet hardness. Nevertheless, in contrast with hardness, the API content has a significant effect on porosity, especially in the case of chitosan-based tablets. However, the decreasing porosity does not result in a significant change of the drug release rate for chitosan matrices (Fig. 4).

5.1.3 Dissolution studies

The negligible change mentioned in the previous section may be due to the complete disintegration of chitosan matrices in the first 24 hours, inducing a burst release of the drug in the initial stage of dissolution (Fig 5). However, the fast disintegration did not result in the completion of the dissolution process. Slow release of drug was detected even after the complete renewal of the dissolution medium, which indicates that the API is entrapped in the chitosan flakes due to a strong interaction. Nevertheless, chitosan-based matrices were unsuitable to achieve the targeted dissolution profile.

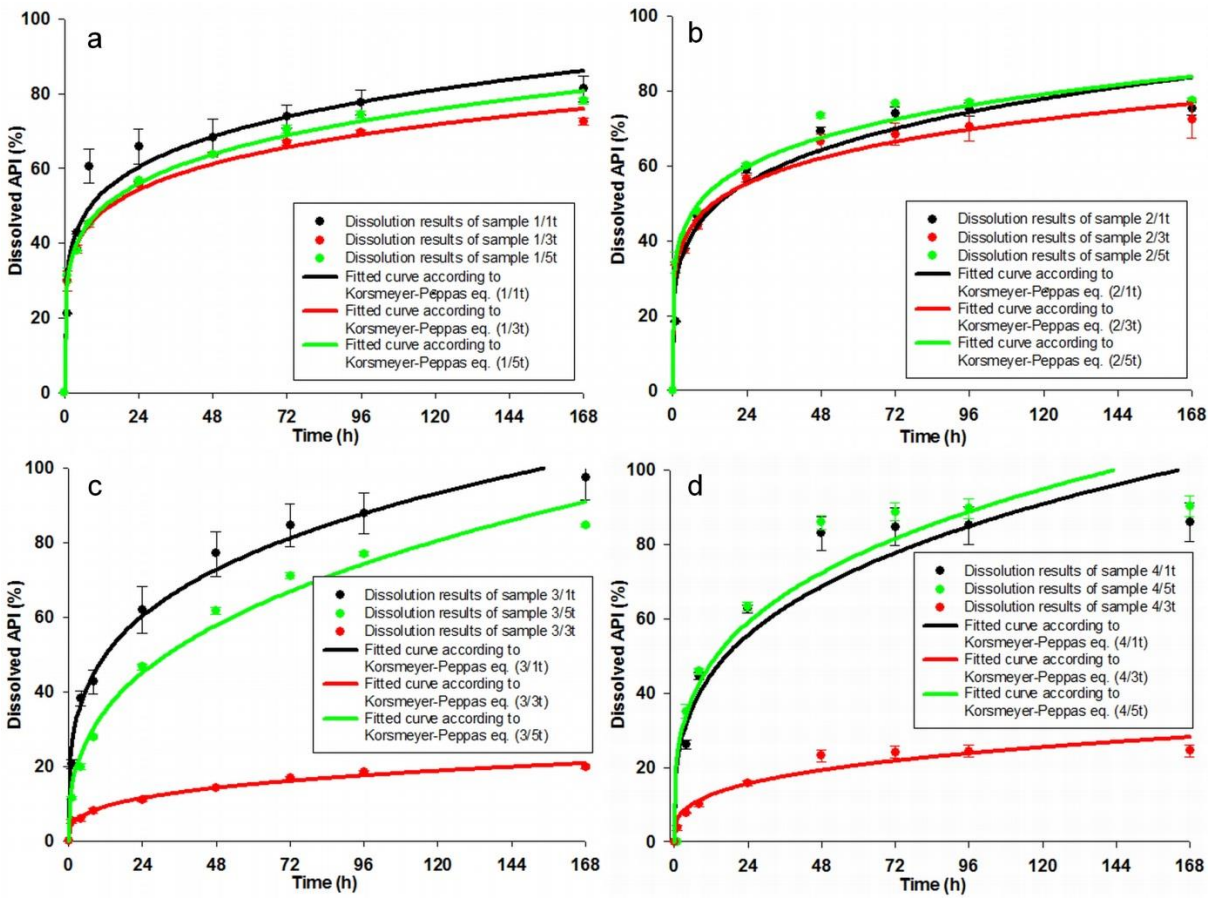

Figure 5. Drug dissolution curves of the CA-1 (a), CA-2 (b), CA-3 (c) and CA-4 (d) samples

The PVC matrices exhibited completely different behaviour during the dissolution process. Due to its hydrophobic nature, the wetting of the PVC matrix is considerably slow, and the texture remained intact during the one-week dissolution process It is also evident from the kinetic data (Table 6) that the PVC based matrices exhibit slower dissolution than the chitosan-based ones under every process condition. Furthermore, even though all the compositions show an inhibited, non-Fickian diffusion-based release of risedronate, it is clearly visible from the

shape parameters (n) that the size of inhibition is smaller in the case of PVC matrices. This is possibly due to the lack of intermolecular associations and may be caused only by the hydrophobic nature of the polymer.

Table 6. Kinetic parameters of drug dissolution

Composition	CA-1			CA-2			CA-3			CA-4		
Compression force (t)	k	n	R^2	k	n	R^2	k	n	R^2	k	n	R^2
1	33.8	0.18	0.91	28.4	0.21	0.95	25.5	0.27	0.97	21.1	0.30	0.88
3	31.4	0.17	0.98	32.4	0.16	0.96	4.33	0.30	0.97	5.97	0.30	0.91
5	30.8	0.18	0.99	34.6	0.17	0.97	14.3	0.36	0.98	23.0	0.29	0.90

It may also be concluded based on the results of statistical analysis (Eq. 14) that the release rate from the matrices is generally determined by the interactions of polymer and compression force and is statistically independent from the drug content of the composition within this range.

$$y=23.84-\mathbf{8.11x_1}+0.45x_2-0.75x_3-\mathbf{3.97x_3^2}+0.55x_1x_2-\mathbf{1.56x_1x_3}-\mathbf{3.96x_1x_3^2}+\mathbf{2.79x_2x_3} \quad (14)$$

The significant factors are highlighted in boldface. The MS residual of the model was 1.0847, R^2=0.9973 and adjR^2=0.9902.

Nevertheless, the drug content has considerable effect on the rate of burst release and therefore the predefined acceptance range of less than 10% drug release within the first 24 hrs may be achieved only at very low API contents.

5.1.4 Investigation of drug-carrier interactions

Although, the supposed interaction between chitosan and the API did not solve the problem of burst release due to the fast disintegration, the phenomenon requires further investigation since it may provide an interesting alternative for tailoring the release from slow-disintegrating matrices. Utilization of micro-environmental drug-polymer interactions is widely used method for solubility improvement and stabilization of spray-dried (11,66) vacuum-dried (67,68), or hot-melt extruded (69,70) solid dispersions or solutions and for modification of drug release (71,72). Nevertheless, most of the referred drug delivery systems are prepared with the

solidification of dissolved or melted materials, where the molecularly dispersed state promotes the formation of interactions during the solidification process. The formation of micro-environmental interactions in directly compressed systems is unlikely, due to the limited contact surface and molecular mobility, but there is a limited amount of data on the in-situ emergence of such interactions during drug dissolution from directly compressed matrices (73). Nguyen et al. (74) described the formation of hydrogen bonds in a hydroxypropyl-cellulose-carbomer matrix, which helped to achieve the required release profile. In another study, Pavli et al. (75) have identified the in-situ emergence of an electrochemical interaction which considerably influenced the release of cationic doxasozin from the anionic polyelectrolyte carrageenan matrix. Nevertheless, in present case the formation of polyelectrolyte complexes is unexpected under the applied preparation and dissolution conditions, since the chitosan matrix is in deprotonated form (see. Section 3.4).

For the confirmation of the nature of interaction FT-IR and NIR investigations were performed, The method is well applicable in various fields where chemical interactions are the area of interest (76,77).

In order to clarify the reason for the release after full disintegration, the influence of the wet media was also tested. A tablet was placed into the dissolution medium until the end of the disintegration process. The remaining flakes were then filtered and dried in drying chamber at 60°C for 24 h and then stored in an exsiccator.

The results of FT-IR measurements (Fig. 6) revealed that presence of drug-polymer interaction may be identified already in the directly compressed samples. The O=P-OH stretching usually gives broad peaks with multiple maxima in the 1600-2400 cm^{-1} region, however in our case these peaks are presented between 1450-2000 cm^{-1} due to distortion caused by the ZnSe HATR crystal, which is resulted in an overlapping with the βOH vibrations of the chitosan molecule. Nevertheless, it is well visible that the most characteristic peak of this region at 1549 cm^{-1} is separated to a peak doublet at 1540 and 1558 cm^{-1}, and the peak at 1567 cm^{-1} exhibits a partial left shift to 1575 cm^{-1}, indicating different strength association between the drug and polymer. Concurrently the peak of chitosan at 1302 cm^{-1} belonging to the νC-N stretching exhibits a left shift to 1321 cm^{-1}, which indicates that the amino groups of the polymer also take part in this interaction. The differences between the spectra of samples before and after dissolution suggests that the associations are being stronger during the dissolution process. The disappearance of the peak 851 cm^{-1} which is associated with the γOH vibrations indicates, the breaking of the dimerized form of the drug. And the shift of the P-OH peak from 975 to 937 cm^{-1} suggests the formation of new intermolecular associations instead of intramolecular ones.

This is also supported by the disappearance of the νP=O vibrations at 1206 cm^{-1}, and the broadening and right shift of the maxima (from 3300 to 3175 cm^{-1}) of the overlapping O-H and N-H stretching peaks. Nevertheless, there was no sign of the presence of POO^- anions, due to the dissociation of the phosphonate groups, nor the appearance of the wide disseminated peaks with multiple maxima in the range of 3100-2600 and 2220-1820 cm^{-1} indicating the protonation of the amino groups of the chitosan. Overall, it may be stated that the present strong drug-polymer interaction is based on hydrogen bonds and not on the formation of a polyelectrolyte complex.

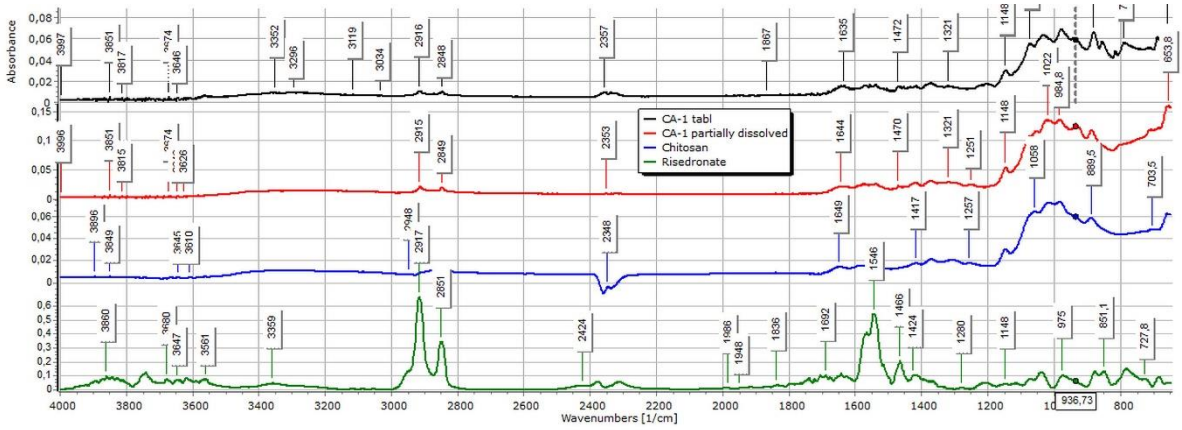

Figure 6. FT-IR spectra of CA-1 sample (CA-1 dry tablet (black), CA-1 tablet after 8h dissolution and drying (red), Chit (blue) and RIS (green)

The presence of hydrogen bond-based interaction was confirmed also with NIR spectroscopic investigations. The NIR spectra of the CA-1 composition are displayed on Fig. 7. It is well visible that although there are some changes on the spectrum of the dry compressed materials, like the merging of the peaks of chitosan at 4235 and 4289 cm^{-1}, it indicates the formation of intra-molecular hydrogen bonds only. It can be seen well in the spectrum of this sample that the intramolecular hydrogen bond ceased since the characteristic peaks of chitosan at 4235 and 4289 cm^{-1} could be identified separately. Nevertheless, new intermolecular associations between chitosan and the API are indicated by the broadening and left shift of the peak of risedronate sodium at 4715 cm^{-1} and the right shift and merging of the peaks of 5195 and 5184 cm^{-1} with the peak at 5022 cm^{-1}. Some smaller characteristic peaks of risedronate sodium have disappeared from the spectrum, but it is not clear whether it is caused by the interaction or may be due to the decreased amount of the drug due to dissolution during the sample treatment.

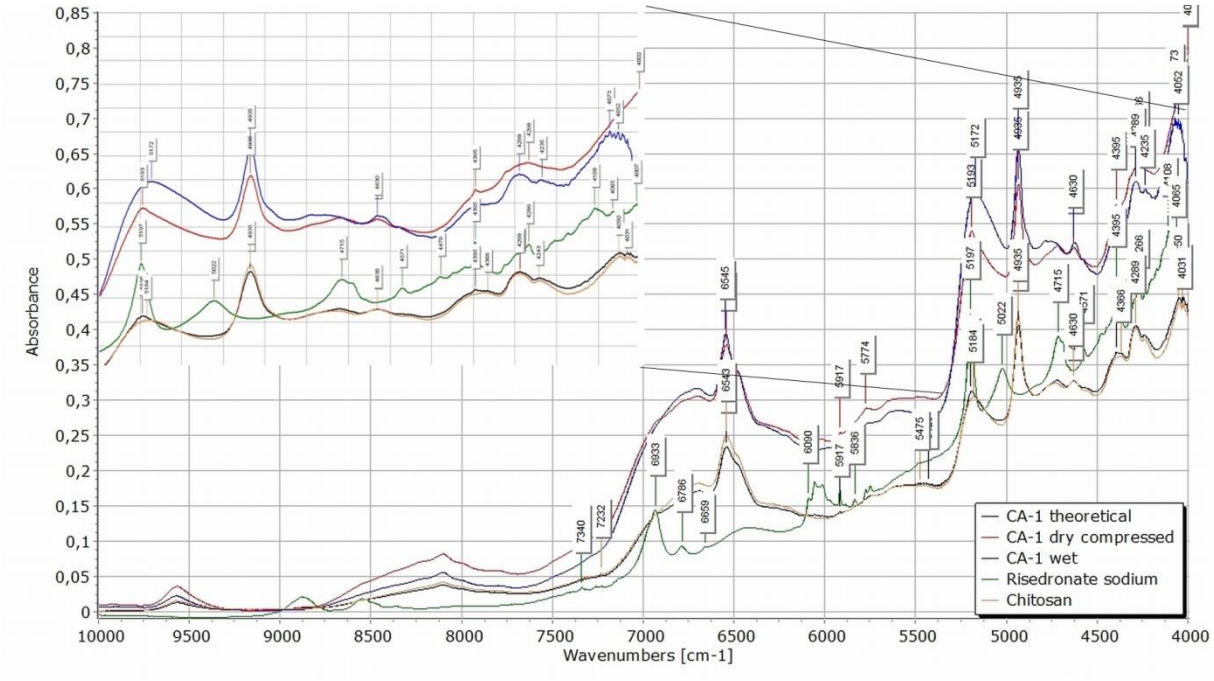

Figure 7. NIR spectra of the CA-1 sample (calculated theoretical spectrum based on weight ratios (black), dry compressed tablet (red), tablet after 8h dissolution and drying (blue)), RIS (green) and CHIT (yellow)

The spectroscopic investigation was also performed in the case of PVC containing samples, and despite of the expectations, major changes were identified in the FT-IR spectrum (Fig. 8) of the partially dissolved sample. The characteristic signal at 1546 cm^{-1} belonging to the O=P-OH stretching of risedronate sodium is separated into a peak doublet. The appearance of the new peak at 1514 cm^{-1} indicates the appearance of the unbonded form of the API, while the right shifted (1539 cm^{-1}) part of the original peak suggests the weakening of the original intramolecular hydrogen bonds. However, these changes in the spectrum may be a general consequence of the dissolution process, it is notable, that a left shift of a characteristic PVC peak from 836 cm^{-1} to 857 cm^{-1} indicating a change in the C-C stretching of the polymer chain, and the appearance of new peaks at 1367 and 1396 cm^{-1} indicating changes in the CH vibrations, suggests the presence of a weak interaction between the drug and the polymer, due the increased reactivity of the hydrogen in the HC-Cl groups.

Nevertheless, the weakness of this bond is indicated well by the NIR studies, where PVC based formulations showed no sign of characteristic changes (Fig. 9). There is no sign of peak shifts or other differences indicating specific interactions either in the dry tablets or in those which were dissolved for 8 hours prior to the analysis. The lack of differences indicates that the slow release of drug is basically determined by the porosity of the matrix, the texture

of which remained intact during the one-week dissolution process. The relationship between porosity and dissolution rates may be followed well from the change of dissolution rate constants (Fig. 5, Table 6.).

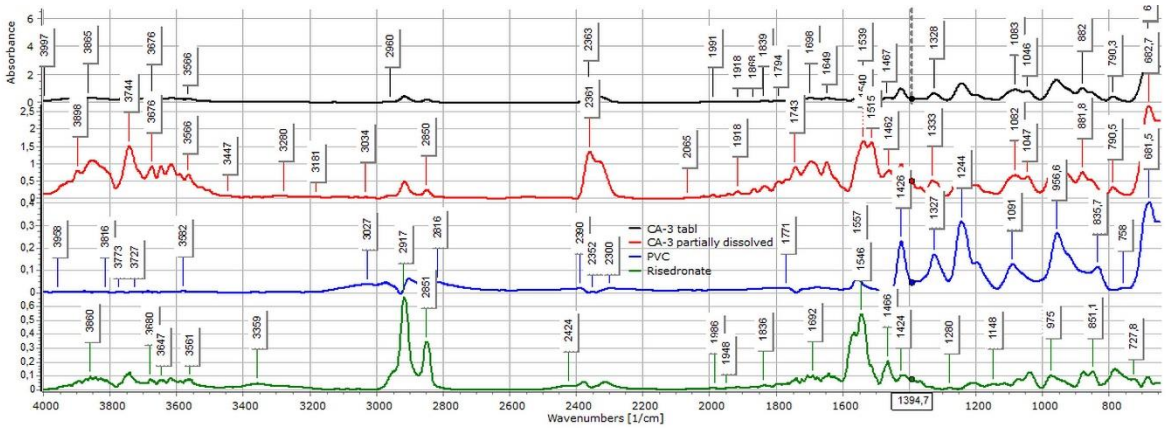

Figure 8. FT-IR spectra of CA-1 sample (CA-3 dry tablet (black), CA-3 tablet after 8h dissolution and drying (red), PVC (blue) and RIS (green)

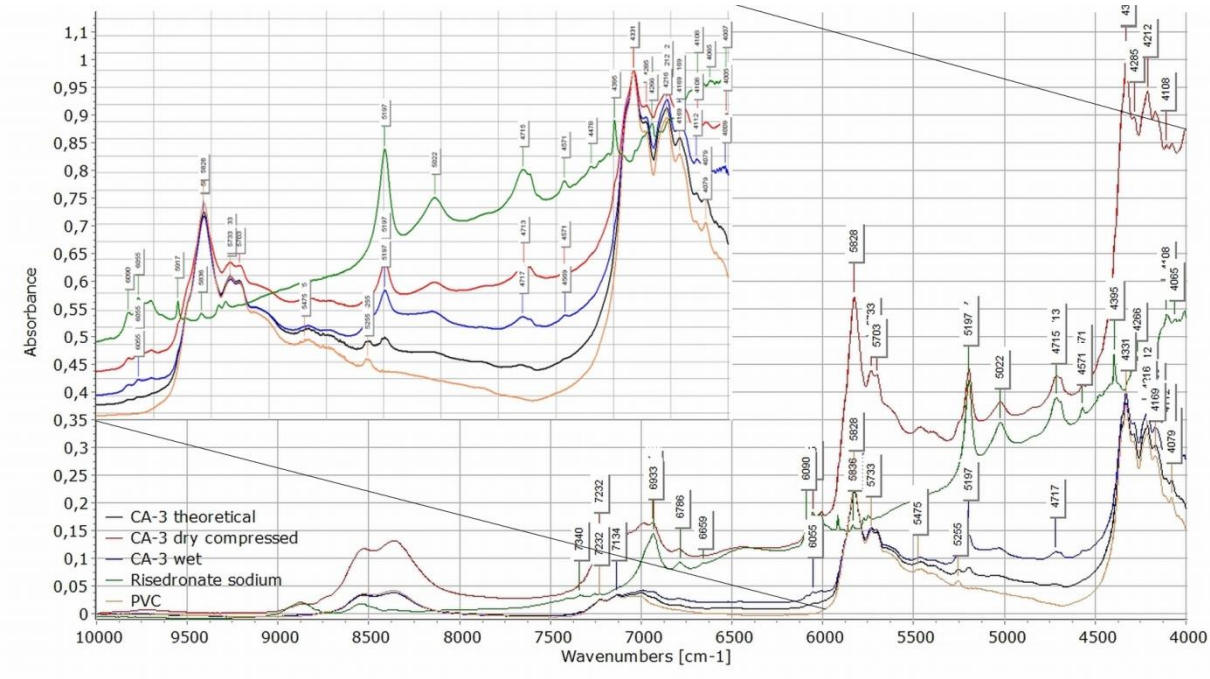

Figure 9: NIR spectra of the CA-3 sample (calculated theoretical spectrum based on weight ratios (black), dry compressed tablet (red), tablet after 8h dissolution and drying (blue), RIS (green) and PVC (yellow))

5.1.5 Brief discussion

The results confirmed that both the chitosan and the PVC based matrix systems may be applicable for long term bisphosphonate delivery, but due fast disintegration and the resulted initial burst release of chitosan-based matrices indicates that direct compression is not appropriate for processing of this system. Nevertheless, the unexpected, in-situ emerging hydrogen bond between the drug and polymer ensuring the prolongation of drug release may have significant importance and enable a new way for modification and tailoring of drug release. A similar, but considerably weaker interaction was also identified between the drug and the PVC matrix, but its strength is unsuitable to considerably influence the drug release rate.

Nevertheless, the PVC-based system mostly fulfilled the predefined QTTP, the hardness of matrices compressed with 3t force was within the optimum 80-120 N hardness range, while the achieved kinetic model projected more than 1 year-long dissolution time. However, the drug release within the first 24 hrs exceeded the predefined 10% limit and it was found to be 11 and 16 % at 10 and 40 % API content, respectively, which requires further optimization. The use of additional excipients are required to utilize the possibilities in interaction-based control of release rate. In the upcoming section results of a more comprehensive systematic approach are detailed for the investigation of the role of chemical interactions between model APIs and co-matrix forming excipients (Eudragit E (EE) and Eudragit L (EL)) in directly compressed PVC matrices, in order to provide more information on the weight of chemical interactions for the modification of dissolution rate.

5.2 Matrices for the investigation of the role of chemical interactions

5.2.1 Physical parameters

The physical parameters of the tablets, prepared for the comprehensive investigation of drug-matrix interactions are shown in Table 7, while the statistical evaluation of the effect of compression pressure (x_1), the amount of excipient (x_2), API (x_3) and excipient used (x_4) on hardness (y_1) and porosity (y_2) of the various compositions are displayed in equations 15 and 16, respectively. The presented equations provided the best fit, for the equations contain the full set of the acquired factor effects and their interactions please see the supplementary materials

in Annex 3. The significant factors and factor interactions are highlighted in boldface in all cases.

$$y_1=110.11+\mathbf{47.02x_1}+\mathbf{9.46x_1^2}+\mathbf{19.31x_2}-\mathbf{10.04x_3}-\mathbf{29.78x_4}+2.45x_1x_2+2.45x_1^2x_2+2.29x_1^2x_2^2-\mathbf{6.31x_1x_3}-\mathbf{4.29x_1^2x_3}+\mathbf{4.96x_1x_3^2}-\mathbf{3.62x_1^2x_3^2}-3.32x_2x_3^2-\mathbf{11.48x_2x_4}-2.24x_2^2x_4-2.33x_3x_4+\mathbf{6.83x_3^2x_4} \quad (15)$$

$R^2=0.9743$ adj. $R^2=0.9599$ MS Res=123.02

$$y_2=0.133-\mathbf{0.053x_1}-\mathbf{0.023x_1^2}-\mathbf{0.046x_3}+\mathbf{0.018x_4}+\mathbf{0.024x_1x_2}-\mathbf{0.019x_1x_2^2}+0.012x_1^2x_3+0.011x_1^2x_3^2-0.014x_1x_4-\mathbf{0.033x_2x_3}-0.009x_2x_3^2+0.010x_2^2x_3^2-0.009x_2x_4+\mathbf{0.016x_2^2x_4} \quad (16)$$

$R^2=0.7627$ adj $R^2=0.6775$ MS Res=0.0023

Table 7. Physical parameters of non-degradable matrices

Eudragit/ PVC ratio (%/%)	Compression pressure (MPa)	Composition	Mass (mg)	Hardness (N)	Porosity	Composition	Mass (mg)	Hardness (N)	Porosity	Composition	Mass (mg)	Hardness (N)	Porosity
25/75	75	PAR-PVC-EL	147.0	15.0	0.307	DIS-PVC-EL	152.1	8.0	0.423	ACE-PVC-EL	144.5	13.5	0.279
	225		147.9	114.3	0.136		135.2	118.5	0.125		131.4	68.2	0.077
	375		141.6	109.1	0.118		202.6	140.7	0.082		131.2	103.6	0.067
50/50	75		149.0	18.7	0.290		154.2	34.0	0.236		152.7	22.9	0.232
	225		135.9	95.8	0.122		138.7	92.0	0.128		137.8	65.8	0.104
	375		142.2	133.6	0.111		146.9	134.4	0.058		142.4	71.3	0.097
75/25	75		147.0	28.2	0.306		153.8	27.3	0.026		147.7	15.2	0.027
	225		151.7	132.6	0.118		136.9	97.0	0.137		134.9	90.7	0.086
	375		149.7	153.8	0.091		121.5	153.8	0.100		137.1	116.7	0.060
25/75	75	PAR-PVC-EE	154.8	113.6	0.223	DIS-PVC-EE	150.4	94.4	0.092	ACE-PVC-EE	147.3	93.4	0.106
	225		142.5	166.6	0.126		129.0	130.7	0.098		151.2	159.1	0.038
	375		136.1	184.5	0.098		130.7	173.7	0.113		152.7	164.7	0.014
50/50	75		149.0	50.1	0.191		151.7	57.4	0.210		151.1	67.6	0.141
	225		152.2	146.7	0.109		138.8	102.6	0.101		137.6	87.5	0.068
	375		145.2	161.8	0.105		138.7	153.8	0.080		139.0	143.6	0.071
75/25	75		149.5	128.6	0.282		137.4	102.9	0.147		146.3	131.2	0.102
	225		137.0	192.4	0.131		135.8	160.6	0.121		145.9	187.9	0.011
	375		148.6	211.2	0.115		151.7	201.0	0.046		141.7	192.8	0.011

The results revealed that there was a general logarithmic relation between the porosity and hardness of the compressed matrices (Fig. 10), while matrices made with use of EE could reach higher breaking hardness and lower porosity than the tablets made with EL. From the

aspect of different weight ratios, the general conclusion is that the composites containing more methacrylate copolymer and less PVC appear to be the strongest systems with the least porosity, while the 25:75 Eudragit-PVC ratio showed the lowest values and the highest porosity. The mean values showed that paracetamol formed the hardest, and ACE formed the weakest matrices, but in general the targeted 80-120 N breaking hardness could be achieved for all APIs. Nevertheless, in contrast with the general expectations the achieved porosities were not directly proportional to the observed drug release rates, which support our primary hypothesis, that in addition of matrix porosity the physicochemical properties of the applied materials and the presence of drug-carrier interactions may considerably influence the drug release.

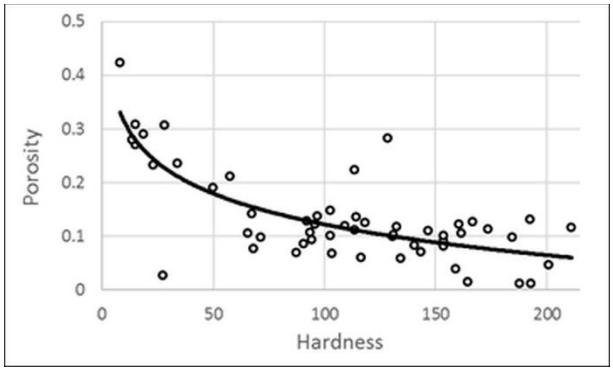

Figure 10. Hardness-porosity plot

5.2.2 Investigation of drug-carrier interactions

The FT-IR spectra of the compressed samples were used to reveal the presence of the drug-excipient interactions. The method is well applicable in various fields where chemical interactions are the area of interest (76,77), the present analysis will focus on selected wavenumber ranges, reasonably where signals of H-bond forming groups can be found.

Interestingly, weak signal intensities were observed in the -OH stretching region (3000-3600 cm^{-1}, data not displayed), for all samples, which made the drawing of proper consequences about the interaction status impossible. The further analysis is focusing therefore on the C=O stretching (1600-1800 cm^{-1}) and the β-OH (β-NH) deformation vibration (1200-1600 cm^{-1}) regions.

According to our primary hypothesis, the interaction potential of the studied APIs is decreasing in the order of ACE>DIS>>PAR and stronger interactions were expected with EE than with EL in all cases. The results generally confirmed this hypothesis.

The Fig. 11 displays the IR spectra of ACE-PVC-EE composition, which exhibits intensive signs of drug-polymer interactions. In the carbonyl signal (C=O stretching) region EE has a characteristic peak at 1722 cm^{-1}, while the ACE at 1712 cm^{-1} and at 1769 cm^{-1}, belonging to the dimerized and monomer forms, respectively. The monomeric peak of ACE (1769 cm^{-1}) almost completely disappears with the increasing amount of EE (Fig. 11). Some further changes, such as the shifting of the deformation vibration of the HNC bonds of ACE 1438 cm^{-1} to 1434 cm^{-1}, and at 1415 cm^{-1} appears to shift to 1420 cm^{-1}, which indicates that the corresponding molecular parts also may take part in the interaction.

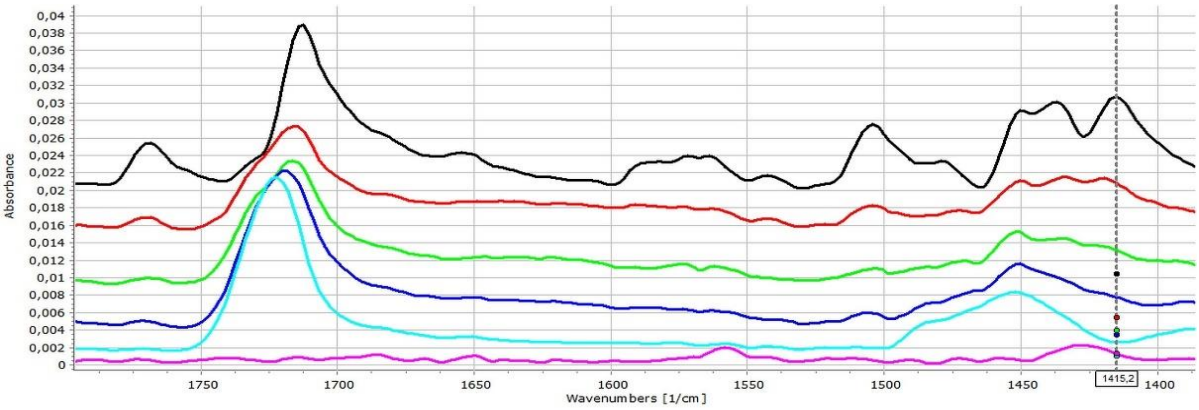

Figure 11. FT-IR spectra (1400-1800 cm^{-1} range) of the ACE (black); ACE-PVC:EE 75:25 (red); ACE-PVC:EE 50:50 (green); ACE-PVC:EE 25:75 (deep blue); EE (light blue) and PVC (purple) samples, multi cursor indicates the place of peak shift in the spectrum.

As it was expected, ACE exhibited fewer signs of interactions in relation to the acidic EL polymer (Fig. 12). The presence of mild interactions by increasing the amount of the EL is supported by the slight shift of the carbonyl signal to 1715 cm^{-1}, 1717 cm^{-1} and 1719 cm^{-1} in the case of 75:25, 50:50 and 25:75 PVC:EL ratios, respectively, and indicated increasing strength of interactions, which is also supported by the decreasing intensity of the unassociated acidic carbonyl absorption peak which appears at 1769 cm^{-1}.

The β-OH vibration of EL appears at 1472.2 cm^{-1}, which cannot be seen clearly in the spectra of matrices. A slight shift of the peak at 1415.3 cm^{-1} towards 1417.8 cm^{-1} can be recognised, which may reflect some further changes in the environment of the diphenylamine group of the drug. This finding is in accordance with the observation of Liu et al. who confirmed that EL may form H-bond based interactions under proper circumstances (78) .

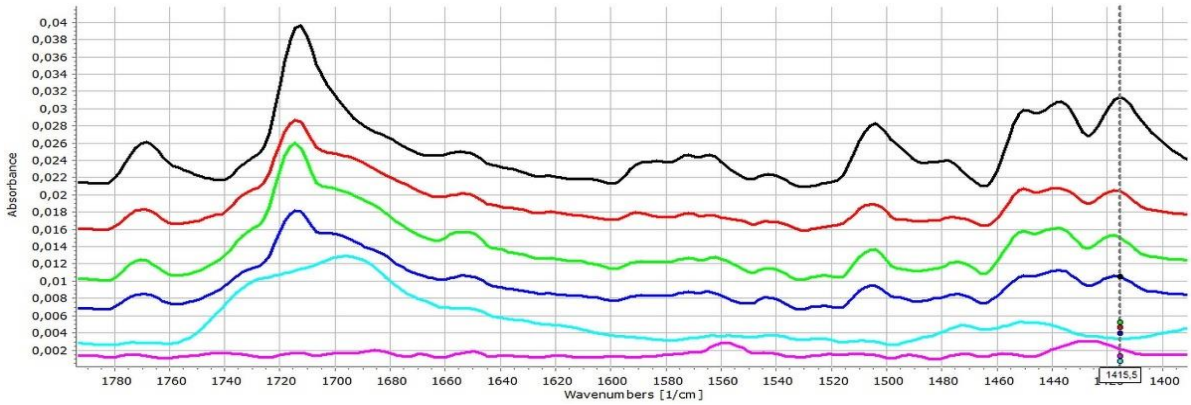

Figure 12. FT-IR spectra (1400-1800 cm^{-1} range) of the ACE (black); ACE-PVC:EL 75:25 (red); ACE-PVC:EL 50:50 (green); ACE-PVC:EL 25:75 (deep blue); EL (light blue) and PVC (purple) samples, multi cursor indicates the place of peak shift in the spectrum.

To clarify the importance of the solid-state interactions, and to analyse the effect of the dissolution medium on the strength of interactions the following experiment was performed. Tablets were dipped into pH 7.4 buffer for 30 min to achieve a complete moisturization of the sample, then the excess of the water was removed, and the samples were measured with FT-IR. Nevertheless, since the presence of water in the pores completely masked the signals in the 3000-3600 cm^{-1} and 1550-1700 cm^{-1} regions, the samples were dried in exsiccator for 24 h, and measured again.

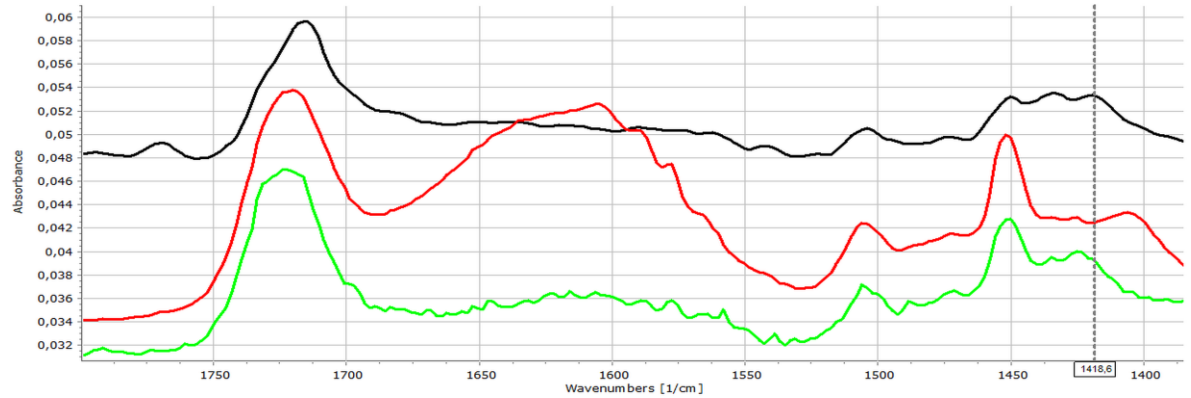

Figure 13. FT-IR spectra of ACE-PVC:EE 75:25 samples: original (black), dipped (red), and dried (green)

Figure 13 displays well, that the strength of intermolecular interaction has increased as effect of water absorption The characteristic peaks of HCN bonds from 1434 cm^{-1} was shifted to 1451 cm^{-1}, while the peak at 1420 cm^{-1} shifted to 1405 cm^{-1}. The characteristic peak of C-N

stretching at 1252 cm^{-1} has shifted to 1272 cm^{-1}. These changes may be observed also in case of the dried samples, despite of some re-organization due to the water loss.

In case of EL containing samples (Fig. 14) similar changes may be observed in the characteristic peaks of HCN vibrations: the peak at 1438 cm^{-1} shifts to 1425 cm^{-1} and its intensity increases considerably, while and C-N stretching signal which may be found at 1279 cm^{-1} shifts to 1291 cm^{-1}.

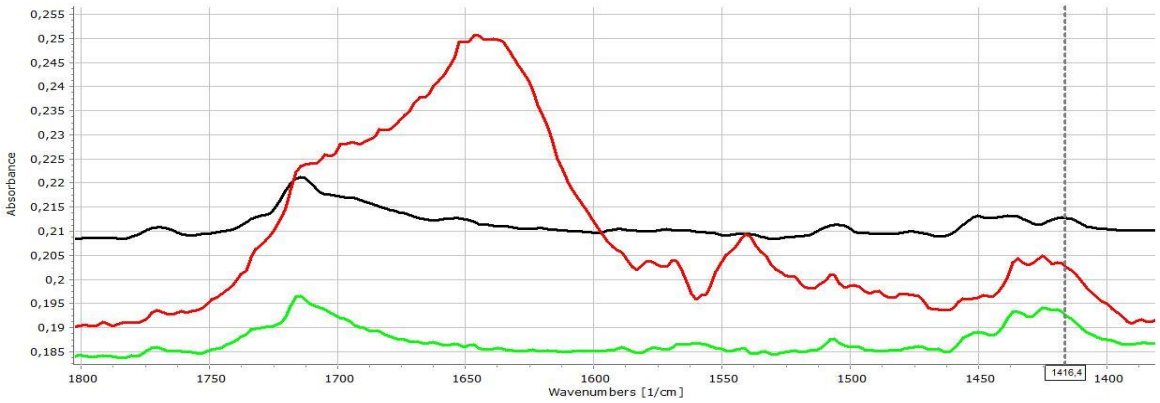

Figure 14. FT-IR spectra of ACE-PVC:EL 75:25 samples: original (black), dipped (red), and dried (green)

As it was expected, the matrices prepared with DIS exhibited fewer spectral changes after compression, primarily due the weaker acidity of the drug, but the higher porosity may also play a possible role in this phenomenon. Similarly to the ACE containing compositions, the most obvious changes may be found in the C=O stretching region. The characteristic peak doublet may be found at 1555 cm^{-1} and 1571 cm^{-1}, where the shift of the peak intensities to the direction of 1571 cm^{-1} may be observed with increasing Eudragit content. As expected, the shift is less intensive in case of EL containing compositions (Fig. S1 in Annex 3) than in EE containing ones (Fig. S2 in Annex 3). Some further signs of mild interaction and increased intramolecular association the C-O bond region of EE containing matrices may also be observed (Fig. S2 in Annex 3). The characteristic peak of DIS at 1279 cm^{-1} and of EE at 1269.5 cm^{-1} overlap around 1274 cm^{-1} in accordance with the increasing amount of EE.

The observed interactions were strongly intensified by the dipping. The ratio of the associated C=O groups was increased for both EE and EL containing (Figs S3 and S4 in Annex 3), which is well visibly from the increasing intensity of the associated C=O peak at 1555 cm^{-1}, and 1549 cm^{-1} for EE and EL, respectively. Further changes such as the increasing intensity of the peak at 1410 cm^{-1} and a peak shift from 1234 cm^{-1} to 1248 cm^{-1}, associated with the βNH and C-N stretching vibration indicates that under these circumstances the secondary

amino group of DIS also involved into the association with EE. In case of EL the corresponding changes may be found at 1409 cm^{-1}, 1232 cm^{-1}, and at 1250 cm^{-1}, respectively. Other peak shifts from 1168 cm^{-1} to 1197 cm^{-1}, and from 1190 $cm^{-}1$ to 1198 cm^{-1}, for EE and EL respectively confirms the presence intermolecular associations from the side of the polymers.

In the case of PAR containing compositions exhibit no obvious signs of interactions neither in case of EL (Fig. S5 in Annex 3) nor for EE (Fig. S6 in Annex 3) containing compositions. The only mentionable change is the slight shift of C-N stretching peak (PAR) from 1221 cm^{-1} to 1224 cm^{-1} or 1226 cm^{-1}, in case of EL and EE containing compositions, respectively. This finding was in accordance with our primary hypothesis, and with the finding of Obediat et al. who also observed no interaction between EE and PAR in compressed matrix systems (79).

Nevertheless, after dipping the tablets into the dissolution medium considerable changes were observed in the FT-IR spectra both the EE and EL containing samples. The shift of the peaks from 1504 cm^{-1} to 1512 cm^{-1} and from 1432 cm^{-1} to 1454 cm^{-1} indicates the participation of the secondary amide group, while the shift of the peak from 1224 cm^{-1} to 1239 cm^{-1} refers on the involvement of the phenolic -OH group, into intermolecular associations (Fig S7 in Annex 3). The shift of the characteristic peak of EE from 1170 cm^{-1} to 1147 cm^{-1} suggest that the drug is connected to tertiary amino groups of the polymer.

The above-mentioned changes may be observed also in case of EL containing samples (peak shifts from 1504 cm^{-1} to 1514 cm^{-1}, from 1434 cm^{-1} to 1424 cm^{-1} and from 1224 cm^{-1} to 1240 cm^{-1}, respectively). While the shift of the characteristic peak of EL from 1169 cm^{-1} to 1186 cm^{-1} indicates that here the carbonyl side groups of the polymer are involved into the association (Fig S8 in Annex 3).

Overall, the results confirmed that solid state drug-polymer interactions may be presented after direct compression of the materials which were in accordance with the findings with de Robertis et al. (73). The weak solid-state H-bonds may further strengthen during the dissolution process and influence the drug release rate (80) or in some cases may even turn into the formation of polyelectrolyte complexes as was observed by Pavli et al. (75).

5.2.3 Dissolution tests and kinetic study

The drug release kinetics was also evaluated with the use of the Korsmeyer-Peppas model (Table 8) which is the most regular type of dissolution in case of hydrophilic matrix systems. It can be noticed from the results that the dissolution followed non-Fickian diffusion. Most n values represent non-Fickian kinetics except those below 0.45. In the case of cylindrical

shapes Fickian diffusion has a value of 0.45, for spherical shapes this value is 0.43. The reason for having smaller values than the limitations of the model is due to the polydisperse nature of the system (81). Particle size has a major influence on the release exponent. Also, the geometry of tablets slightly varies from the ideal cylindrical shape.

Table 8. Release rates and release exponents derived from the Korsmeyer-Peppas model (24-h-long non-biodegradable test)

Eudragit/PVC ratio (%/%)	Compression pressure (MPa)	Composition	R^2	k	n	Composition	R^2	k	n	Composition	R^2	k	n
25/75	75	PAR-PVC-EL	0.9230	5.7937	0.3858	DIS-PVC-EL	0.9966	0.0419	0.9833	ACE-PVC-EL	0.9945	0.4184	0.7325
	225		0.9840	1.4970	0.5635		0.9997	0.0092	1.1609		0.9979	0.0540	0.9340
	375		0.9870	1.7224	0.5345		0.9999	0.0054	1.2765		0.9976	0.0850	0.8940
50/50	75		0.9410	6.8732	0.3534		0.9867	1.4394	0.4317		0.9994	0.1289	0.8756
	225		0.9845	1.6004	0.5377		0.9979	0.0265	0.9560		0.9691	0.1877	0.8271
	375		0.9712	1.5522	0.5594		0.9942	0.0435	0.9105		0.9899	0.0829	0.8931
75/25	75		0.9920	1.7155	0.5058		0.9789	1.5287	0.5567		0.9906	0.2466	0.7311
	225		0.9974	0.7570	0.6298		0.9902	0.1828	0.7850		0.9990	0.2002	0.7389
	375		0.9928	1.5108	0.5239		0.9976	0.2207	0.6573		0.9991	0.2055	0.7260
25/75	75	PAR-PVC-EE	0.9936	0.9010	0.5693	DIS-PVC-EE	0.9660	1.3715	0.2623	ACE-PVC-EE	0.9998	0.0376	0.5936
	225		0.9977	0.6775	0.5774		0.9609	1.4599	0.2306		0.9933	0.0097	0.7596
	375		0.9755	0.8078	0.5483		0.9286	1.4502	0.2176		0.9820	0.0106	0.7241
50/50	75		0.9915	1.1441	0.5441		0.9974	1.7063	0.2739		0.9877	0.2063	0.4619
	225		0.9973	0.4156	0.6751		0.9846	0.9046	0.3542		0.9972	0.0704	0.5474
	375		0.9978	0.3755	0.6785		0.9823	0.9284	0.3404		0.9969	0.0805	0.4910
75/25	75		0.9920	1.6898	0.5056		0.9867	1.5953	0.3265		0.9839	0.2829	0.6100
	225		0.9983	0.7675	0.5535		0.9659	1.0545	0.3185		0.9933	0.1695	0.5134
	375		0.9918	0.8430	0.5239		0.9641	1.5575	0.2903		0.9670	0.2069	0.4661

The PAR loaded matrices released the most drug from 40 to 90 % within 24 h, the acidic ACE containing ones released between 2 and 80%, while the DIS loaded systems released 6-50%. These differences cannot be explained with the different solubility of the APIs since the applied dissolution environment ensures sink conditions for all tested drugs and therefore the solubility may be no limiting factor. Nevertheless, the results of statistical analysis (Eq. 17) revealed that the main governing forces of the drug dissolution rate (y_3) are the physicochemical properties, especially the acidic strength of the drug (x_3), and the applied compression force (x_1), which confirms that the release rate is primarily determined by the porosity of the tablets, since PAR loaded matrices have the lowest hardness and highest porosity (Table 7).

$$y3=0.937-\mathbf{0.380x_1}-\mathbf{0.284x_1^2}-\mathbf{0.804x_3}+0.185x_4-0.242x_1x_2^2+\mathbf{0.403x_1x_3}+0.116x_1x_3^2+\mathbf{0.289x_1^2x_3}-0.208x_1x_4-0.181x_1^2x_4-0.241x_2x_3-0.135x_2x_3^2+0.197x_2x_4+0.116x_2^2x_4-\mathbf{0.440x_3x_4}-\mathbf{0.427x_3^2x_4} \quad (17)$$

R2=0.7669 adj R2=0.6661 MS Res=0.5176

The amount of excipient (x_2), and excipient used (x_4) exhibited non-significant effect on dissolution rate, but regarding the significant factor interactions, the compressibility of the API and its possible chemical interactions with the polymer also have considerable influence on drug liberation. To confirm this observation, and minimize the effect of the mechanical differences, the dissolution rates of tablets with similar porosities (0.13±0.02) were compared (Fig 15a).

The results met with the expectations since EE-based compositions exhibited considerably lower dissolution rates in all cases. Furthermore, in contrast to the observation of Mustafine et al., with acidic APIs a dissolution rate of 100% is expected between 2 to 8 hours with the application of EE and EL (82), slower dissolution was achieved with all tested systems, which also support the importance of drug-matrix interactions on the dissolution rate.

The amount of the released drug decreased to 50.6 % from 78.5 %, to 10.9 % from 45.7 % and to 6.2 % from 58.5 % in the case of PAR, DIS and ACE containing systems, respectively, if EL was switched to EE in the matrix (Fig. 15b-d). This may be partially explained by the bigger hardness and smaller overall porosity of EE containing samples, but the tendency is same if the dissolution rates of samples with similar porosities are compared. In contrast, the observed results are in good accordance with the strength of drug-carrier interactions, since stronger interactions were expected between the acidic drugs and the alkaline EE. This finding supports our previous observation on the role of in situ forming drug-polymer interactions in drug dissolution (80) and were in accordance with the similar findings of Priemel et al. (83), or Mustafine et al. (84), and ultimately confirms our hypothesis, that the utilization of drug-carrier interactions enabled the decrease of initial burst release, and may help in the tailoring of release kinetic.

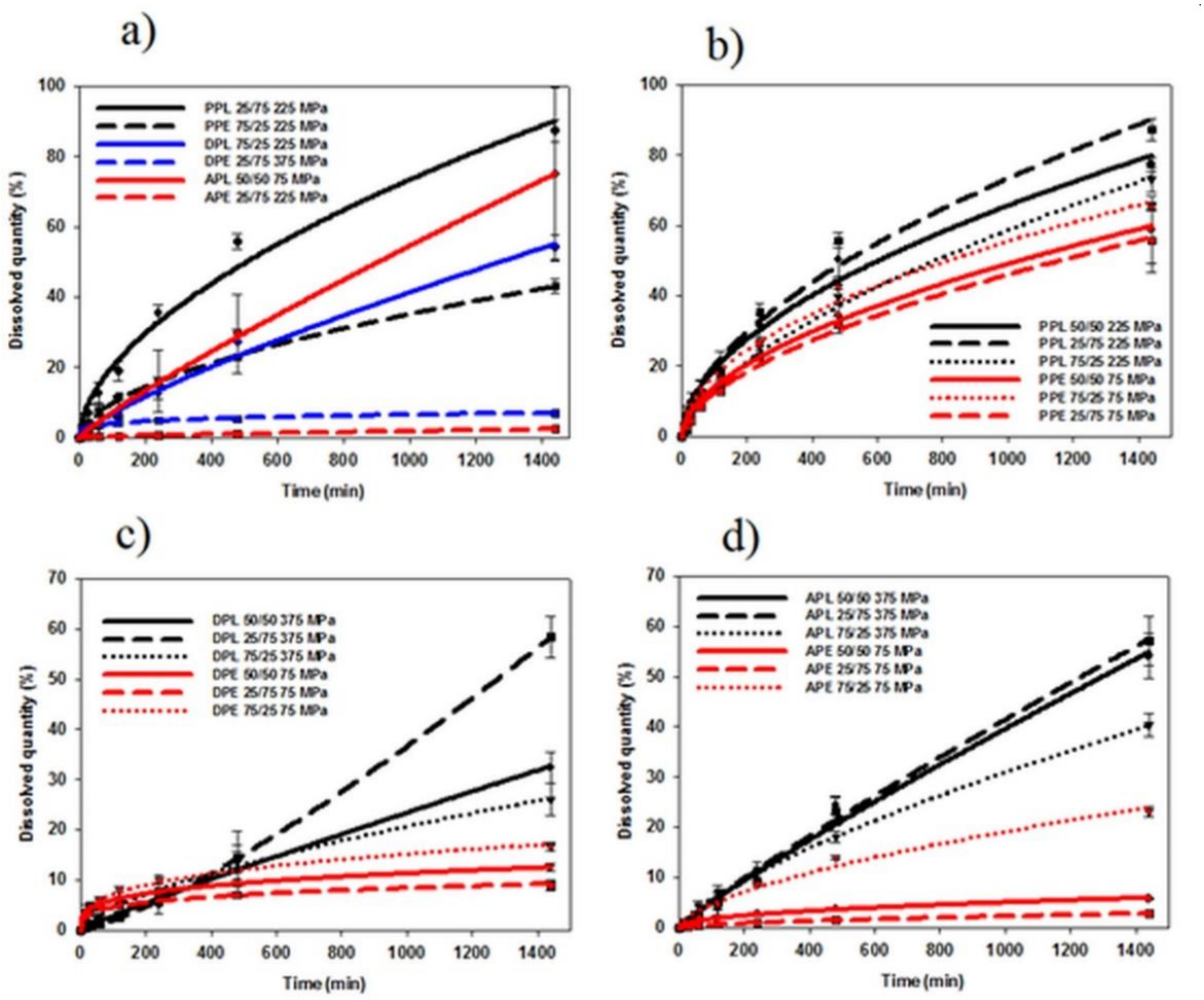

Figure 15. 24 h drug release from various non-degradable matrices: effect of the drug and polymer properties (a) and effect of the composition and compression force for PAR (b), DIS (c) and ACE (d) containing matrices

Finally, to confirm that the selected matrices are suitable for long-term drug delivery, and get more accurate kinetic model, one-week long dissolution study was also performed with some selected compositions. The detailed results can be found in the supplementary material in Annex 3.

5.2.4 Compressibility studies

In order to obtain more information on the formation of matrix texture, the compressibility and the cohesiveness of the compressed systems were determined with the Kawakita and Walker method. The data presents samples compressed at 75, 225 and 375 MPa were plotted according to the out-of-the-die method. Results are shown in Table 9.

Constant *a* shows the rearrangement of particles during compression, i.e. the compressibility of powder mixtures. It can be noticed from the data that the best compactable mixture possessing the lowest value of the constant slightly varies according to the properties of the materials used. Nevertheless, the values usually decrease with increasing Eudragit content, which indicates a positive effect on this property, but the values generally indicate still loosely arranged particles for all compositions. Constant *1/b* represents the energy needed for the reduction of the initial powder volume to its half. These numbers are not in accordance with compressibility (*a*), which suggests that while *a* is related to the particle size distribution of the compressed sample, *1/b* is rather related to the overall surface free energy and adhesiveness of the mixture. This was in accordance with previous findings (63).

Table 9. Parameters of different equations calculated from linear regression analysis

Composition	Primary/ Secondary exc. ratio (%/%)	*a*	*1/b*	*L*	*W*
PAR:PVC:EL	25/75	0.7593	2.7431	3.394	6.9927
	50/50	0.8096	8.3404	10.085	9.9138
	75/25	0.7707	5.6384	12.453	7.9879
PAR:PVC:EE	25/75	0.7827	2.1802	46.997	2.0927
	50/50	0.7702	2.6644	11.855	5.9611
	75/25	0.7440	1.4176	13.849	4.2773
DIS:PVC:EL	25/75	0.7936	3.2601	14.348	5.6154
	50/50	0.7906	5.2812	8.101	9.4141
	75/25	0.7783	2.8007	10.206	6.5001
DIS:PVC:EE	25/75	0.7901	0.1744	18.218	2.3197
	50/50	0.7948	0.7074	25.571	2.3090
	75/25	0.7865	2.0998	-17.815	-0.7867
ACE:PVC:EL	25/75	0.7742	0.7171	11.471	4.3500
	50/50	0.7901	3.3134	9.509	7.5198
	75/25	0.7939	3.6390	10.559	6.9251
ACE:PVC:EE	25/75	0.7925	2.3332	10.088	6.2481
	50/50	0.7625	2.1441	19.075	4.0566
	75/25	0.7355	5.3289	17.199	5.6337

The increment of coefficient *L* means the decrement in volume reduction. According to the results, this parameter shows a complex relation of the composition and the deformation properties. Generally, the increasing amount of Eudragit has a negative effect on this property, but EL containing compositions exhibit slightly better deformation properties than EE containing ones. Nevertheless, all conclusions should be drawn with reservations since both Walker plots (Figs. S10 and S11 in Annex 4) indicate considerable elasticity of the compositions at high compression pressures, which makes the models based on linear

approximations unreliable in the investigated range. This is best visible in the case of the sample where DIS is mixed with mixture PVC:EE of 75:25 weight ratios, where the Walker coefficients show negative values due to the very intensive elastic relaxation, which resulted in looser tablet texture at high compression forces than at smaller ones, and indicates that similarly to the first part of the study, the use of moderate compression forces is the best selection to achieve the targeted mechanical strength of tablets.

5.2.5 ANN modelling

The previous results confirmed, that the targeted QTTP may be achieved with the selected compositions, but tailored drug release requires accurate predictions and consideration of factors which cannot be involved into a regular DoE, which necessitates the use of alternative modelling methods during the development process. In present study, ANN modelling was performed for a dual purpose: to cross check the DoE-based results on the importance of various descriptors on drug dissolution, and to compare the effectiveness of kinetic-based and point-to-point approaches in the predictability of the dissolution data. The use of various predictor sets may help the further clarification of which material attributes play crucial role in the dissolution from the developed implantable matrices.

The results revealed that the overall perfection of point-to-point modelling was significantly ($p<0.05$) better as of kinetic parameter-based models (0.92±0.02 and 0.87±0.03, respectively). No significant difference was observed between the prediction performance of retained networks related to the applied hidden neuron number (Table S3 in Annex 3), the results were inconsistent and more dependent on network initialization. Similarly, the use of the various predictor sets caused no considerable change in the overall prediction performance, but an interesting difference was observed between the point-to-point and kinetic parameter-based models when the prediction performance was compared on the train, test, and validation subsets. In case of kinetic parameter-based modelling the RMSE of predictions on train (0.22±0.08, 0.15±0.07, 0.09±0.05) and test (0.30±0.04, 0.29±0.05, 0.19±0.05) datasets was significantly improved in order of Approach 1, 2 and 3, respectively, while no significant change was observed on validation dataset. In contrast, for point-to-point modelling the RMSE of predictions on train and test datasets remained unchanged, while it was a significant improvement on the validation dataset (328±19, 235±18, 158±10) in order of Approach 5, 4, and 6, respectively.

Nevertheless, despite of the observed differences it can be stated, that the use of continuous inputs with appropriate descriptors of the tablet texture (hardness, porosity) enable

the best prediction performance for both point-to-point and kinetic parameter-based approaches, despite of the fact that texture parameters exhibited relatively low importance in predictivity according to the results of the global sensitivity analysis (Table S4 in Annex 3).

The results of the global sensitivity analysis, which show the relative importance of various predictors (inputs) on the prediction outcome, are partly consistent with the results of the experimental design. The greatest effect was observed for drug solubility, but the pKa of the excipients and the peak shift indicating drug-excipient interactions exhibits similar importance than the compression pressure, tablet texture or the amount of excipient (Table S4 in Annex 3).

To ultimately compare the prediction effectiveness of point-to-point and kinetic parameter-based modelling approaches the best performing networks (best overall training perfection and lowest prediction error on validation dataset, with no negative prediction values) was selected for both modelling approaches. The best network for kinetic parameter-based modelling had 9 input, 7 hidden and 2 output neurons, with logistic activation on hidden and exponential on output neurons (training perfection: 0.9103, validation error: 0.0760). The structure of the best point-to-point network was 9 input, 16 hidden and 7 output neurons, with exponential activation on hidden and logistic on output neurons (training perfection: 0.9286, validation error: 83.06). Figure 16 shows the predicted dissolution curves of the best and worst predicted cases.

It is clearly visible the point-to-point modeling approach showed more consistent accuracy, especially in cases where drug release was nearly linear (Fig. 16a, c). In other cases, the most considerable inaccuracies were observed at the 2, 4, and 8 h data points. Nevertheless, the predicted results were closer to the observed ones as for kinetic parameter-based models.

The main problem of the kinetic parameter-based approaches that the dissolution data obtained showed large differences, so the corresponding dissolution rates were scattered by two orders of magnitude. This posed a certain limitation on the predictivity, since small inaccuracies in the predicted values of low release rates were resulted in predictions of 3-5-fold faster or slower dissolution (Fig. 16 a, c). The prediction of release exponents, which scattered in a significantly smaller range was more accurate, but the presence of small inaccuracies can also cause large differences between the observed and predicted data at the end of the dissolution curves. It can be stated that the obtained models provide the desired accuracy only in the first 4-8 hours of dissolution (Fig. 16 b, d).

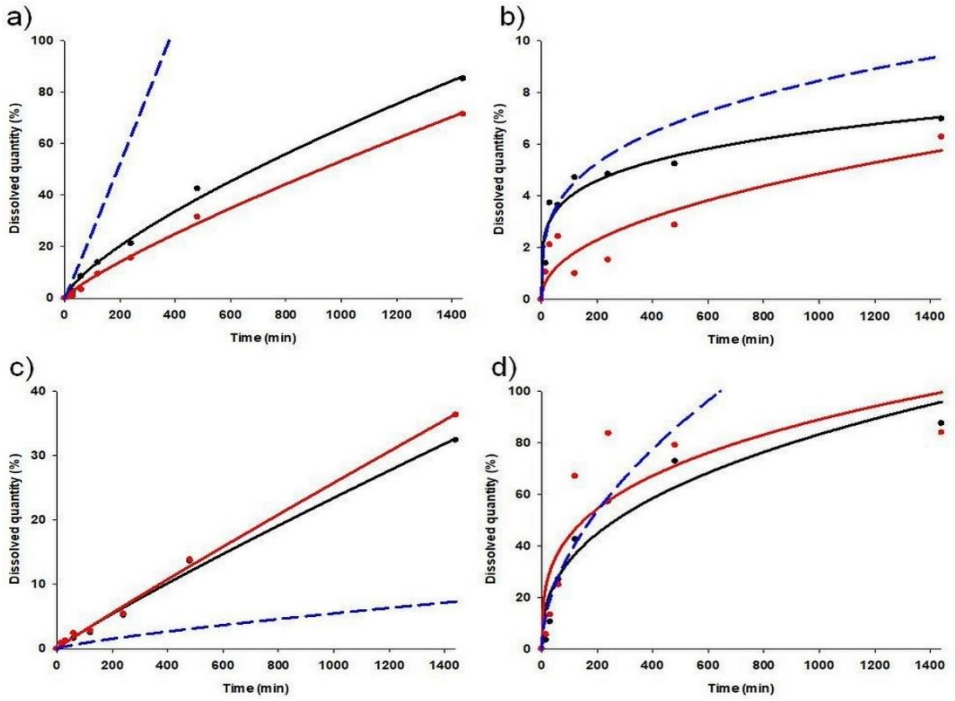

Figure 16. Observed and predicted dissolution curves of case 43 (a), case 36 (b), case 24 (c) and case 7 (d). Black dots: observed data points, black line: fitted model on observed data, red dots: predicted data points, red line: fitted model on predicted data points, blue line: predicted model.

5.2.6 Brief discussion

The present work introduced a comprehensive systematic approach for the investigation of the role of chemical interactions between APIs and excipients in directly compressed matrices. With help of FT-IR studies it was confirmed that solid-state interactions may be induced also in directly compressed matrix systems. The results also confirmed that the presence of solid-state interactions may not always presented in directly compressed systems, but their presence will definitely predict strong in-situ forming interactions during the drug dissolution process. The interactions are mostly H-bond based, but the forming of polyelectrolyte complexes cannot be excluded. With minimizing the influence of the solubility of the API and the porosity of the matrix, we have proven that interactions exert considerable influence on drug liberation by retaining the drug in the matrix. This helped to decrease the initial burst release of the drug, and to achieve the targeted QTTP with 80+N hardness, drug release for more than 3 month and less than 10% of drug release in the first 24 hrs. This study provides better understanding of the correlation of the physicochemical properties of materials with the drug liberation process, thereby promoting a more evolved formulation design.

6 CONCLUSION AND PRACTICAL RELEVANCE

The present dissertation introduces a comprehensive work on the development on implantable pharmaceutical drug delivery systems. Despite its indisputable advantage that it is completely absorbed by the body, the biodegradable chitosan was unsuitable to achieve the targeted QTTP, due to the fast disintegration and the initial burst release of the drug. In contrast, the non-biodegradable PVC-based matrix systems found to be applicable for long term bisphosphonate delivery. However, the burst release required further optimalization, but the utilization of in-situ emerging hydrogen bonds, firstly observed in case of chitosan-based systems between the drug and polymer enables further prolongation and tailoring of drug release.

To better understand the relevance of these interactions a systematic investigation was used. A Design of Experiments plan was set with the addition of varying APIs and excipients. Overall, the results confirmed that solid state drug-polymer interactions may be presented after direct compression of the materials. The weak solid-state H-bonds may further strengthen during the dissolution process and influence the drug release rate or in some cases, may even turn into the formation of polyelectrolyte complexes. According to our hypothesis, the interaction potential of the studied APIs can be predicted and is decreasing in the order of ACE>DIS>>PAR and stronger interactions were expected with EE than with EL in all cases, which was confirmed by the results, noting that the dissolution rate is primarily determined by the physical properties of the matrix, and interactions play only secondary role in the process. Nevertheless, the utilization of the drug-carrier interactions enabled the further decrease of the initial burst release and helped to achieve the targeted QTTP.

Nevertheless, the achievement of tailored drug release requires accurate estimation of factor effects, which may be limited by the rigid structure and requirements of DoE planning. and better predictability may be achieved using ANNs. ANNs are capable of predicting dissolution profiles from general physicochemical properties of materials and possess the advantage that their network system is fine tuneable throughout development process. The efficacy of different ANN models was compared, and was confirmed, that ANNs may provide useful complimentary tool for better understanding of the importance of various factors in the modelled processes. However, our secondary hypothesis, that kinetic-based modelling approach, which allows a simplified network structure and faster generalization process will provide faster and more accurate predictions was not confirmed. On the contrary, according to

our findings the point-to-point modelling approach proved more consistent accuracy, especially in cases where drug release was nearly linear. The wide range of dissolution rates in the training dataset posed a certain limitation on the predictivity of kinetic parameter-based models.

Summary of the present work regarding to hypotheses:

1. The primary aim of the study was only partially confirmed, as the QTTP of tablet hardness above 80 N and long term bisphosphonate delivery up to 12 months could be only achieved with the use of non-biodegradable PVC, and the fulfilment of the burst release requirements required further optimization
2. The secondary hypothesis on the correlation of the strength of solid-state interactions with acidic strength of API was confirmed, and further in-situ forming bonds are predictable prior dissolution.
3. The third hypothesis on the priority of kinetic parameter-based modelling over point-to-point approach was rejected. Comparing the effectiveness of the two approaches despite our expectations point to point modelling proved more consistent accuracy regarding to generalized prediction of drug dissolution rates from different matrices.

Nevertheless, due to their advantageous properties, such as their high degree of flexibility, the ANN-based DDS design will soon became vast pillar of personalised medicine, overcoming individual differences among patients with chronic diseases. The fundaments of interaction-based matrix design are presented in this work still requires further investigations and model adjustments, but opens new ways to achieve tailored drug release.

REFERENCES

1. Rajam N. Policy strategies for personalising medicine “in the data moment”. Health Policy and Technology. 2020 Sep;9(3):379–83.
2. Curtis EM, Dennison EM, Cooper C, Harvey NC. Osteoporosis in 2022: Care gaps to screening and personalised medicine. Best Practice & Research Clinical Rheumatology. 2022 Jun;101754.
3. Verza BS, van den Beucken JJJP, Brandt JV, Jafelicci Junior M, Barão VAR, Piazza RD, et al. A long-term controlled drug-delivery with anionic beta cyclodextrin complex in layer-by-layer coating for percutaneous implants devices. Carbohydrate Polymers. 2021 Apr;257:117604.
4. Chansanroj K, Petrović J, Ibrić S, Betz G. Drug release control and system understanding of sucrose esters matrix tablets by artificial neural networks. European Journal of Pharmaceutical Sciences. 2011 Oct;44(3):321–31.
5. Clynes MA, Harvey NC, Curtis EM, Fuggle NR, Dennison EM, Cooper C. The epidemiology of osteoporosis. Br Med Bull. 2020 May 15;133(1):105–17.
6. Cadarette SM, Katz JN, Brookhart MA, Stürmer T, Stedman MR, Levin R, et al. Comparative gastrointestinal safety of weekly oral bisphosphonates. Osteoporos Int. 2009 Oct;20(10):1735–47.

7. Lichtenberger LM, Romero JJ, Gibson GW, Blank MA. Effect of bisphosphonates on surface hydrophobicity and phosphatidylcholine concentration of rodent gastric mucosa. Digestive Diseases and Sciences. 2000;45(9):1792–801.

8. Thomson ABR, Marshall JK, Hunt RH, Provenza JM, Lanza FL, Royer MG, et al. 14 day endoscopy study comparing risedronate and alendronate in postmenopausal women stratified by Helicobacter pylori status. J Rheumatol. 2002 Sep 1;29(9):1965.

9. Hur W, Park M, Lee JY, Kim MH, Lee SH, Park CG, et al. Bioabsorbable bone plates enabled with local, sustained delivery of alendronate for bone regeneration. Journal of Controlled Release. 2016 Jan;222:97–106.

10. Peter B, Pioletti DP, Laïb S, Bujoli B, Pilet P, Janvier P, et al. Calcium phosphate drug delivery system: influence of local zoledronate release on bone implant osteointegration. Bone. 2005 Jan;36(1):52–60.

11. Medarević D, Kachrimanis K, Djurić Z, Ibrić S. Influence of hydrophilic polymers on the complexation of carbamazepine with hydroxypropyl-β-cyclodextrin. European Journal of Pharmaceutical Sciences. 2015 Oct;78:273–85.

12. Perugini P, Genta I, Conti B, Modena T, Pavanetto F. Long-term release of clodronate from biodegradable microspheres. AAPS PharmSciTech. 2001 Sep;2(3):6–14.

13. Anselmo AC, Mitragotri S. An overview of clinical and commercial impact of drug delivery systems. Journal of Controlled Release. 2014 Sep;190:15–28.

14. Kleiner LW, Wright JC, Wang Y. Evolution of implantable and insertable drug delivery systems. Journal of Controlled Release. 2014 May;181:1–10.

15. Avgoustakis K, Nixon JR. Biodegradable controlled release tablets 1: Preparative variables affecting the properties of poly(lactide-co-glycolide) copolymers as matrix forming material. International Journal of Pharmaceutics. 1991 Mar;70(1–2):77–85.

16. Krier F, Riva R, Defrère S, Mestdagt M, Van Langendonckt A, Drion P, et al. Device-based controlled local delivery of anastrozol into peritoneal cavity: in vitro and in vivo evaluation. Journal of Drug Delivery Science and Technology. 2014;24(2):198–204.

17. Campiñez MD, Ferris C, de Paz MV, Aguilar-de-Leyva A, Galbis J, Caraballo I. A new biodegradable polythiourethane as controlled release matrix polymer. International Journal of Pharmaceutics. 2015 Mar;480(1–2):63–72.

18. Miller-Chou BA, Koenig JL. A review of polymer dissolution. Progress in Polymer Science. 2003 Aug;28(8):1223–70.

19. Thomas NL, Windle AH. A theory of case II diffusion. Polymer. 1982 Apr;23(4):529–42.

20. Campos-Aldrete ME, Villafuerte-Robles L. Influence of the viscosity grade and the particle size of HPMC on metronidazole release from matrix tablets. European Journal of Pharmaceutics and Biopharmaceutics. 1997 Apr;43(2):173–8.

21. Costa P, Sousa Lobo JM. Modeling and comparison of dissolution profiles. European Journal of Pharmaceutical Sciences. 2001 May;13(2):123–33.

22. Lee PI, Peppas NA. Prediction of polymer dissolution in swellable controlled-release systems. Journal of Controlled Release. 1987 Dec;6(1):207–15.

23. Kaunisto E, Abrahmsen-Alami S, Borgquist P, Larsson A, Nilsson B, Axelsson A. A mechanistic modelling approach to polymer dissolution using magnetic resonance microimaging. Journal of Controlled Release. 2010 Oct;147(2):232–41.

24. Kaunisto E, Marucci M, Borgquist P, Axelsson A. Mechanistic modelling of drug release from polymer-coated and swelling and dissolving polymer matrix systems. International Journal of Pharmaceutics. 2011 Oct;418(1):54–77.

25. Crowley MM, Schroeder B, Fredersdorf A, Obara S, Talarico M, Kucera S, et al. Physicochemical properties and mechanism of drug release from ethyl cellulose matrix tablets prepared by direct compression and hot-melt extrusion. International Journal of Pharmaceutics. 2004 Jan;269(2):509–22.

26. Korsmeyer RW, Gurny R, Doelker E, Buri P, Peppas NA. Mechanisms of solute release from porous hydrophilic polymers. International Journal of Pharmaceutics. 1983 May;15(1):25–35.

27. Huanbutta K, Cheewatanakornkool K, Terada K, Nunthanid J, Sriamornsak P. Impact of salt form and molecular weight of chitosan on swelling and drug release from chitosan matrix tablets. Carbohydrate Polymers. 2013 Aug;97(1):26–33.

28. Ravi Kumar MNV, Kumar§ N. Polymeric Controlled Drug-Delivery Systems: Perspective Issues and Opportunities. Drug Development and Industrial Pharmacy. 2001 Jan;27(1):1–30.

29. Rime A. Compressibility and compactibility of powdered polymers: poly(vinyl chloride) powders. European Journal of Pharmaceutics and Biopharmaceutics. 1997 Nov;44(3):315–22.

30. am Ende MT, Peppas NA. Transport of ionizable drugs and proteins in crosslinked poly(acrylic acid) and poly(acrylic acid-co-2-hydroxyethyl methacrylate) hydrogels. II. Diffusion and release studies. Journal of Controlled Release. 1997 Sep;48(1):47–56.

31. Khunawattanakul W, Puttipipatkhachorn S, Rades T, Pongjanyakul T. Novel chitosan−magnesium aluminum silicate nanocomposite film coatings for modified-release tablets. International Journal of Pharmaceutics. 2011 Apr;407(1–2):132–41.

32. Szakonyi G, Zelkó R. Carbopol®-crospovidone interpolymer complex for pH-dependent desloratadine release. Journal of Pharmaceutical and Biomedical Analysis. 2016 May;123:141–6.

33. Li L, Li J, Si S, Wang L, Shi C, Sun Y, et al. Effect of formulation variables on in vitro release of a water-soluble drug from chitosan–sodium alginate matrix tablets. Asian Journal of Pharmaceutical Sciences. 2015 Jul;10(4):314–21.

34. Sreekanth Reddy O, Subha MCS, Jithendra T, Madhavi C, Chowdoji Rao K. Curcumin encapsulated dual cross linked sodium alginate/montmorillonite polymeric composite beads for controlled drug delivery. Journal of Pharmaceutical Analysis. 2021 Apr;11(2):191–9.

35. Phaechamud T, Koizumi T, Ritthidej GC. Chitosan citrate as film former: compatibility with water-soluble anionic dyes and drug dissolution from coated tablet. International Journal of Pharmaceutics. 2000 Mar;198(1):97–111.

36. AlKhatib HS, Aiedeh KM, Bustanji Y, Hamed S, Mohammad MK, AlKhalidi B, et al. Modulation of buspirone HCl release from hypromellose matrices using chitosan succinate: Implications for pH-independent release. European Journal of Pharmaceutics and Biopharmaceutics. 2008 Nov;70(3):804–12.

37. Sogias IA, Williams AC, Khutoryanskiy VV. Chitosan-based mucoadhesive tablets for oral delivery of ibuprofen. International Journal of Pharmaceutics. 2012 Oct;436(1–2):602–10.

38. Li L, Wang L, Li J, Jiang S, Wang Y, Zhang X, et al. Insights into the mechanisms of chitosan–anionic polymers-based matrix tablets for extended drug release. International Journal of Pharmaceutics. 2014 Dec;476(1–2):253–65.

39. Shao Y, Li L, Gu X, Wang L, Mao S. Evaluation of chitosan–anionic polymers based tablets for extended-release of highly water-soluble drugs. Asian Journal of Pharmaceutical Sciences. 2015 Feb;10(1):24–30.

40. Rege PR, Shukla DJ, Block LH. Chitinosan-drug complexes: effect of electrolyte on naproxen release in vitro. International Journal of Pharmaceutics. 2003 Jan;250(1):259–72.

41. Claeys B, Coen RD, De Geest BG, de la Rosa VR, Hoogenboom R, Carleer R, et al. Structural modifications of polymethacrylates: Impact on thermal behavior and release characteristics of glassy solid solutions. European Journal of Pharmaceutics and Biopharmaceutics. 2013 Nov;85(3):1206–14.

42. Gandhi A, Jana S, Sen KK. In-vitro release of acyclovir loaded Eudragit RLPO® nanoparticles for sustained drug delivery. International Journal of Biological Macromolecules. 2014 Jun;67:478–82.

43. Ramyadevi D, Rajan KS. Interaction and release kinetics study of hybrid polymer blend nanoparticles for pH independent controlled release of an anti-viral drug. Journal of the Taiwan Institute of Chemical Engineers. 2015 May;50:1–11.

44. Dai W, Guo Y, Zhang H, Wang X, Zhang Q. Sylysia 350/Eudragit S100 solid nanomatrix as a promising system for oral delivery of cyclosporine A. International Journal of Pharmaceutics. 2015 Jan;478(2):718–25.

45. Ali ME, Lamprecht A. Polyethylene glycol as an alternative polymer solvent for nanoparticle preparation. International Journal of Pharmaceutics. 2013 0 1;456(1):135–42.

46. Balaguer-Fernández C, Femenía-Font A, del Rio-Sancho S, Merino V, López-Castellano A. Sumatriptan Succinate Transdermal Delivery Systems for The Treatment of Migraine. Journal of Pharmaceutical Sciences. 2008 0 1;97(6):2102–9.

47. Basarkar A, Singh J. Poly (lactide-co-glycolide)-polymethacrylate nanoparticles for intramuscular delivery of plasmid encoding interleukin-10 to prevent autoimmune diabetes in mice. Pharm Res. 2009 Jan;26(1):72–81.

48. Caputo A, Brocca-Cofano E, Castaldello A, De Michele R, Altavilla G, Marchisio M, et al. Novel biocompatible anionic polymeric microspheres for the delivery of the HIV-1 Tat protein for vaccine application. Vaccine. 2004 0 29;22(21):2910–24.

49. Hari BNV, Narayanan N, Dhevendaran K, Ramyadevi D. Engineered nanoparticles of Efavirenz using methacrylate co-polymer (Eudragit-E100) and its biological effects in-vivo. Materials Science and Engineering: C. 2016 0 1;67:522–32.

50. Schlocker W, Gschließer S, Bernkop-Schnürch A. Evaluation of the potential of air jet milling of solid protein-poly(acrylate) complexes for microparticle preparation. European Journal of Pharmaceutics and Biopharmaceutics. 2006 0 1;62(3):260–6.

51. Thomas TT, Kohane DS, Wang A, Langer R. Microparticulate Formulations for the Controlled Release of Interleukin-2. Journal of Pharmaceutical Sciences. 2004 0 1;93(5):1100–9.

52. Sovány T, Papós K, Kása P, Ilič I, Srčič S, Pintye-Hódi K. Application of Physicochemical Properties and Process Parameters in the Development of a Neural Network Model for Prediction of Tablet Characteristics. AAPS PharmSciTech. 2013 Jun;14(2):511–6.

53. Sovány T, Kása P, Pintye-Hódi K. Modeling of subdivision of scored tablets with the application of artificial neural networks. Journal of Pharmaceutical Sciences. 2010 Feb;99(2):905–15.

54. Galata, Farkas, Könyves, Mészáros, Szabó, Csontos, et al. Fast, Spectroscopy-Based Prediction of In Vitro Dissolution Profile of Extended Release Tablets Using Artificial Neural Networks. Pharmaceutics. 2019 Aug 9;11(8):400.

55. Kása P, Bajdik J, Zsigmond Z, Pintye-Hódi K. Study of the compaction behaviour and compressibility of binary mixtures of some pharmaceutical excipients during direct compression. Chemical Engineering and Processing: Process Intensification. 2009 Apr;48(4):859–63.

56. Schliecker G, Schmidt C, Fuchs S, Ehinger A, Sandow J, Kissel T. In vitro and in vivo correlation of buserelin release from biodegradable implants using statistical moment analysis. Journal of Controlled Release. 2004 Jan;94(1):25–37.

57. Yi HG, Choi YJ, Kang KS, Hong JM, Pati RG, Park MN, et al. A 3D-printed local drug delivery patch for pancreatic cancer growth suppression. Journal of Controlled Release. 2016 Sep;238:231–41.

58. Chang HI, Williamson MR, Perrie Y, Coombes AGA. Precipitation casting of drug-loaded microporous PCL matrices: Incorporation of progesterone by co-dissolution. Journal of Controlled Release. 2005 Sep;106(3):263–72.

59. Hernandez C, Gawlik N, Goss M, Zhou H, Jeganathan S, Gilbert D, et al. Macroporous acrylamide phantoms improve prediction of in vivo performance of in situ forming implants. Journal of Controlled Release. 2016 Dec;243:225–31.

60. Park ES, Maniar M, Shah JC. Biodegradable polyanhydride devices of cefazolin sodium, bupivacaine, and taxol for local drug delivery: preparation, and kinetics and mechanism of in vitro release. Journal of Controlled Release. 1998 Mar;52(1–2):179–89.

61. Ramchandani M, Robinson D. In vitro and in vivo release of ciprofloxacin from PLGA 50:50 implants. Journal of Controlled Release. 1998 Jul;54(2):167–75.

62. Fuchs K, Bize PE, Denys A, Borchard G, Jordan O. Sunitinib-eluting beads for chemoembolization: Methods for in vitro evaluation of drug release. International Journal of Pharmaceutics. 2015 Mar;482(1–2):68–74.

63. Sovány T, Kása P, Pintye-Hódi K. Comparison of the Halving of Tablets Prepared with Eccentric and Rotary Tablet Presses. AAPS PharmSciTech. 2009 Jun;10(2):430–6.

64. Khlibsuwan R, Pongjanyakul T. Chitosan-clay matrix tablets for sustained-release drug delivery: Effect of chitosan molecular weight and lubricant. Journal of Drug Delivery Science and Technology. 2016 0 1;35:303–13.

65. Mir V, Heinamaki J, Antikainen O, Revoredo O, Colarte A, Nieto O, et al. Direct compression properties of chitin and chitosan. European Journal of Pharmaceutics and Biopharmaceutics. 2008 Aug;69(3):964–8.

66. Punčochová K, Heng JYY, Beránek J, Štěpánek F. Investigation of drug–polymer interaction in solid dispersions by vapour sorption methods. International Journal of Pharmaceutics. 2014 Jul;469(1):159–67.

67. Meng F, Trivino A, Prasad D, Chauhan H. Investigation and correlation of drug polymer miscibility and molecular interactions by various approaches for the preparation of amorphous solid dispersions. European Journal of Pharmaceutical Sciences. 2015 Apr;71:12–24.

68. Sun M, Wu C, Fu Q, Di D, Kuang X, Wang C, et al. Solvent-shift strategy to identify suitable polymers to inhibit humidity-induced solid-state crystallization of lacidipine amorphous solid dispersions. International Journal of Pharmaceutics. 2016 Apr;503(1–2):238–46.

69. Pudlas M, Kyerematen SO, Williams LAM, Kimber JA, van Lishaut H, Kazarian SG, et al. Analyzing the impact of different excipients on drug release behavior in hot-melt extrusion formulations using FTIR spectroscopic imaging. European Journal of Pharmaceutical Sciences. 2015 Jan;67:21–31.

70. Raviña-Eirin E, Azuaje J, Sotelo E, Gomez-Amoza JL, Martinez-Pacheco R. Drug structural features affect drug delivery from hyperbranched polyesteramide hot melt extrudates. European Journal of Pharmaceutics and Biopharmaceutics. 2016 May;102:1–8.

71. Hifumi H, Ewing AV, Kazarian SG. ATR-FTIR spectroscopic imaging to study the drying and dissolution of pharmaceutical polymer-based films. International Journal of Pharmaceutics. 2016 Dec;515(1–2):57–68.

72. Luciani-Giacobbe LC, Ramírez-Rigo MV, Garro-Linck Y, Monti GA, Manzo RH, Olivera ME. Very fast dissolving acid carboxymethylcellulose-rifampicin matrix: Development and solid-state characterization. European Journal of Pharmaceutical Sciences. 2017 Jan;96:398–410.

73. De Robertis S, Bonferoni MC, Elviri L, Sandri G, Caramella C, Bettini R. Advances in oral controlled drug delivery: the role of drug–polymer and interpolymer non-covalent interactions. Expert Opinion on Drug Delivery. 2015 Mar 4;12(3):441–53.

74. Van Nguyen H, Nguyen VH, Lee BJ. Dual release and molecular mechanism of bilayered aceclofenac tablet using polymer mixture. International Journal of Pharmaceutics. 2016 Dec;515(1–2):233–44.

75. Pavli M, Baumgartner S, Kos P, Kogej K. Doxazosin–carrageenan interactions: A novel approach for studying drug–polymer interactions and relation to controlled drug release. International Journal of Pharmaceutics. 2011 Dec;421(1):110–9.

76. Jangir DK, Charak S, Mehrotra R, Kundu S. FTIR and circular dichroism spectroscopic study of interaction of 5-fluorouracil with DNA. Journal of Photochemistry and Photobiology B: Biology. 2011 Nov;105(2):143–8.

77. Mihaylov MY, Ivanova EZ, Vayssilov GN, Hadjiivanov KI. Revisiting ceria-NOx interaction: FTIR studies. Catalysis Today. 2019 May;S0920586119302317.

78. Liu X, Ma X, Kun E, Guo X, Yu Z, Zhang F. Influence of lidocaine forms (salt vs. freebase) on properties of drug–eudragit® L100-55 extrudates prepared by reactive melt extrusion. International Journal of Pharmaceutics. 2018 Aug;547(1–2):291–302.

79. Obeidat WM, Nokhodchi A, Alkhatib H. Evaluation of Matrix Tablets Based on Eudragit®E100/Carbopol®971P Combinations for Controlled Release and Improved Compaction Properties of Water Soluble Model Drug Paracetamol. AAPS PharmSciTech. 2015 Oct;16(5):1169–79.

80. Sovány T, Csüllög A, Benkő E, Regdon G, Pintye-Hódi K. Comparison of the properties of implantable matrices prepared from degradable and non-degradable polymers for bisphosphonate delivery. International Journal of Pharmaceutics. 2017 Nov;533(2):364–72.

81. Ritger PL, Peppas NA. A simple equation for description of solute release I. Fickian and non-fickian release from non-swellable devices in the form of slabs, spheres, cylinders or discs. Journal of Controlled Release. 1987 Jun;5(1):23–36.

82. Moustafine RI, Zaharov IM, Kemenova VA. Physicochemical characterization and drug release properties of Eudragit® E PO/Eudragit® L 100-55 interpolyelectrolyte complexes. European Journal of Pharmaceutics and Biopharmaceutics. 2006 May;63(1):26–36.

83. Priemel PA, Laitinen R, Grohganz H, Rades T, Strachan CJ. In situ amorphisation of indomethacin with Eudragit® E during dissolution. European Journal of Pharmaceutics and Biopharmaceutics. 2013 Nov;85(3):1259–65.

84. Moustafine RI, Sitenkov AY, Bukhovets AV, Nasibullin SF, Appeltans B, Kabanova TV, et al. Indomethacin-containing interpolyelectrolyte complexes based on Eudragit ® E PO/S 100 copolymers as a novel drug delivery system. International Journal of Pharmaceutics. 2017 May;524(1–2):121–33.

ACKNOWLEDGEMENTS

I would like to express my sincere gratitude and thanks to my supervisors **Dr. Tamás Sovány** and **Prof. Dr. Ildikó Csóka** for their guidance, encouragement and continuous support throughout the present work and my career as a Ph.D. student.

This endeavour would not have been possible without the support of **Dr. Géza Regdon jr**., leader of our research group, **Prof. Dr. Piroska Szabó-Révész** as the former and **Prof. Dr. Ildikó Csóka** as the current Head of the Institute of Pharmaceutical Technology and Regulatory Affairs.

I would like to express my very great appreciation to **Prof. Dr. Klára Pintye-Hódi** for the valuable advice in my research work.

I'm extremely grateful to **Prof. Dr. Stane Srčič**, **Dr. Ilija German Ilič**, and **Blaž Grilc** from University of Ljubljana, Faculty of Pharmacy, Chair of Pharmaceutical Technology, for their continuous help and support, and their group colleagues who helped me a lot feel myself like home in Slovenia.
And for the CEEPUS MOBILITY: CIII-RS-1113-01-1718-M-113871 grand for being able to work in Slovenia.

I express my kindest gratitude to **Dr. Kriszinta Ludasi**, and **Dr. Katalin Kristó** for their support, and kind presence.

Many thanks to the **colleagues** of the **research group**, the **institute** and the **faculty** for their support and encouragement during my work and studies.

And finally, I could not have undertaken this journey without the complete support of **my family, relatives** and **friends**, Thank you!

Project no. TKP2021-EGA-32 also has been implemented with the support provided by the Ministry of Innovation and Technology of Hungary from the National Research, Development, and Innovation Fund, financed under the TKP2021-EGA funding scheme.

ANNEXES

Annex 1.

T. Sovány, A. Csüllög, **E. Benkő**, G. Regdon, and K. Pintye-Hódi, 'Comparison of the properties of implantable matrices prepared from degradable and non-degradable polymers for bisphosphonate delivery', *International Journal of Pharmaceutics*, vol. 533, no. 2, pp. 364-372, Nov. 2017, doi: 10.1016/j.ijpharm.2017.07.023.

Annex 2.

E. Benkő et al., 'Predicting Drug Release Rate of Implantable Matrices and Better Understanding of the Underlying Mechanisms through Experimental Design and Artificial Neural Network-Based Modelling', *Pharmaceutics*, vol. 14, no. 2, pp. 228, Jan. 2022, doi: 10.3390/pharmaceutics14020228.

Annex 3.

Supplementary material for **Annex 2**

Annex 4.

Supplementary material

ANNEX 1

International Journal of Pharmaceutics 533 (2017) 364–372

Contents lists available at ScienceDirect

International Journal of Pharmaceutics

journal homepage: www.elsevier.com/locate/ijpharm

Comparison of the properties of implantable matrices prepared from degradable and non-degradable polymers for bisphosphonate delivery

Tamás Sovány*, Anna Csüllög, Ernő Benkő, Géza Regdon Jr., Klára Pintye-Hódi

Institute of Pharmaceutical Technology and Regulatory Affairs, University of Szeged, H-6720, Eötvös u. 6, Szeged, Hungary

ARTICLE INFO

Article history:
Received 4 January 2017
Received in revised form 6 June 2017
Accepted 8 July 2017
Available online 13 July 2017

Keywords:
Implantable matrix
PVC
Chitosan
Near-infrared spectroscopy
Design of experiments

ABSTRACT

The aim of the present study was the development of directly compressed tablets for implantable delivery of risedronate sodium for osteoporosis treatment and the comparison of the mechanism and kinetics of drug release from biogradable (chitosan) and non-degradable (PVC) polymer matrices.

The compositions and process parameters were optimized in accordance to a mixed 2 and 3 level full factorial design. Critical Quality Attributes (CQA), such as diametral breaking hardness, porosity and speed of drug dissolution were investigated.

The results revealed significant differences between the behaviours of the two polymers. Chitosan exhibited poor compressibility, which resulted in poor mechanical properties and the fast disintegration of chitosan based tablets. Nevertheless, despite the fast disintegration, the chitosan based matrices exhibited one-week-long continuous drug release, which can be due to a strong drug-carrier interaction. The presence of intermolecular hydrogen bonds was confirmed with FT-IR and NIR measurements.

In contrast, PVC based compositions exhibited excellent compressibility, good tablet hardness and low porosity. The tablets remained intact during the dissolution and exhibited a slower release rate than what was measured in the case of chitosan based matrices. There was no sign of intermolecular association on NIR spectra, suggesting that the dissolution rate is basically determined by the porosity of tablets, but FT-IR measurements revealed some details of the molecular background of drug release mechanism.

1. Introduction

Bisphosphonates are widely used drugs for osteoporosis treatment, but have poor (approx. 0.4–0.7% of iv.) oral bioavailability and severe side effects, such as irritation and necrosis of the gastrointestinal mucosa (Cadarette et al., 2009). Some experimental results suggest the effect of bisphosphonates on gastric mucosa is based on the modification of the hydrophobicity of the phospholipid bilayer surfaces. The strength of this effect was different amongst the investigated bisphosphonates and risedronate exhibited the lowest effect (Lichtenberger et al., 2000). This result was in accordance with the findings of Thomson et al. (2002), who confirmed that risedronate exhibits considerably higher safety over alendronate from the aspect of mucosal irritation applied in the regularly used 5 or 10 mg doses in daily oral administration. Based on these results, the use of risedronate may be generally considered as safe also in alternative routes.

Numerous investigations confirm that the long term local delivery of bisphosphonates has a great advantage in bone regeneration after injuries (Hur et al., 2016) or implantation of hip or femoral neck prosthesis (Peter et al., 2005; Mazurkiewicz et al., 2013). In these studies, the drug was mixed into the bone cement (Mazurkiewicz et al., 2013), the hydroxyapatite coating of the titanium implant (Peter et al., 2005) or into the modified chitosan coating of a commercial bone platelet (Hur et al., 2016), which ensured the targeted local delivery of the drug to the injured bone parts. Under these conditions a 4 μg daily dose may be enough to ensure successful bone remodelling under a 2-month treatment period, without any sign of adverse reactions or cytotoxic effect. The lack of cytotoxicity in the case of extended release local delivery suggests that the adverse reactions related to the irritative effect of bisphonates are dose dependent and the use of controlled release implants may help to overcome the limitations and risks of oral, intravenous or intramuscular injection use, offering a good way for the systemic delivery of these drugs in osteoporosis, where localized therapy cannot be used due to the generalized nature of the disease (Perugini et al., 2001).

There are numerous methods for implantable delivery of drugs using passive (degradable or non-degradable reservoir or

* Corresponding author.
E-mail addresses: t.sovany@pharm.u-szeged.hu, sovanytamas@gmail.com (T. Sovány).

http://dx.doi.org/10.1016/j.ijpharm.2017.07.023
0378-5173/

monolithic matrix systems, micro- or nanospheres) or active (osmotic or programmable pump systems) release and delivery of drugs (Anselmo and Mitragotri, 2014; Kleiner et al., 2014). Although the use of pump systems may ensure a better control on drug release, the production of reservoir or monolithic systems is easier and cheaper, therefore they are currently of greater interest from the industrial aspect. Although the use of degradable (chitosan, polylactide (PLA), poly(lactide-*co*-glycolide) (PLGA) or polythiourethane) polymers is considerably more advantageous as compared to non-degradable (polyvinylchloride (PVC), poly(dimethyl siloxan), polyurethanes (PU), polyethylene (PE), poly (ethylene-co-vinyl-acetate) (PEVA), poly(methyl methacrylate (PMMA)) ones because the removal of the device after the complete release of the drug is not necessary, it is a major drawback that the release rate is concurrently determined by diffusion, erosion and the degradation rate of the polymers. In comparison, the release from non-degradable matrices is completely diffusion determined (Avgoustakis and Nixon, 1991; Krier et al., 2014; Campiñez et al., 2015).

The aim of present study was therefore the comparison of the potential of biodegradable (chitosan) and non-degradable (PVC) polymers as directly compressed, polymer based monolithic matrices for the implantable delivery of risedronate sodium based on the evaluation of mechanical properties and mechanism and rate of the drug release.

PVC is a widely used polymer for fabrication of medical and drug delivery devices, and was maybe first polymer used for compression of non-degradable, "inert" polymer matrices, despite of the various compressibility depending of the grade used (Rime et al., 1997). Due to its chemical inertness, the drug release is determined by the physical parameters (e.g. pore size and volume distribution) of the matrix, and is not affected by drug-polymer interactions. In contrast, the free amino side chains of chitosan are highly capable to form various physico-chemical interactions (e.g hydrogen bonds or polyelectrolyte complexes) with drugs or polymers, which may significantly influence the drug release rate from chitosan matrices (am Ende and Peppas, 1997; Puttipipatkhachorn et al., 2001; Szakonyi and Zelkó, 2016). The formation of polyelectrolyte complexes is common in chitosan nanoparticles or films, where the free amino groups of the chitosan are undergoing protonation during the dissolution in diluted acids (Phaechamud et al., 2000; Khunawattanakul et al., 2011), but not evident in the case of matrix tablets, where the chitosan is in mostly deprotonated form during preparation (AlKhatib et al., 2008; Sogias et al., 2012). Under these circumstances the formation of polyelectrolyte complexes may be expected only in the GI tract, if the deprotonation of the jellified chitosan in the small intestine is slower as the dissociation of the drug (Li et al., 2013, 2014, 2015; Shao et al., 2015). Therefore, in present study where the dissolution medium is slightly alkaline, the formation of drug-polymer interactions is unexpected (Rege et al., 2003).

2. Materials and methods

2.1. Materials

Risedronate sodium was kindly gifted by TEVA Pharmaceuticals Plc. (Debrecen, Hungary). This drugexhibits excellent (10,4 mg/ml) aqueous solubility its strongest acidic pKa is −0.68. These properties are resulted in an extremely low permeability (logP = −0.75), which may explain its poor oral bioavailability. The non-degradable Halvic PVC powder (MW: 60–150 kDa) and the lubricant calcium stearate were supplied by Gedeon Richter Plc. (Budapest, Hungary). Biodegradable, 1000 cP average viscosity and 80% deacetyled chitosan (MW: 400–600 kDa) was purchased from Heppe Medical Chitosan GmbH (Halle an der Saale, Germany).

The chemical structures of the compounds may be seen in Fig. 1.

2.2. Methods

2.2.1. Preformulation studies

The flow properties (flow time, angle of repose, bulk density) of the powders were studied with a Pharmatest PTG-1 (Pharmatest GmbH, Germany) powder rheological tester.

The plasticity of materials and mixtures was determined with a computer-connected Korsch EK0 eccentric tablet press (E. Korsch Machienenfabrik, Berlin, Germany), instrumented with strain gauges on both punches and a displacement transducer (Micropulse, BTL5-A11-M0050-P-532, Balluff, Germany) on the upper punch. The strain gauges were calibrated with a Wazau HM-HN-30kN-D cell (Kaliber Ltd., Budapest, Hungary). The transducer distance accuracy was checked by using five measuring pieces of accurately known thickness (1.0, 2.0, 5.0, 7.5 and 10.0 mm) under zero load (Mitutoyo, Tokyo, Japan). The materials were filled into the die and compressed manually (to ensure similar conditions for the well- and poorly-compressible materials) in the compression

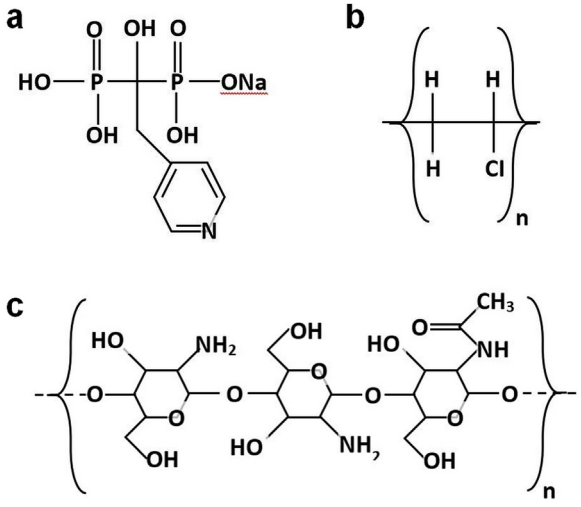

Fig. 1. Chemical structures of risedronate sodium (a), PVC (b) and chitosan (c).

force range from 1–30 kN, using 10 mm in-diameters flat-faced punches, with beveled edge. The plasticity was calculated from the results of force displacement measurements with the Stamm-Mathis equation (Eq. (1)):

$$Pl = E2/(E2 + E3)^{*}100 \quad (1)$$

where E2 and E3 are the given areas of the force-displacement curve (Kása et al., 2009).

A DataPhysics OCA 20 (DataPhysics Instruments GmbH, Fielderstadt, Germany) optical contact angle tester was used for the determination of the surface free energies and wettability of the materials using sessile drop method. This method is based on the measurement of the equilibrium contact angle, which is determined by the surface energy of the solid, and the surface tension of the liquid and vapor phases, as described by the Young equation (Eq. (2)):

$$\gamma_{SV} - \gamma_{SL} - \gamma \cos\theta = 0 \quad (2)$$

where θ is the equilibrium contact angle, γ is the surface tension between the given phases, S is solid, L is liquid and V is vapor. The disperse and polar components of the solid surface energy γ_{SV} were calculated with the Wu equations (Eqs. (3) and (4)) with the consideration of the surface tensions of polar and nonpolar test liquids (water and diiodomethane). The liquids were dropped onto the surface of solid comprimates 10 mm in diameter, prepared with a Specac hydraulic press (Specac Inc, Orpington, UK) at a pressure of 4 tons.

$$(1 + \cos\theta)\gamma_1 = ((\gamma_1^{d}\gamma_s^{d})/(\gamma_1^{d} + \gamma_s^{d}) + (\gamma_1^{p}\gamma_s^{p})/(\gamma_1^{p} + \gamma_s^{p})) \quad (3)$$

$$(1 + \cos\theta)\gamma_2 = ((\gamma_2^{d}\gamma_s^{d})/(\gamma_2^{d} + \gamma_s^{d}) + (\gamma_2^{p}\gamma_s^{p})/(\gamma_2^{p} + \gamma_s^{p})) \quad (4)$$

where γ^d is the disperse and γ^p is the polar component of the liquid surface tension, γ_1 is the surface tension of the first, and γ_2 is the surface tension of the second test liquid, and γ_s is the surface free energy of the solid material.

2.2.2. Tablet preparation

The composition of the matrix tablets are displayed in Table 1. The drug and the polymer were homogenized with a Turbula mixer (Willy A. Bachofen Maschienenfabrik, Switzerland) for 8 min +2 min after the addition of the lubricant. The homogenous powder mixture was compressed with the Specac hydraulic tablet press (Specac Inc, Orpington, UK), applying 13 mm in diameter flat punches, manual filling and compression. The mass of the tablets was 0.35 g.

2.2.3. Tablet testing

The mass, geometry and hardness of the tablets were determined with a Kraemer UTS tablet tester (Kraemer Elektronik GmbH, Germany).

The porosity of the samples was calculated according to the following equation (Eq. (5)):

$$\varepsilon = 1 - (\rho_{app}/\rho_{true}) \quad (5)$$

Table 1
Tablet compositions.

Materials	Biodegradable		Non-biodegradable	
	CA-1 (%)	CA-2 (%)	CA-3 (%)	CA-4 (%)
Risedronate sodium	10	40	10	40
PVC	–	–	89	59
Chitosan	89	59	–	–
Ca-stearate	1	1	1	1

where, ρ_{app} is the apparent density (calculated from the mass and geometry data) and ρ_{true} is the true density of the tablets.

The true density of the tablets was determined with the use of a Quantachrome helium Multipycnometer (Quantachrome, USA).

There are several methods described in the literature for the testing of dissolution from implantable devices. According to the most commonly used methods, the implants are soaked into the dissolution medium in a watertight container without any agitation (Schliecker et al., 2004; Yi et al., 2016) or applying shaking water bath for continuous mixing of the dissolution liquid (Ramchandani and Robinson, 1998; Park et al., 1998; Chang et al., 2005; Cheng et al., 2010; Hernandez et al., 2016). Nevertheless, Fuchs et al. (2015) have performed a comparative study on various testing methods, and have described that despite the results obtained with shaking bath are good for comparison of different samples, give not so good correlation with in-vivo data as flow–through cell dissolution, due to the different shear rates. In the lack of flow-through tester, a special apparatus was developed for the testing of the dissolution rate of risedronate sodium from the implantable matrix tablets, mimicking the shear rates obtained with flow-through cells. The tablets were placed into Erlenmeyer flasks containing 50 ml of pH 7.4 phosphate buffered saline solution ensuring sink condition for the drug during the whole dissolution study. The continuous closed-loop flow of the dissolution medium was ensured with an Alitea-XV (Alitea, Sweden) peristaltic pump using 2 ml/min flow rate. The dissolution medium was periodically renewed to maintain the concentration gradient, considering a time-dependent manner. Therefore, 5 ml, 5 ml, 10 ml and 20 ml samples were taken and replaced with fresh medium after 1, 2, 4 and 8 h respectively. After 24, 48, 72 and 186 h the full amount of the dissolution medium was renewed.

The dissolution process was evaluated according to the Korsmeyer Peppas equation (Eq. (6)).

$$M_t/M_0 = kt^n \quad (6)$$

where M_0 is the initial drug amount in the matrix, M_t is the drug amount at the given time, k is the dissolution rate constant and n is the shape parameter regarding the diffusion mechanism.

The matrix-drug interactions were studied with the use of a ThermoNicolet Avatar 330 FT-IR with ZnSe HATR accessory and a ThermoScientific Antaris II FT-NIR spectrometer (ThermoFisher Scientific, USA). In both cases, the resolution was set to 4 cm^{-1}, the scan number was 128 and H_2O and CO_2 corrections were applied.

The spectra were evaluated with the use of Spekwin32 optical spectroscopy software v1.72.2 (Dr. F. Menges, Berchtesgaden, Germany).

2.2.4. Statistical analysis

The experiments were performed according to a mixed 2 and 3 level full factorial design, where the effect of the polymer (biodegradable/non-biodegradable) as a 2 level, qualitative, the amount of the API (10% or 40%) as 2 level, quantitative and the applied compression force (1, 3 or 5 tons equal with 58, 174 or 290 MPa compression pressure, respectively) as a 3 level quantitative factor was studied. The critical quality attributes of tablets, e.g. hardness, porosity, drug dissolution rate and the amount of the dissolved drug after one week were used as optimization parameters.

The results of the design experiments were evaluated with the help of Statistica for Windows v12 software package (Statsoft Inc., Tulsa, OK, USA).

The general equation of the response surface was the following (Eq. (7)):

$$y = b_0 + b_1x_1 + b_2x_2 + b_3x_3 + b_{33}x_3^2 + b_{12}x_1x_2 + b_{13}x_1x_3 + b_{133}x_1x_3^2 + b_{23}x_2x_3 + b_{233}x_2x_3^2 \quad (7)$$

Table 2
Results of the preformulation tests.

	PVC	Chitosan	Risedronate sodium
Flow time (s)	71.5 (±0.76)	344.7 (±13.75)	n.m.
Angle of repose (°)	25.1 (±1.10)	48.7 (±1.76)	n.m.
Bulk density (g/ml)	0.541 (±0.0166)	0.072 (±0.003)	n.m.
γ (J/m^2)	54.75 (±0.53)	52.16 (±0.71)	76.26 (±0.48)
γ^d (J/m^2)	39.14 (±0.27)	40.49 (±1.15)	41.46 (±0.26)
γ^p (J/m^2)	15.61 (±0.45)	11.12 (±0.70)	34.80 (±0.41)
Polarity (%)	28.51	21.32	45.63
Plasticity (%)	97.76	81.28	84.81
Decrease of elasticity (%/kN)	1.1344	0.6671	0.1765

where b_0 is the average of the results of the given parameter and the other b coefficients show the change in the value of the optimization parameter if the value of the given factor increased from the 0 to the +1 level. The unnecessary determinants were deleted from the full equation during the evaluation to avoid overdetermination and improve the model fitting. The optimal number of determinants was selected on the basis of the maximization of the adjusted goodness of fit (adjR^2) and the minimization of the mean square of residuals (MS residual).

3. Results and discussion

The results of the powder rheological test revealed that in accordance with the expectations, the micronized risedronate sodium exhibited no measurable flow properties, which may be due to its high surface area and moderately high surface free energy (Table 2). The rheological properties of chitosan platelets confirmed the poor flow properties and extremely low bulk density despite their considerably big size, low surface free energy and low polarity, which was expected based on literature data and may cause problems during tablet preparation (Rege et al., 1999; Mir et al., 2008; Khlibsuwan and Pongjanyakul, 2016). The PVC has similar surface properties and smaller but more regular particles than chitosan, which resulted in moderate flow properties, bulk density and, in accordance with the value of the angle of repose, excellent arrangement profile.

The result of the deformability tests also reveals considerable differences amongst the 3 materials. The ratio of the plastic/elastic properties (plasticity) of the materials is in negative correlation with the applied compression force. In Table 2 the theoretical maximum (extrapolated to 0 force) of the plasticity and the size of the decrease when the compression force is increased with one kN are displayed.

It can be seen that PVC basically deforms plastically but this value highly depends on the compression force. Chitosan and risedronate sodium exhibits higher elasticity but their behavior is less dependent on compression force.

The differences in the rheological and mechanical properties of the raw materials are clearly visible when comparing the mechanical properties of the different samples.

The response surface of the best fitting model regarding diametric tablet hardness can be described with the following equation (Eq. (8)):

$$y = 70.71 + 42.37x_1 + 14.76x_3 + 5.57x_3^2 - 12.72x_1x_2 + 2.56x_1x_3 + 3.52 \times {}_2x_3 \quad (8)$$

where the significant factors are highlighted in boldface. The value of the MS residual was 38.93, R^2 was 0.9935 and the adjR^2 value was 0.9867, indicating the excellent fit of the applied model.

It can be seen that the hardness of the tablets mostly depends on the properties of the matrix former polymers, and the amount of the API plays a negligible role in this aspect. However, the strong interaction of the type of the polymer indicates that the two polymers behave differently (Fig. 2). The mixing of plastic PVC with the elastic API considerably decreases the hardness of tablets, especially at small compression forces. At high compression forces

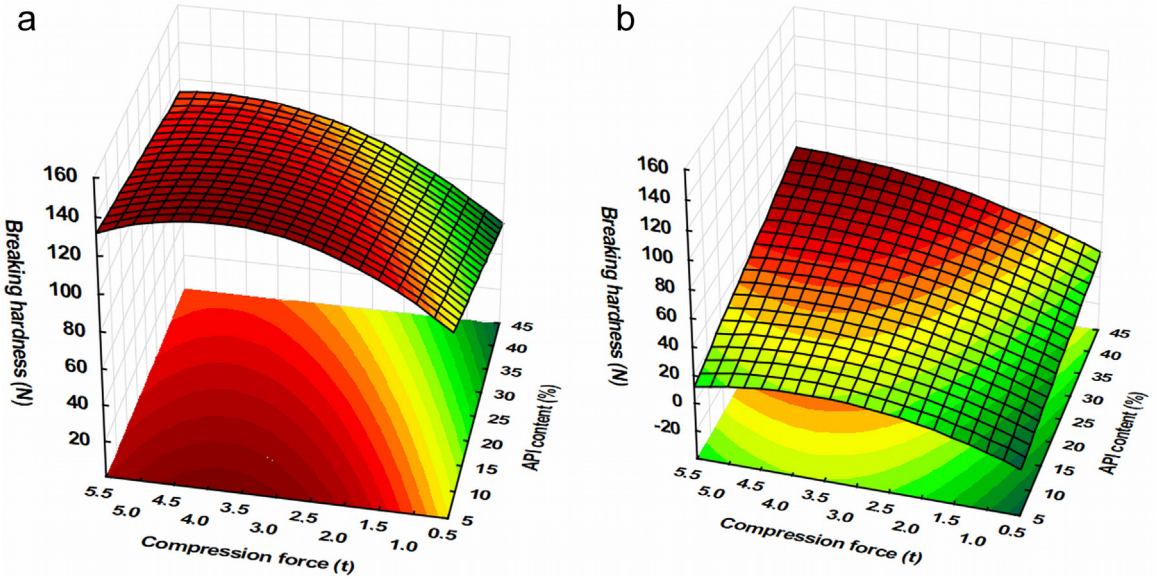

Fig. 2. Breaking hardness of PVC (a) and chitosan (b) tablets.

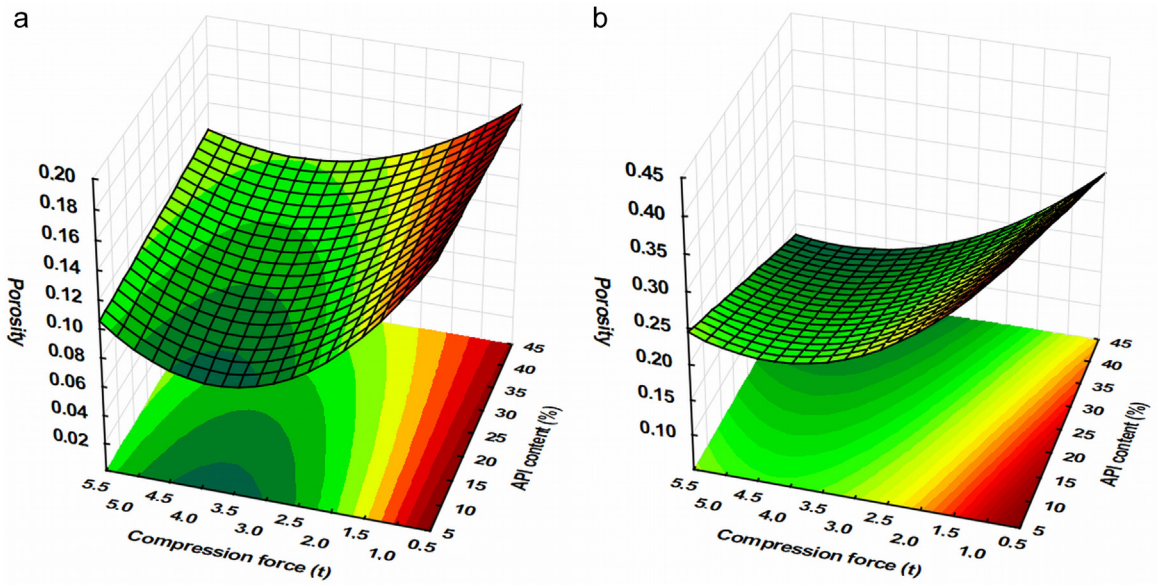

Fig. 3. Porosity of PVC (a) and chitosan (b) tablets.

the difference is negligible due the compression force dependence of the behavior of PVC. In contrast, the increasing amount of API improves the hardness of chitosan based tablets both at low and high compression forces due to its higher surface free energy, and less compression force dependency of its plastic-elastic behavior.

The high elastic recovery of compositions resulted in increasing porosity (Fig. 3) and accelerated drug release rate (Fig. 4) at high compression forces.

The change in the porosity of the systems can be described with Eq. (9).

$$y = 0.175 - 0.057x_1 - 0.016x_2 - 0.047x_3 - 0.019x_3^2 + 0.023x_1x_2 + 0.021x_1x_3 \quad (9)$$

The MS residual value of the model is 0.0002, $R^2 = 0.9856$ and $adjR^2 = 0.9682$. As expected, the porosity of the tablets exhibits a negative exponential correlation with tablet hardness.

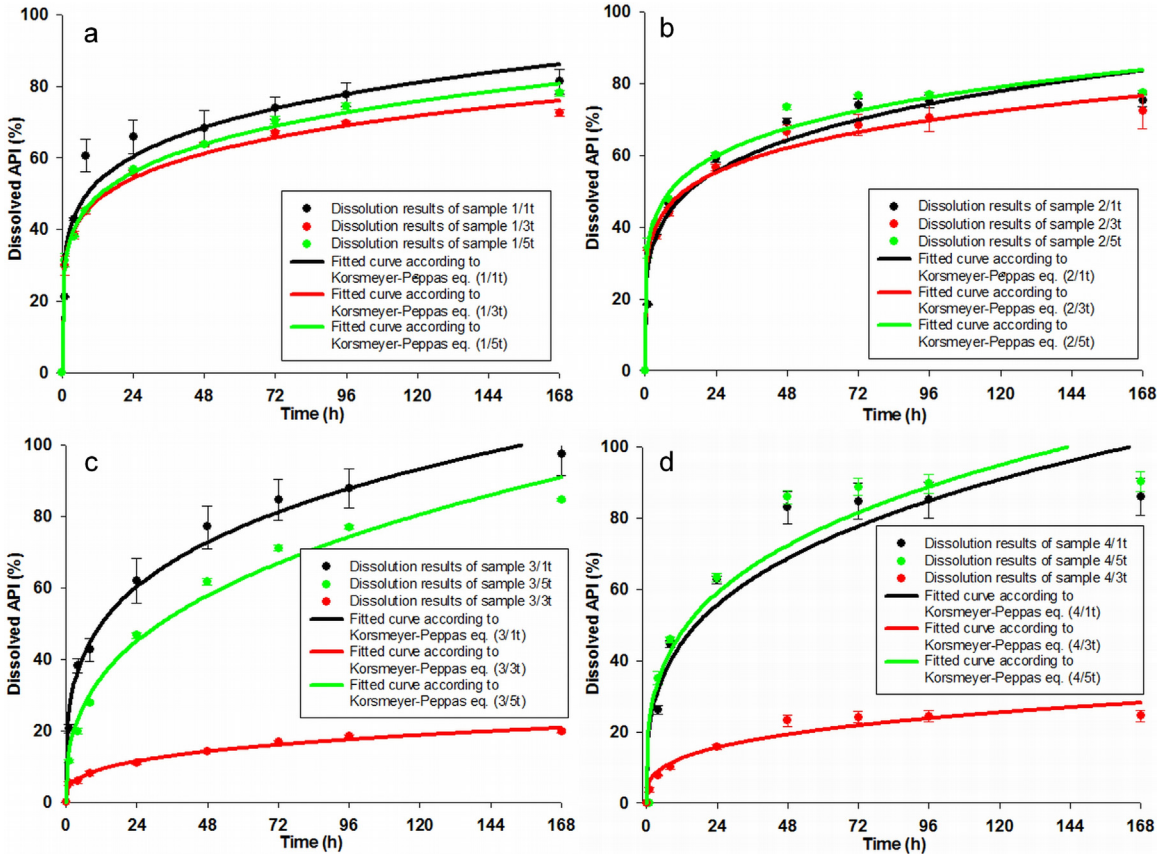

Fig. 4. Drug dissolution curves of the CA-1 (a), CA-2 (b), CA-3 (c) and CA-4 (d) samples.

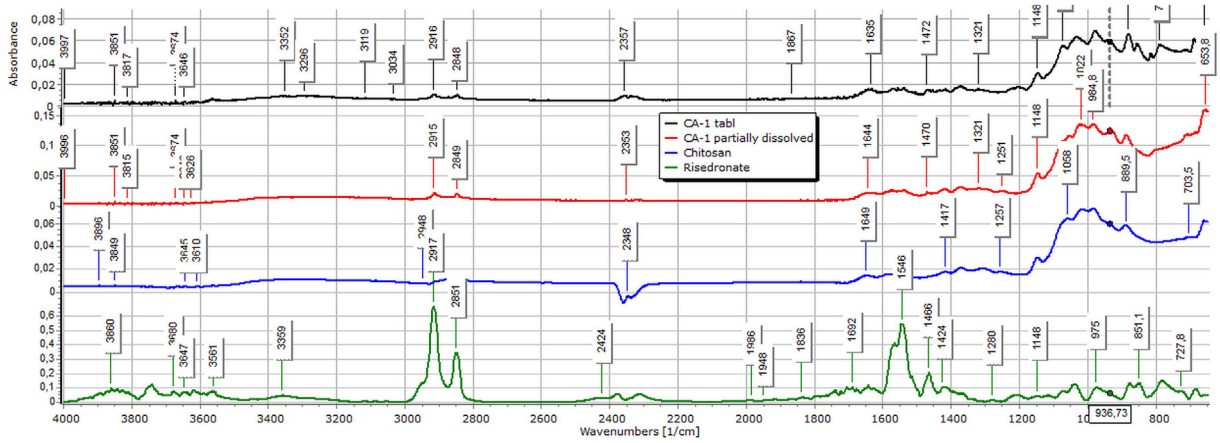

Fig. 5. FT-IR spectra of CA-1 sample CA-1 dry tablet (black), CA-1 tablet after 8 h dissolution and drying (red), chitosan (blue) and risedronate sodium (green). (For interpretation of the references to colour in this figure legend, the reader is referred to the web version of this article.)

Nevertheless, in contrast with hardness, the API content has a significant effect on porosity, especially in the case of chitosan based tablets. However, the decreasing porosity does not result in a significant change of the drug release rate for chitosan matrices (Fig. 3).

This negligible change may be due to the complete disintegration of chitosan matrices in the first 24 h, inducing a burst release of the drug in the initial stage of dissolution. However, the fast disintegration did not result in the completion of the dissolution process. Slow release of drug was detected even after the complete renewal of the dissolution medium, which indicates that the API is entrapped in the chitosan flakes due to a strong interaction.

Utilization of micro-environmental drug-polymer interactions is widely used method for solubility improvement and stabilization of spray-dried (Puncochová et al., 2014; Medarević et al., 2015; Ngo et al., 2016), vacuum-dried (Meng et al., 2015; Sun et al., 2016), or hot-melt extruded (Pudlas et al., 2015; Raviña-Eirin et al., 2016) solid dispersions or solutions and for modification of drug release (Dürig and Fassihi, 2002; Chambin et al., 2004; Ravishankar et al., 2006; Glaessl et al., 2010; Hifumi et al., 2016; Luciani-Giacobbe et al., 2017). Nevertheless, most of the referred drug delivery systems are prepared with the solidification of dissolved or melted materials, where the molecularly dispersed state promotes the formation of interactions during the solidification process. The formation of micro-environmental interactions in directly compressed systems is unlikely, due to the limited contact surface and molecular mobility, but there is a limited number of data on the in-situ emergence of such interactions during drug dissolution from directly compressed matrices (De Robertis et al., 2015). Nguyen et al. (2016) described the formation of hydrogen bonds in a hydroxypropyl-cellulose-carbomer matrix, which helped to achieve the required release profile. In another study, Pavli et al. (2011) have identified the in-situ emergence of an electrochemical interaction which considerably influenced the release of cationic doxasozin from the anionic polyelectrolyte carrageenan matrix. Nevertheless, in present case the formation of polyelectrolyte complexes is unexpected under the applied preparation and dissolution conditions, since the chitosan matrix is in deprotonated form (see. Introduction section).

For the confirmation of the nature of interaction FT-IR and NIR investigations were performed, in order to clarify the reason for the release after full disintegration, the influence of the wet media was also tested. A tablet was placed into the dissolution medium until the end of the disintegration process. The remaining flakes were then filtered and dried in drying chamber at 60 °C for 24 h and then stored in an exsiccator.

The results of FT-IR measurements (Fig. 5) revealed that presence of drug-polymer interaction may be identified already in the directly compressed samples. The O = P-OH stretching usually gives broad peaks with multiple maxima in the 1600–2400 cm^{-1} region, however in our case these peaks are presented between 1450 and 2000 cm^{-1} due to distortion caused by the ZnSe HATR crystal, which is resulted in an overlapping with the βOH vibrations of the chitosan molecule. Nevertheless, it is well visible that the most characteristic peak of this region at 1549 cm^{-1} is separated to a peak doublet at 1540 and 1558 cm^{-1}, and the peak at 1567 cm^{-1} exhibits a partial left shift to 1575 cm^{-1}, indicating different strength association between the drug and polymer. Concurrently the peak of chitosan at 1302 cm^{-1} belonging to the νC—N stretching exhibits a left shift to 1321 cm^{-1}, which indicates that the amino groups of the polymer also takes part in this interaction. The differences between the spectra of samples before and after dissolution suggests that the associations are being stronger during the dissolution process. The disappearance of the peak 851 cm^{-1} which is associated with the γOH vibrations indicates, the breaking of the dimerized form of the drug. And the shift of the P-OH peak from 975 to 937 cm^{-1} suggest the formation of new intermolecular associations instead of intramolecular ones. This is also supported by the disappearance of the νP=O vibrations at 1206 cm^{-1}, and the broadening and right shift of the maxima (from 3300 to 3175 cm^{-1}) of the overlapping O—H and N—H stretching peaks. Nevertheless, there was no sign of the presence of POO^- anions, due to the dissociation of the phosphonate groups, nor the appearance of the wide disseminated peaks with multiple maxima in the range of 3100–2600 and 2220–1820 cm^{-1} indicating the protonation of the amino groups of the chitosan. Overall, it may be stated that the present strong drug-polymer interaction is based on hydrogen bonds and not on the formation of a polyelectrolyte complex.

The presence of hydrogen bond based interaction was confirmed also with NIR spectroscopic investigations. The NIR spectra of the CA-1 composition are displayed on Fig. 6. It is well visible that although there are some changes on the spectrum of the dry compressed materials, like the merging of the peaks of chitosan at 4235 and 4289 cm^{-1}, it indicates the formation of intramolecular hydrogen bonds only. It can be seen well in the spectrum of this sample that the intramolecular hydrogen bond ceased since the characteristic peaks of chitosan at 4235 and 4289 cm^{-1} can be

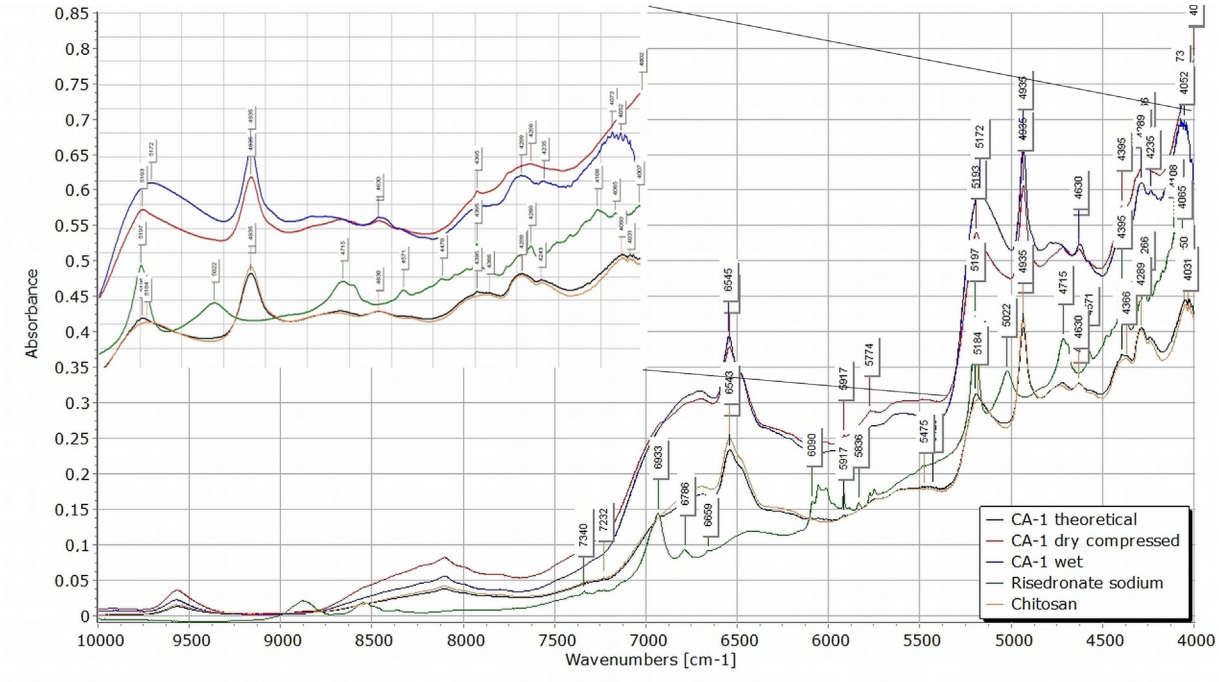

Fig. 6. NIR spectra of the CA-1 sample (calculated theoretical spectrum based on weight ratios (black), dry compressed tablet (red), tablet after 8 h dissolution and drying (blue), risedronate sodium (green) and chitosan (yellow)). (For interpretation of the references to colour in this figure legend, the reader is referred to the web version of this article.)

identified separately. Nevertheless, new intermolecular associations between chitosan and the API are indicated by the broadening and left shift of the peak of risedronate sodium at 4715 cm^{-1} and the right shift and merging of the peaks of 5195 and 5184 cm^{-1} with the peak at 5022 cm^{-1}. Some smaller characteristic peaks of risedronate sodium have disappeared from the spectrum, but it is not clear whether it is caused by the interaction or may be due to the decreased amount of the drug due to dissolution during the sample treatment.

The spectroscopic investigation was also performed in the case of PVC containing samples, and despite of the expectations, major changes were identified in the FT-IR spectrum (Fig. 7) of the partially dissolved sample. The characteristic signal at 1546 cm^{-1} belonging to the O=P-OH stretching of risedronate sodium is separated into a peak doublet. The appearance of the new peak at 1514 cm^{-1} indicates the appearance of the unbonded form of the API, while the right shifted (1539 cm^{-1}) part of the original peak suggest the weakening of the original intramolecular hydrogen bonds. However, these changes in the spectrum may be a general consequence of the dissolution process, it is notable, that a left shift of a characteristic PVC peak from 836 cm^{-1} to 857 cm^{-1} indicating a change in the C—C stretching of the polymer chain, and the appearance of new peaks at 1367 and 1396 cm^{-1} indicating changes in the CH vibrations, suggests the presence of a weak interaction between the drug and the polymer, due the increased reactivity of the hydrogen in the HC—Cl groups.

Nevertheless, the weakness of this bond is indicated well by the NIR studies, where PVC based formulations showed no sign of characteristic changes (Fig. 8). There is no sign of peak shifts or other differences indicating specific interactions either in the dry

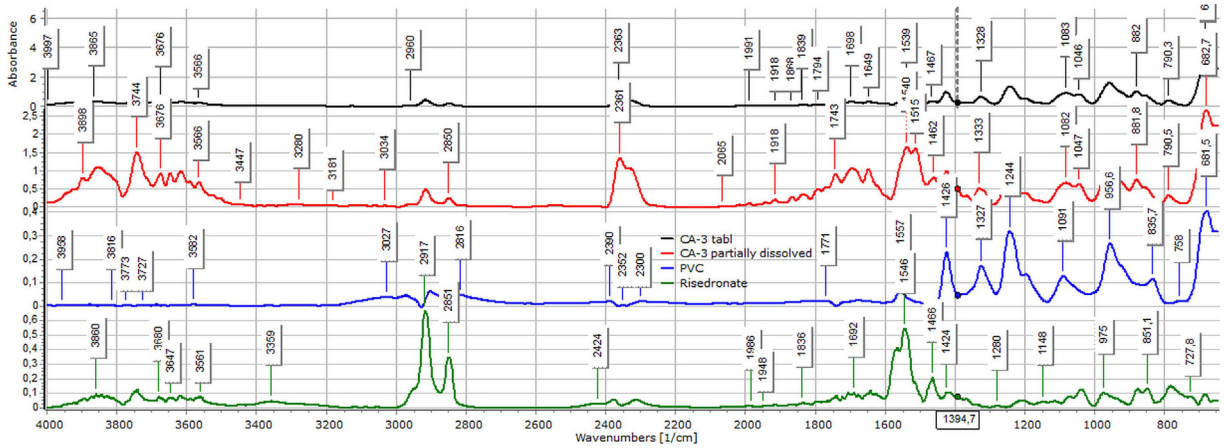

Fig. 7. FT-IR spectra of CA-1 sample CA-3 dry tablet (black), CA-3 tablet after 8 h dissolution and drying (red), PVC (blue) and risedronate sodium (green). (For interpretation of the references to colour in this figure legend, the reader is referred to the web version of this article.)

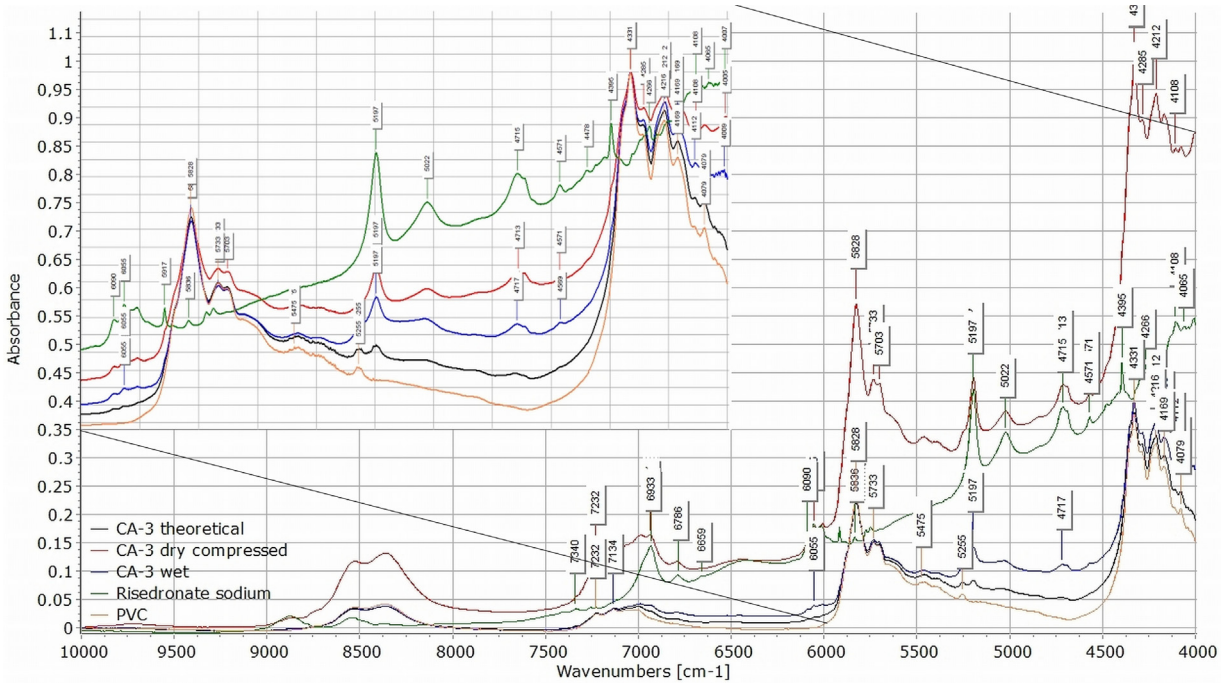

Fig. 8. NIR spectra of the CA-3 sample (calculated theoretical spectrum based on weight ratios (black), dry compressed tablet (red), tablet after 8 h dissolution and drying (blue), risedronate sodium (green) and PVC (yellow)). (For interpretation of the references to colour in this figure legend, the reader is referred to the web version of this article.)

Table 3
Kinetic parameters of drug dissolution.

Composition	CA-1			CA-2			CA-3			CA-4		
Compression force (t)	k	n	R^2	k	n	R^2	k	n	R^2	k	n	R^2
1	33.8	0.18	0.91	28.4	0.21	0.95	25.5	0.27	0.97	21.1	0.30	0.88
3	31.4	0.17	0.98	32.4	0.16	0.96	4.33	0.30	0.97	5.97	0.30	0.91
5	30.8	0.18	0.99	34.6	0.17	0.97	14.3	0.36	0.98	23.0	0.29	0.90

tablets or in those which were dissolved for 8 h prior to the analysis. The lack of differences indicates that the slow release of drug is basically determined by the porosity of the matrix, the texture of which remained intact during the one-week dissolution process. The relationship between porosity and dissolution rates may be followed well from the change of dissolution rate constants (Fig. 4, Table 3).

The PVC matrices exhibited completely different behavior during the dissolution process. Due to its hydrophobic nature, the wetting of the PVC matrix is considerably slow, and the texture remained intact during the one-week dissolution process.

It is also evident from the kinetic data that the PVC based matrices exhibit slower dissolution than the chitosan based ones under every process condition. Furthermore, despite the fact that all the compositions show an inhibited, non-Fickian diffusion based release of risedronate, it is clearly visible from the shape parameters (n) that the size of inhibition is smaller in the case of PVC matrices. This is possibly due to the lack of intermolecular associations, and may be caused only by the hydrophobic nature of the polymer.

It may also be concluded on the basis of the results of statistical analysis (Eq. (10)) that the release rate from the matrices is generally determined by the interactions of polymer and compression force and is independent from the drug content of the composition within this range.

$$y = 23.84 - 8.11x_1 + 0.45x_2 - 0.75 \times {}_3 - 3.97x_3{}^2 + 0.55 \times {}_1x_2 - 1.56\ x_1x_3 - 3.96x_1x_3{}^2 + 2.79x_2x_3 \quad (10)$$

The significant factors are highlighted in boldface. The MS residual of the model was 1.0847, $R^2 = 0.9973$ and $adjR^2 = 0.9902$.

4. Conclusions

The results confirmed that both the chitosan and the PVC based matrix systems may be applicable for long term bisphosphonate delivery, but the fast disintegration of chitosan based matrices and the resulted initial burst release requires further optimization of these matrices. Nevertheless, the unexpected, in-situ emerging hydrogen bond between the drug and polymer ensuring the prolongation of drug release may have significant importance, and help the better understanding of hydrogen bond based modification of drug release. A similar, but considerably weaker interaction was also identified between the drug and the PVC matrix, but it may have no or only minor influence on the drug release rate. Therefore, the drug dissolution rate is better controllable for PVC matrices, especially since the texture remained intact during the whole dissolution process.

Conflict of interest

The authors declare no conflict of interest.

References

AlKhatib, H.S., Aiedeh, K.M., Bustanji, Y., Hamed, S., Mohammad, M.K., AlKhalidi, B., Najjar, S., 2008. Modulation of buspirone HCl release from hypromellose matrices using chitosan succinate: implications for pH-independent release. Eur. J. Pharm. Biopharm. 70, 804–812.

Anselmo, A.C., Mitragotri, S., 2014. An overview of clinical and commercial impact of drug delivery systems. J. Control. Release 190, 15–28.

Avgoustakis, K., Nixon, J.R., 1991. Biodegradable controlled release tablets 1: Preparative variables affecting the properties of poly(lactide-co-glycolide) copolymers as matrix forming material. Int. J. Pharm. 70, 77–85.

Cadarette, S.M., Katz, J.M., Brookhart, M.A., Stürmer, T., Stedman, M.R., Levin, R., Solomon, D.H., 2009. Comparative gastrointestinal safety of weekly oral bisphosphonates. Osteoporos. Int. 20, 1735–1747.

Campiñez, M.D., Ferris, C., de Paz, M.V., Aguilar-de-Leyva, A., Galbis, J., Caraballo, I., 2015. A new biodegradable polythiourethane as controlled release matrix polymer. Int J. Pharm. 480, 63–72.

Chambin, O., Champion, D., Debray, C., Rochat-Gonthier, M.H., Le Mesteb, M., Pourcelot, Y., 2004. Effects of different cellulose derivatives on drug release mechanism studied at a preformulation stage. J. Control. Release 95, 101–108.

Chang, H.-I., Williamson, M.R., Perrie, Y., Coombes, A.G.A., 2005. Precipitation casting of drug-loaded microporous PCL matrices: incorporation of progesterone by co-dissolution. J. Control. Release 106, 263–272.

Cheng, L., Lei, L., Guo, S., 2010. In vitro and in vivo evaluation of praziquantel loaded implants based on PEG/PCL blends. Int. J. Pharm. 387, 129–138.

Dürig, T., Fassihi, R., 2002. Guar-based monolithic matrix systems: effect of ionizable and non-ionizable substances and excipients on gel dynamics and release kinetics. J. Control. Release 80, 45–56.

De Robertis, S., Bonferoni, M.C., Elviri, L., Sandri, G., Caramella, C., Bettini, R., 2015. Advances in oral controlled drug delivery: the role of drug-polymer andinterpolymer non-covalent interactions. Exp. Opin. Drug Deliv. 12, 441–453.

Fuchs, K., Bize, P.E., Denys, A., Borchard, G., Jordan, O., 2015. Sunitinib-eluting beads for chemoembolization: methods for in vitro evaluation of drug release. Int. J. Pharm. 482, 68–74.

Glaessl, B., Siepmann, F., Tucker, I., Rades, T., Siepmann, J., 2010. Deeper insight into the drug release mechanisms in Eudragit RL-based delivery systems. Int. J. Pharm. 389, 139–146.

Hernandez, C., Gawlik, N., Goss, M., Zhou, H., Jeganathan, S., Gilbert, D., Exner, A.A., 2016. Macroporous acrylamide phantoms improve prediction of in vivo performance of in situ forming implants. J. Control. Release 243, 225–231.

Hifumi, H., Ewing, A.V., Kazarian, S.G., 2016. ATR-FTIR spectroscopic imaging to study the drying and dissolution of pharmaceutical polymer-based films. Int. J. Pharm. 515, 57–68.

Hur, W., Park, M., Lee, J.Y., Kim, M.Y., Lee, S.H., Park, C.G., Kim, S.-N., Min, H.S., Min, H. J., Chai, J.H., Lee, S.J., Kim, S., Choi, T.H., Choy, Y.B., 2016. Bioabsorbable bone plates enabled with local, sustained delivery of alendronate for bone regeneration. J. Control. Release 222, 97–106.

Kása, P., Bajdik, J., Zsigmond, Zs., Pintye-Hódi, K., 2009. Study of the compaction behaviour and compressibility of binary mixtures of some pharmaceutical excipients during direct compression. Chem. Eng. Process. 48, 859–863.

Khlibsuwan, R., Pongjanyakul, T., 2016. Chitosan-clay matrix tablets for sustained-release drug delivery: effect of chitosan molecular weight and lubricant. J. Drug Deliv. Sci. Technol. 35, 303–313.

Khunawattanakul, W., Puttipipatkhachorn, S., Rades, T., Pongjanyakul, T., 2011. Novel chitosan-magnesium aluminum silicate nanocomposite film coatings for modified-release tablets. Int. J. Pharm. 407, 132–141.

Kleiner, L.W., Wright, J.C., Wang, Y., 2014. Evolution of implantable and insertable drug delivery systems. J. Control. Release 181, 1–10.

Krier, F., Riva, R., Defrère, S., Mestdagt, M., Van Langendonckt, A., Drion, P., Dehoux, J.-P., Donnez, J., Foidart, J.-M., Jérome, C., Evrard, B., 2014. Device-based controlled local delivery of anastrozol into peritoneal cavity: in vitro and in vivo evaluation. J. Drug Deliv. Sci. Technol. 24, 198–204.

Li, L., Wang, L., Shao, Y., Tian, Y., Li, C., Li, Y., Mao, S., 2013. Elucidation of release characteristics of highly soluble drug trimetazidine hydrochloride from chitosan–carrageenan matrix tablets. J. Pharm. Sci. 102, 2644–2653.

Li, L., Wang, L., Li, J., Jiang, S., Wang, Y., Zhang, X., Ding, J., Yu, T., Mao, S., 2014. Insights into the mechanisms of chitosan–anionic polymers-based matrix tablets for extended drug release. Int. J. Pharm. 476, 253–265.

Li, L., Li, J., Si, S., Wang, L., Shi, C., Sun, Y., Liang, Z., Mao, S., 2015. Effect of formulation variables on in vitro release of a water-soluble drug from chitosane sodium alginate matrix tablets. Asian J. Pharm. Sci. 10, 314–321.

Lichtenberger, L.M., Romero, J.J., Gibson, G.W., Blank, M.A., 2000. Effect of bisphosphonates on surface hydrophobicity and phosphatidylcholine concentration of rodent gastric mucosa. Digest. Dis. Sci. 45, 1792–1801.

Luciani-Giacobbe, L.C., Ramírez-Rigo, M.V., Garro-Linck, Y., Monti, G.A., Manzo, R.H., Olivera, M.E., 2017. Very fast dissolving acid carboxymethylcellulose-rifampicin matrix: development and solid-state characterization. Eur. J. Pharm. Sci. 96, 398–410.

Mazurkiewicz, T., Matuszewsk, L., Matuszewska, A., Jaszek, M., 2013. Implanted bisphosphonates in bone cement affect bone markers in rat serum. Int. Orthop. 37, 969–974.

Medarević, D., Kachrimanis, K., Djurić, Z., Ibrić, S., 2015. Influence of hydrophilic polymers on the complexation of carbamazepine with hydroxypropyl-b-cyclodextrin. Eur. J. Pharm. Sci. 78, 273–285.

Meng, F., Trivino, A., Prasad, D., Chauhan, H., 2015. Investigation and correlation of drug polymer miscibility and molecular interactions by various approaches for the preparation of amorphous solid dispersions. Eur. J. Pharm. Sci. 71, 12–24.

Mir, V.G., Heinämäki, J., Antikainen, O., Revoredo, O.B., Colarte, A.I., Nieto, O.M., Yliruusi, J., 2008. Direct compression properties of chitin and chitosan. Eur. J. Pharm. Biopharm. 69, 964–968.

Ngo, H.V., Nguyen, P.K., Vo, T.V., Duan, W., Tran, W.-T., Tran, P.H.-L., Tran, T.T.-D., 2016. Hydrophilic-hydrophobic polymer blend for modulation of crystalline changes and molecular interactions in solid dispersion. Int. J. Pharm. 513, 148–152.

Nguyen, H.V., Nguyen, V.H., Lee, B.-J., 2016. Dual release and molecular mechanism of bilayered aceclofenac tablet using polymer mixture. Int. J. Pharm. 515, 233–244.

Park, E.-S., Maniar, M., Shah, J.C., 1998. Biodegradable polyanhydride devices of cefazolin sodium, bupivacaine, and taxol for local drug delivery: preparation, and kinetics and mechanism of in vitro release. J. Control. Release 52, 179–189.

Pavli, M., Baumgartner, S., Kos, P., Kogej, P., 2011. Doxazosin–carrageenan interactions: a novel approach for studying drug–polymer interactions and relation to controlled drug release. Int. J. Pharm. 421, 110–119.

Perugini, P., Genta, I., Conti, B., Modena, T., Pavanetto, F., 2001. Long-term release of clodronate from biodegradable microspheres. AAPS PharmSciTech 2, 1–9.

Peter, B., Pioletti, D.P., Laib, S., Bujoli, B., Pilet, P., Janvier, P., Guicheux, J., Zambelli, P.-Y., Bouler, J.-M., Gauthier, O., 2005. Calcium phosphate drug delivery system: influence of local zoledronate release on bone implant osteointegration. Bone 36, 52–60.

Phaechamud, T., Koizumi, T., Ritthidej, G.C., 2000. Chitosan citrate as film former: compatibility with water-soluble anionic dyes and drug dissolution from coated tablet Int. J. Pharm. 198, 97–111.

Pudlas, M., Kyerematen, S.O., Williams, L.A.M., Kimber, J.A., van Lishaut, H., Kazarian, S.G., Woehrle, G.H., 2015. Analyzing the impact of different excipients on drug release behavior in hot-melt extrusion formulations using FTIR spectroscopic imaging. Eur. J. Pharm. Sci. 67, 21–31.

Puncochová, K., Heng, J.Y.Y., Beránek, J., Štepánek, F., 2014. Investigation of drug–polymer interaction in solid dispersions by vapour sorption methods. Int. J. Pharm. 469, 159–167.

Ramchandani, M., Robinson, D., 1998. In vitro and in vivo release of ciprofloxacin from PLGA 50:50 implants. J. Control. Release 54, 167–175.

Raviña-Eirin, E., Azuaje, J., Sotelo, E., Gomez-Amoza, J.L., Martinez-Pacheco, R., 2016. Drug structural features affect drug delivery from hyperbranched polyesteramide hot melt extrudates. Eur. J. Pharm. Biopharm. 102, 1–8.

Ravishankar, H., Patil, P., Samel, A., Petereit, H.-U., Lizio, R., Iyer-Chavan, J., 2006. Modulated release metoprolol succinate formulation based on ionic interactions: in vivo proof of concept. J. Control. Release 111, 65–72.

Rege, P.R., Shukla, D.J., Block, L.H., 1999. Chitinosans as tableting excipients for modified release delivery systems. Int J. Pharm. 40, 49–60.

Rege, P.R., Shukla, D.J., Block, L.H., 2003. Chitinosan-drug complexes: effect of electrolyte on naproxen release in vitro. Int. J. Pharm. 250, 259–272.

Rime, A.-F., Massuelle, D., Kubel, F., Hagemann, H.-R., Doelker, E., 1997. Compressibility and compactibility of powdered polymers: poly(vinyl chloride) powders. Eur. J. Pharm. Biopharm. 44, 315–322.

Schliecker, G., Schmidt, C., Fuchs, S., Ehinger, A., Sandow, J., Kissel, T., 2004. In vitro and in vivo correlation of buserelin release from biodegradable implants using statistical moment analysis. J. Control. Release 94, 25–37.

Shao, Y., Li, L., Gu, X., Wang, L., Mao, S., 2015. Evaluation of chitosane anionic polymers based tablets for extended-release of highly water soluble drugs. Asi. J. Pharm. Sci. 10, 24–30.

Sogias, I.A., Williams, A.C., Khutoryanskiy, V.V., 2012. Chitosan-based mucoadhesive tablets for oral delivery of ibuprofen. Int. J. Pharm. 436, 602–610.

Sun, M., Wu, C., Fu, Q., Di, D., Kuang, X., Wang, C., He, Z., Wang, J., Sun, J., 2016. Solvent-shift strategy to identify suitable polymers to inhibit humidity-induced solid-state crystallization of lacidipine amorphous solid dispersions. Int. J. Pharm. 503, 238–246.

Szakonyi, G., Zelkó, R., 2016. Carbopol®-crospovidone interpolymer complex for pH-dependent desloratadine release. J. Pharm. Biomed. Anal. 123, 141–146.

Thomson, A.B.R., Marshall, J.K., Hunt, R.H., Provenza, J.M., Lanza, F.L., Royer, M.G., Li, Z., Blank, M.A., 2002. 14 day endoscopy study comparing risedronate and alendronate in postmenopausal women stratified by helicobacter pylori status. J. Rheumatol. 29, 1965–1974.

Yi, H.-G., Choi, Y.-J., Kang, K.S., Hong, J.M., Pati, R.G., Park, M.N., Shim, I.K., Lee, C.M., Kim, S.C., Cho, D.-W., 2016. A 3D-printed local drug delivery patch for pancreatic cancer growth suppression. J. Control. Release 238, 231–241.

am Ende, M.T., Peppas, N.A., 1997. Transport of ionizable drugs and proteins in crosslinked poly(acrylic acid) and poly(acrylic acid-co-2-hydroxyethyl methacrylate) hydrogels. II. Diffusion and release studies. J. Control. Release 48, 47–56.

ANNEX 2

pharmaceutics

MDPI

Article

Predicting drug release rate of implantable matrices and better understanding the underlying mechanisms through experimental design and artificial neural network-based modelling

Ernő Benkő[1], Ilija German Ilič[2], Katalin Kristó[1], Géza Regdon Jr.[1], Ildikó Csóka[1], Klára Pintye-Hódi[1], Stane Srčič[2] and Tamás Sovány[1]*

[1] Institute of Pharmaceutical Technology and Regulatory Affairs, University of Szeged, Eötvös u. 6., H-6720, Szeged, Hungary
[2] Chair of Pharmaceutical Technology, University of Ljubljana, Aškerčeva cesta 7, SI-1000, Ljubljana, Slovenia
* Correspondence: author: Tamás Sovány, Institute of Pharmaceutical Technology and Regulatory Affairs, University of Szeged, Eötvös u. 6., H-6720, Szeged, Hungary, tel: +3662545576, e-mail: sovany.tamas@szte.hu

Abstract: There is a growing interest in implantable drug delivery systems (DDS) in pharmaceutical science. The aim of the present study is to investigate whether it is possible to customize drug release from implantable DDSs through drug-carrier interactions. Therefore, a series of chemically similar active ingredients (APIs) were mixed with different matrix-forming materials and then compressed directly. Compression and dissolution interactions were examined by FT-IR spectroscopy. Regarding the effect of the interactions on the drug release kinetics, a custom-made dissolution device designed for implantable systems was used. The data obtained were used to construct models based on the artificial neural networks (ANNs) to predict drug dissolution. FT-IR studies confirmed the presence of H-bond-based solid-state interactions that intensified during dissolution. These results confirmed our hypothesis that interactions could significantly affect both the release rate and the amount of the released drug. The efficiencies of the kinetic parameter-based and point-to-point ANN models were also compared, where the results showed that the point-to-point models better handle predictive inaccuracies and provide better overall predictive efficiency.

Keywords: Drug-excipient interaction; polymers; non-degradable; matrix tablet; controlled release; Design of Experiments; Artificial Neural Networks

Citation: Benkő, E.; Ilič, I.G.; Kristó, K., Géza Regdon Jr.1.; Csóka, I.; Pintye-Hódi, K.; Srčič, S.; Sovány, T. Predicting drug release rate of implantable matrices and better understanding the underlying mechanisms through experimental design and artificial neural network-based modelling. *Pharmaceutics* **2022**, *13*, x. https://doi.org/10.3390/xxxxx

Academic Editor(s):

Received: date
Accepted: date
Published: date

Publisher's Note: MDPI stays neutral with regard to jurisdictional claims in published maps and institutional affiliations.

1. Introduction

Matrix tablets belong to the most popular systems for controlled delivery of drugs. The drug liberation from porous matrices is complex process, influenced by numerous parameters such as solubility, matrix porosity [1], swelling [2] and gel formation [3] of polymers. The gel properties are influenced by the particle size [1,4] or molecular weight of polymers [5] and generally determines the drug transport within the matrix, which could be diffusion-driven [2], relaxation-driven [6], external mass-transport-driven or anomalous [7]. Especially the anomalous transport mechanism presupposes the presence of interparticle interactions within the system [5,7]. Novel achievements require the reconsideration of the traditional thinking about inert excipients and turns the investigation and utilization of drug-excipient interactions into the focus of the development of tailored drug delivery systems.

Most of the polymers used as pharmaceutical excipients can form supramolecular conjugates [8], and the resulting H-bond-based or ionic drug excipient [9] or excipient-excipient [10] interactions may provide an ideal way to customize drug release. The formation of supramolecular interactions is most likely in dissolution or melt-based production processes, but de Robertis et al. described the occurrence of similar interactions in directly compressed systems [11]. In our previous study, we examined the release of

risedronate sodium from biodegradable and non-degradable implants. Although the slowest release rate has been shown in low porosity non-degradable systems, unexpectedly prolonged, sustained release was observed in the degradable systems even after complete matrix disintegration. This was due to a strong H-bond-based interaction between risedronate sodium and chitosan, suggesting that the role and presence of intermolecular interactions in the drug release rate of directly compressed matrices could be significantly underestimated [12].

Therefore, the primary goal of the present study is to confirm the hypothesis that drug-excipient interactions can be used to further prolong drug release from non-degradable matrices, while the strength of the interactions can be predicted based on the acid strength of the drugs.

To confirm the primary hypothesis, the original PVC matrix was combined with Eudragit of different grades as a model excipient, which allowed the development of drug-binder interactions, which are mentioned as a favorable choice to produce controlled-release DDSs. Weak base Eudragit E100 and acidic Eudragit L100-55 are commonly used for oral administration, but recent reports [13-19] investigate their applicability in parenteral drug administration. Following intramuscular administration of Eudragit-based nanoparticles, safety tests were performed [18] to examine liver and skeletal muscle damage during the 6-week experiment. Tissue samples from the liver were as in the control group, the skeletal muscle showed inflammation in the first week, which decreased by the second week, and at the end of the experiment it became like the control group as well. In the case of intravenous microparticulate administration [13] also only local inflammation was observed. Overall, the use of these materials as implantable excipients is considerable, especially because quaternerised Eudragit can facilitate paracellular API permeation at pH 7.4, which highlights the benefits of Eudragit copolymers.

A Quality by Design based approach was used to investigate the effect of critical material attributes on the mechanical properties of the matrices, the strength of the interaction, and the drug release rate. Design of Experiments (DoE) was used to reveal basic relationships while artificial neural networks (ANN) were used for the prediction of drug dissolution of the designed matrices. ANNs are commonly used types of machine learning/deep learning methods, which mimic the signal transduction and learning mechanism of the human brain. ANNs can self-accommodate to the learning environment, and therefore are widely applied for modelling of difficult nonlinear problems in a wide range of applications, including pharmaceutics. Previous studies [20, 21] have demonstrated that ANNs are excellent tools for modeling the mechanical properties of tablets, whereas Galata et al. has successfully used ANNs to model drug release from hydrophilic, sustained-release matrix systems [22] by point-to-point modeling of drug release. Nevertheless, the question how the developed network may be used for the modelling of general problems remained open. A secondary objective of the present study was to reveal if the tested material attributes will enable a generalized prediction of drug dissolution and furthermore to compare the efficiency of point-to-point modeling with another method where kinetic parameters (shape parameters of the dissolution curve) served as output variables.

2. Materials and Methods

2.1. Materials

Aceclofenac (ACE) was a kind gift from ExtractumPharma Ltd. (Budapest, Hungary), while diclofenac sodium (DIS), paracetamol (PAR) and polyvinyl chloride (polymerization degree: 60-150) (PVC) were kindly gifted by Gedeon Richter Plc. (Budapest, Hungary). A powder form of Eudragit E100, Eudragit EPO (EE) and Eudragit L100-55 (EL) was supplied by Evonik Industries AG (Essen, Germany). The main physicochemical properties of raw materials are summarized in Table 1.

Table 1. Physicochemical properties of raw materials

	Paracetamol	**Diclofenac Sodium**	**Aceclofenac**	**EUDR-E**	**EUDR-L**	**PVC**
Solubility (pH 7.4)	18-21 mg/ml	5.15 mg/ml	4.0-12.8 mg/ml	<10 μg/ml (> pH 5)	< 0,03 mg/ml (> pH 6)	<10 μg/ml
logP	0.34	3.10	4.16	-	-	-
pKa	9.46	4.00	3.44	10	6	-
H+ acceptor	2	2	4	3/n*	3/n*	-
H+ donor	2	2	2	0/n*	1/n*	-
Rotable bonds	3	3	5	-	-	-

*x/n: represents the number of H+ acceptor/donor groups per monomer

2.2. Methods

2.2.1. Tablet preparation

Tablets were prepared according to a mixed 2- and 3-level factorial design, where the acidic or basic nature of excipients (e.g. the use of Eudragit E or L) was studied as 2-level, while the acidic strength of API, the weight ratio of excipients and the applied compression force as 3-level factors. The detailed experimental plan is shown in Table 2.

Powder mixing was made with a Paul Schatz principle based 1.5L mixer (Inversina, BioEngineering, Wald, Switzerland) at 45 rpm for 8 minutes and then for another 2 minutes with the addition of 1% magnesium stearate as lubricant. The mixtures were compressed with an instrumented Kilian SP 300 hydraulic press (IMA Kilian GmbH & Co., KG, Cologne, Germany) using 7-mm-diameter punches with beveled edge. The mixtures were loaded into the die manually then compressed in a semi-automatic 'jogging' mode with the application of 2.9, 8.7, or 14.4 kN compression force (75, 225 and 375 MPa compression pressure, respectively).

2.2.2. Physical properties

The physical characterization of tablets was made with a Kraemer UTS tablet tester (Kraemer Elektronik GmbH, Germany). Mass, hardness, thickness and diameter were measured. The true density of matrices (ρ_{true}) was determined with a helium gas pycnometer (AccuPyc 1330, Micromeritics, Norcross, GA, USA), while apparent density (ρ_{app}) was calculated from their mass and physical dimensions. Then porosity (ε) was obtained according to the following equation (Eq. (1)):

$$\varepsilon = 1 - (\rho_{app}/\rho_{true}) \quad (1)$$

2.2.3. Physicochemical characterization

For the specific identification and characterization of interactions, FT-IR spectra were acquired. ZeSe HATR accessory was used and measurements were taken with a resolution of 4 cm^{-1}, a scan number of 128, with CO_2 and H_2O correction. Spectral data were evaluated with SpectraGryph software v1.2.10 (Dr. F. Menges, Berchtesgaden, Germany).

Table 2. DoE plan

Compression pressure (MPa) (x_1)		Eudragit/PVC ratio (%/%) (x_2)		API (x_3)		Eudragit type (x_4)	
Level	**Value**	**Level**	**Value**	**Level**	**Value**	**Level**	**Value**
-1	75	-1	25/75	-1	Paracetamol	-1	Eudragit E
						+1	Eudragit L
				0	Diclofenac Sodium	-1	Eudragit E
						+1	Eudragit L
				+1	Aceclofenac	-1	Eudragit E
						+1	Eudragit L
		0	50/50	-1	Paracetamol	-1	Eudragit E
						+1	Eudragit L
				0	Diclofenac Sodium	-1	Eudragit E
						+1	Eudragit L
				+1	Aceclofenac	-1	Eudragit E
						+1	Eudragit L
		+1	75/25	-1	Paracetamol	-1	Eudragit E
						+1	Eudragit L
				0	Diclofenac Sodium	-1	Eudragit E
						+1	Eudragit L
				+1	Aceclofenac	-1	Eudragit E
						+1	Eudragit L
0	225	-1	25/75	-1	Paracetamol	-1	Eudragit E
						+1	Eudragit L
				0	Diclofenac Sodium	-1	Eudragit E
						+1	Eudragit L
				+1	Aceclofenac	-1	Eudragit E
						+1	Eudragit L
		0	50/50	-1	Paracetamol	-1	Eudragit E
						+1	Eudragit L
				0	Diclofenac Sodium	-1	Eudragit E
						+1	Eudragit L
				+1	Aceclofenac	-1	Eudragit E
						+1	Eudragit L
		+1	75/25	-1	Paracetamol	-1	Eudragit E
						+1	Eudragit L
				0	Diclofenac Sodium	-1	Eudragit E
						+1	Eudragit L
				+1	Aceclofenac	-1	Eudragit E
						+1	Eudragit L
+1	375	-1	25/75	-1	Paracetamol	-1	Eudragit E
						+1	Eudragit L
				0	Diclofenac Sodium	-1	Eudragit E
						+1	Eudragit L
				+1	Aceclofenac	-1	Eudragit E
						+1	Eudragit L
		0	50/50	-1	Paracetamol	-1	Eudragit E
						+1	Eudragit L

		0	Diclofenac Sodium	-1	Eudragit E
				+1	Eudragit L
		+1	Aceclofenac	-1	Eudragit E
				+1	Eudragit L
		-1	Paracetamol	-1	Eudragit E
				+1	Eudragit L
+1	75/25	0	Diclofenac Sodium	-1	Eudragit E
				+1	Eudragit L
		+1	Aceclofenac	-1	Eudragit E
				+1	Eudragit L

2.2.4. Dissolution tests

According to the requirements of implantable matrix systems, a custom-made dissolution tester was applied imitating the dissolution environment of the tissue matrix and the shearing properties of other flow-through equipment [13]. Tablets were placed into Erlenmeyer flasks containing 50 ml of pH 7.4 phosphate buffered saline solution. The dissolution medium was circulated with an Alitea-XV (Alitea, Sweden) peristaltic pump using a flow rate of 2 ml/min. Due to the vast number of samples to be studied, 24-hour dissolution tests were conducted for all compositions to obtain the most important kinetic parameters, and only those samples were selected afterwards for a one-week study in which the lowest release rates were observed. The concentration gradient was continuously maintained by mimicking the time related systemic renewing of the body fluids. Therefore, in the 24-hour-long experiments 2.5 ml, 5 ml, 5 ml, 5 ml, 10 ml, 20 ml samples were taken and replaced with fresh medium after 15 min, 30 min, 1 h, 2 h, 4 h, 8 h, respectively, while the last samples were taken after 24 h. In the case of the one-week study 5 ml, 5 ml, 10 ml, 20 ml, 35 ml, 35 ml, 35 ml volume was sampled and refreshed as above after 1 h, 2 h, 4 h, 8 h, 24 h, 48 h, 72 h, respectively, while the last samples were taken after 168 h. From each composition three parallel measurements were taken. Quantitative analysis was made with a ThermoGenesys UV-spectrometer at a wavelength of 274 nm for aceclofenac, 276 nm for diclofenac sodium and 244 nm in the case of paracetamol. The dissolution kinetics was characterized according to the Korsmeyer-Peppas equation (Eq. (2)).

$$M_t/M_0 = kt^n \quad (2)$$

where M_0 is the initial drug amount in the matrix, M_t is the drug amount at the given time (t), k is the dissolution rate constant and n is the release exponent regarding the diffusion mechanism.

2.2.5. Design of Experiments and Artificial Neural Networks

DoE analysis and ANN modeling was performed with Statistica v.13.5.0.17 (Tibco Software Inc., Palo Alto, CA, USA). Compression pressure (x_1), amount of excipient (x_2), API (x_3) and excipient used (x_4) were examined as independent factors, while hardness (y_1), porosity (y_2) and release rate (y_3) were used as optimization parameters in the DoE analysis.

The secondary objective of the present study was to compare the effectiveness of various modeling approaches to enable generalized prediction of drug dissolution rates from different matrices. In kinetic-based modelling, the release rate and release exponent were used as the output of the ANN model, while in point-to-point modeling the dissolved amount of drug at the various sampling times was applied according to Galata et al. [22], which included 7 data points. Our hypothesis is that kinetic-based modelling allows for a simplified network structure and faster generalization. To clarify the importance of different input parameters for predictive accuracy, 3 different parameter combinations were

used to train the ANNs for both kinetic based and point-to-point modelling. A list of inputs used in the different training approaches is provided in Table 3, while a detailed data set for training, testing, and validating ANNs is provided in Table S1.

Table 3. Input variables of the various ANN training approaches.

Modelling type	Approach 1	Approach 2	Approach 3	Approach 4	Approach 5	Approach 6
	Kinetic based	Kinetic based	Kinetic based	Point-to-point	Point-to-point	Point-to-point
Input variable						
Drug	x			x		
Drug solubility (mg/ml)		x	x		x	x
Drug pKa		x	x		x	x
Excipient	x			x		
Excipient solubility (mg/ml)		x	x		x	x
Excipient pKa		x	x		x	x
Excipient amount (%)	x	x	x	x	x	x
Compression pressure (MPa)	x	x	x	x	x	x
Hardness			x			x
Porosity			x			x
Peak Shift	x	x	x	x	x	x

Feed-forward, back-propagation Multilayer Perceptron networks were developed in all cases. The networks were trained with BFGS algorithm. The number of hidden neurons was gradually increased in a dynamic system depending on the number of input and output neurons: $I+O-3 \leq n \leq I+O+1$, where I is the number of inputs O is the number outputs and n is number of hidden neurons., so hidden neuron number was varied from 4-8, 6-10, 8-12, 9-13, 11-15, 13-17 in case of approach 1-6, respectively.

A multistart method including 10.000 networks was applied using the Automated Neural Networks module of Statistica with each hidden neuron number, and training approach to screen the best performing network with different initialization patterns, and activation functions for hidden and output neurons. The training was stopped, when the root mean square error (RMSE) of test dataset reached its minimum. The 5 best preforming networks from each multistart run were retained for further analysis.

The prediction performance of the networks was evaluated based on network perfection, which is the mean R^2 of the observed vs. predicted data of each output neurons, and on the RMSE of predictions on the validation subset.

3. Results and discussion

3.1. Physical parameters

The physical parameters of the tablets are shown in Table 4, while the statistical evaluation of the effect of compression pressure (x_1), amount of excipient (x_2), API (x_3) and

excipient used (x_4) on hardness (y_1) and porosity (y_2) of the various compositions are displayed in equations 3 and 4, respectively. The presented equations provided the best fit, for the equations contain the full set of the acquired factor effects and their interactions please see the supplementary materials. The significant factors and factor interactions are highlighted in boldface in all cases.

$$y_1=110.11+\mathbf{47.02x_1}+\mathbf{9.46x_1^2}+\mathbf{19.31x_2}-\mathbf{10.04x_3}-\mathbf{29.78x_4}+2.45x_1x_2+2.45x_1^2x_2+2.29x_1^2x_2^2-\mathbf{6.31x_1x_3}-\mathbf{4.29x_1^2x_3}+\mathbf{4.96x_1x_3^2}-\mathbf{3.62x_1^2x_3^2}-3.32x_2x_3^2-\mathbf{11.48x_2x_4}-2.24x_2^2x_4-2.33x_3x_4+\mathbf{6.83x_3^2x_4} \quad (3)$$

$R^2=0.9743$ adj. $R^2=0.9599$ MS Res=123.02

$$y_2=0.133-\mathbf{0.053x_1}-\mathbf{0.023x_1^2}-\mathbf{0.046x_3}+\mathbf{0.018x_4}+\mathbf{0.024x_1x_2}-\mathbf{0.019x_1x_2^2}+0.012x_1^2x_3+0.011x_1^2x_3^2-0.014x_1x_4-\mathbf{0.033x_2x_3}-0.009x_2x_3^2+0.010x_2^2x_3^2-0.009x_2x_4+\mathbf{0.016x_2^2x_4} \quad (4)$$

$R^2=0.7627$ adj $R^2=0.6775$ MS Res=0.0023

Table 4. Physical parameters of matrices

Eudragit / PVC ratio (%/%)	Compression pressure (MPa)	Composition	Mass (mg)	Hardness (N)	Porosity	Composition	Mass (mg)	Hardness (N)	Porosity	Composition	Mass (mg)	Hardness (N)	Porosity
25/75	75	PAR-PVC-EL	147.0	15.0	0.307	DIS-PVC-EL	152.1	8.0	0.423	ACE-PVC-EL	144.5	13.5	0.279
	225		147.9	114.3	0.136		135.2	118.5	0.125		131.4	68.2	0.077
	375		141.6	109.1	0.118		202.6	140.7	0.082		131.2	103.6	0.067
50/50	75		149.0	18.7	0.290		154.2	34.0	0.236		152.7	22.9	0.232
	225		135.9	95.8	0.122		138.7	92.0	0.128		137.8	65.8	0.104
	375		142.2	133.6	0.111		146.9	134.4	0.058		142.4	71.3	0.097
75/25	75		147.0	28.2	0.306		153.8	27.3	0.026		147.7	15.2	0.027
	225		151.7	132.6	0.118		136.9	97.0	0.137		134.9	90.7	0.086
	375		149.7	153.8	0.091		121.5	153.8	0.100		137.1	116.7	0.060
25/75	75	PAR-PVC-EE	154.8	113.6	0.223	DIS-PVC-EE	150.4	94.4	0.092	ACE-PVC-EE	147.3	93.4	0.106
	225		142.5	166.6	0.126		129.0	130.7	0.098		151.2	159.1	0.038
	375		136.1	184.5	0.098		130.7	173.7	0.113		152.7	164.7	0.014
50/50	75		149.0	50.1	0.191		151.7	57.4	0.210		151.1	67.6	0.141
	225		152.2	146.7	0.109		138.8	102.6	0.101		137.6	87.5	0.068
	375		145.2	161.8	0.105		138.7	153.8	0.080		139.0	143.6	0.071
75/25	75		149.5	128.6	0.282		137.4	102.9	0.147		146.3	131.2	0.102
	225		137.0	192.4	0.131		135.8	160.6	0.121		145.9	187.9	0.011
	375		148.6	211.2	0.115		151.7	201.0	0.046		141.7	192.8	0.011

The porosity of the system exhibited a well-established logarithmic correlation with tablet hardness (Fig. 1), the increase of pressure resulted in stronger matrices and decrement in porosity. Nevertheless, there are some outliers, where tablets with low breaking hardness showed extremely low porosity. In such cases radically increased dwell time was required to avoid critical tableting problems, e.g. capping, lamination, cracking, or picking. This phenomenon caused poorer fitting accuracy in case of porosity (y_2) values, so the results of the statistical analysis and the related conclusions should be treated with cautions.

The results revealed that matrices made of EE could reach higher breaking hardness and lower porosity than the tablets made of EL. From the aspect of different weight ratios, the general conclusion is that the composites containing more methacrylate copolymer and less PVC appear to be the strongest systems with the least porosity, while the 25:75 Eudragit-PVC ratio showed the lowest values and the highest porosity. The mean values showed that paracetamol formed the hardest, and aceclofenac formed the weakest matrices, but in contrast with the general expectations this was not directly proportional to the drug release rate, which support our primary hypothesis, that beside of the matrix porosity the physicochemical properties of the applied materials and the presence of drug-carrier interactions may considerably influence the drug release.

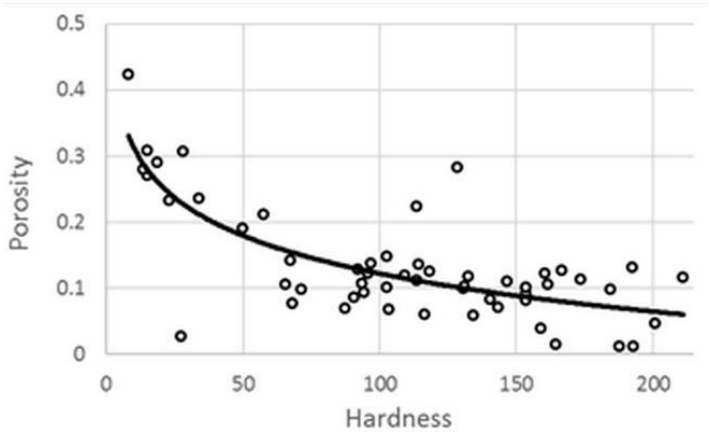

Figure 1. Hardness-porosity plot

3.2. Investigation of drug-carrier interactions

The FT-IR spectra of the compressed samples were used to reveal the presence of the drug-excipient interactions. The method is well applicable in various fields where chemical interactions are the area of interest [23, 24], the present analysis will focus on selected wavenumber ranges, reasonably where signals of H-bond forming groups can be found.

Interestingly, weak signal intensities were observed in the -OH stretching region (3000-3600 cm^{-1}, data not displayed), for all samples, which made the drawing of proper consequences about the interaction status impossible. The further analysis is focusing therefore on the C=O stretching (1600-1800 cm^{-1}) and the β-OH (β-NH) deformation vibration (1200-1600 cm^{-1}) regions.

According to our primary hypothesis, the interaction potential of the studied APIs is decreasing in the order of ACE>DIS>>PAR and stronger interactions were expected with EE than with EL in all cases. The results generally confirmed this hypothesis.

The Fig. 2 displays the IR spectra of ACE-PVC-EE composition, which exhibits intensive signs of drug-polymer interactions. In the carbonyl signal (C=O stretching) region EE has a characteristic peak at 1722 cm^{-1}, while the ACE at 1712 cm^{-1} and at 1769 cm^{-1}, belonging to the dimerized and monomer forms, respectively. The monomeric peak of ACE (1769 cm^{-1}) exhibits decreasing intensity with the increasing amount of EE (Fig. 2) indicating strong conjugation between the drug and excipient. Some further changes, such as the shifting of the deformation vibration of the HNC bonds at 1415 cm^{-1} appears to shift to 1420 cm^{-1}, which indicates that the corresponding molecular parts also may take part in the interaction.

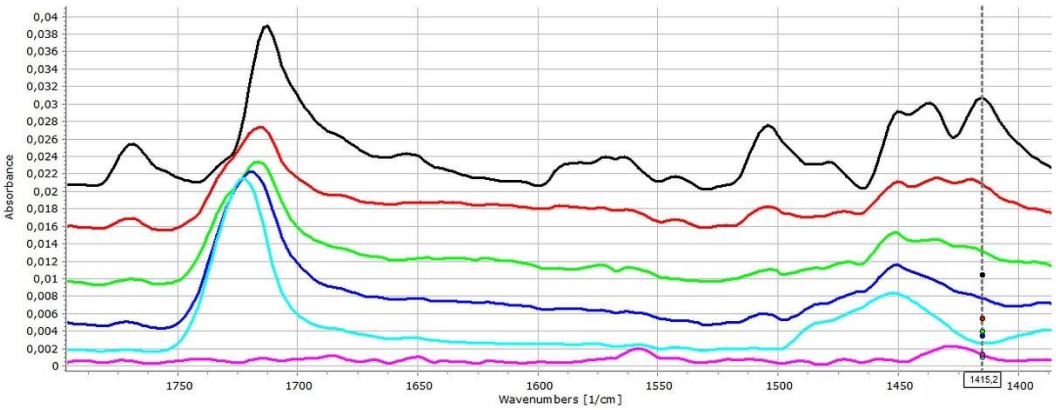

Figure 2. FT-IR spectra (1400-1800 cm^{-1} range) of the ACE (black); ACE-PVC:EE 75:25 (red); ACE-PVC:EE 50:50 (green); ACE-PVC:EE 25:75 (deep blue); EE (light blue) and PVC (purple) samples, multi cursor indicates the place of peak shift in the spectrum.

As it was expected, ACE exhibited fewer signs of interactions in relation to the acidic EL polymer (Fig. 3). The presence of mild interactions by increasing the amount of the EL is supported by the slight shift of the carbonyl signal to 1715 cm^{-1}, 1717 cm^{-1} and 1719 cm^{-1} in the case of 75:25, 50:50 and 25:75 PVC:EL ratios, respectively, and indicated increasing strength of interactions, which is also supported by the decreasing intensity of the unassociated acidic carbonyl absorption peak which appears at 1769 cm^{-1}.

The β-OH vibration of EL appears at 1472.2 cm^{-1}, which cannot be seen clearly in the spectra of matrices. A slight shift of the peak at 1415.3 cm-1 towards 1417.8 cm^{-1} can be recognised, which may reflect some further changes in the environment of the diphenylamine group of the drug. This finding is in accordance with the observation of Liu et al. who confirmed that EL may form H-bond based interactions under proper circumstances [25].

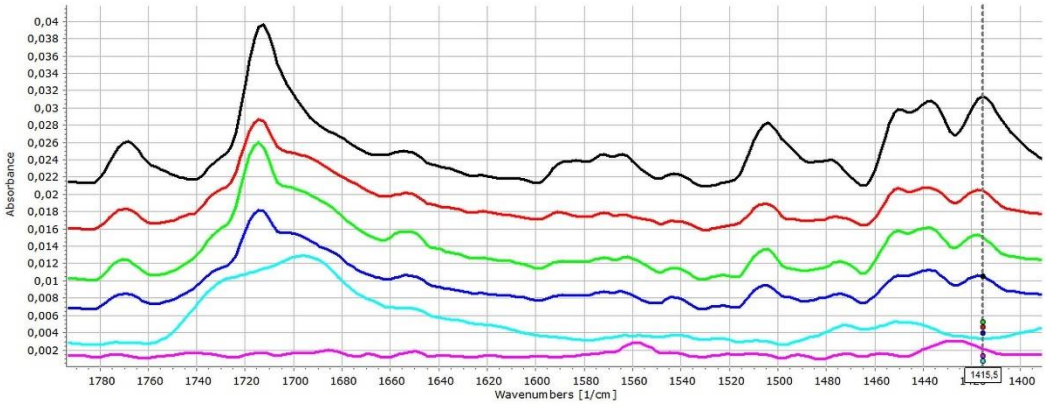

Figure 3. FT-IR spectra (1400-1800 cm^{-1} range) of the ACE (black); ACE-PVC:EL 75:25 (red); ACE-PVC:EL 50:50 (green); ACE-PVC:EL 25:75 (deep blue); EL (light blue) and PVC (purple) samples, multi cursor indicates the place of peak shift in the spectrum.

To clarify the importance of the solid-state interactions, and to analyse the effect of the dissolution medium on the strength of interactions the following experiment was performed. Tablets were dipped into pH 7.4 buffer for 30 min to achieve a complete moisturization of the sample, then the excess of the water was removed, and the samples were measured with FT-IR. Nevertheless, since the presence of water in the pores completely masked the signals in the 3000-3600 cm^{-1} and 1550-1700 cm^{-1} regions, the samples were dried in desiccator for 24 h, and measured again.

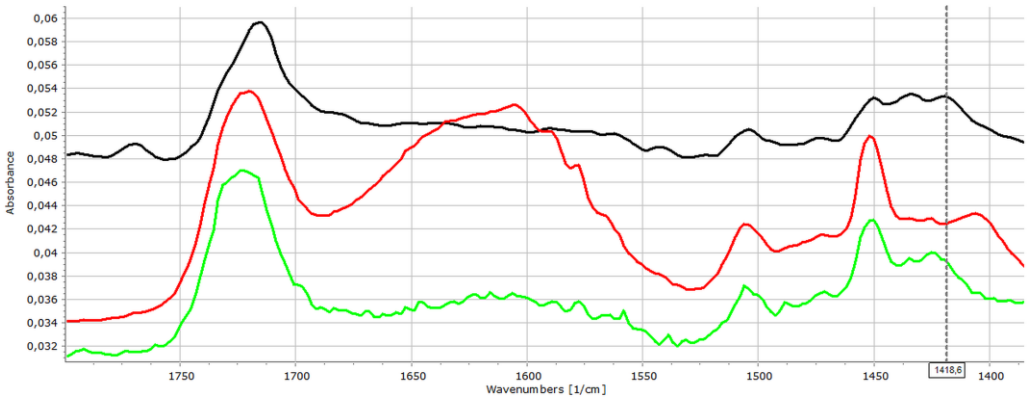

Figure 4. FT-IR spectra of ACE-PVC:EE 75:25 samples: original (black), dipped (red), and dried (green)

Figure 4 displays well, that the strength of intermolecular interaction has increased as effect of water absorption. The characteristic peaks of HCN bonds from 1434 cm^{-1} was shifted to 1451 cm^{-1}, while the peak at 1420 cm^{-1} shifted to 1405 cm^{-1}. The characteristic peak of C-N stretching at 1252 cm^{-1} has shifted to 1272 cm^{-1}. These changes may be observed also in case of the dried samples, despite of some re-organization due to the water loss.

In case of EL containing samples (Fig. 5) similar changes may be observed in the characteristic peaks of HCN vibrations: the peak at 1438 cm^{-1} shifts to 1425 cm^{-1} and its intensity increases considerably, while and C-N stretching signal which may be found at 1279 cm^{-1} shifts to 1291 cm^{-1}.

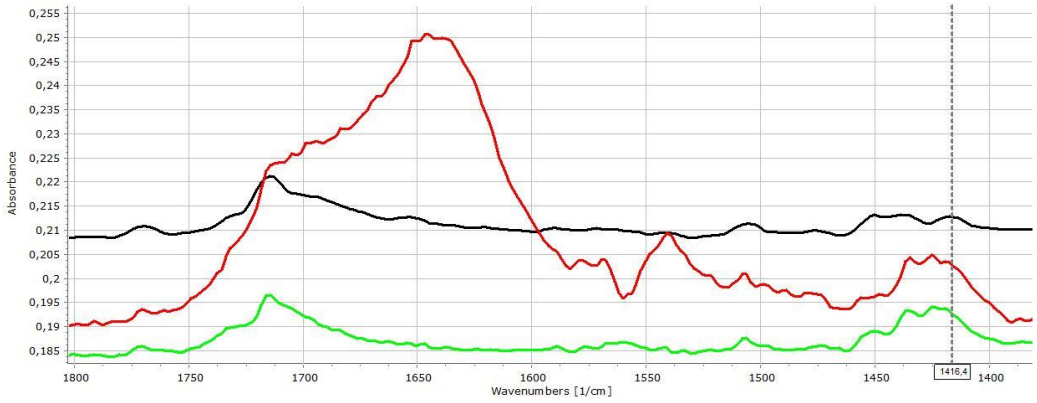

Figure 5. FT-IR spectra of ACE-PVC:EL 75:25 samples: original (black), dipped (red), and dried (green)

As it was expected, the matrices prepared with DIS exhibited fewer spectral changes after compression, primarily due the weaker acidity of the drug, but the higher porosity may also play a possible role in this phenomenon. Similarly as in the ACE containing compositions, the most obvious changes may be found in the C=O stretching region. The characteristic peak doublet may be found at 1555 cm^{-1} and 1571 cm^{-1}, where the shift of the peak intensities to the direction of 1571 cm^{-1} may be observed with increasing Eudragit content. As expected, the shift is less intensive in case of EL containing compositions (Fig. S1) than in EE containing ones (Fig. S2). Some further signs of mild interaction and increased intramolecular association the C-O bond region of EE containing matrices may also be observed (Fig. S2). The characteristic peak of DIS at 1279 cm^{-1} and of EE at 1269.5 cm^{-1} overlap around 1274 cm^{-1} in accordance with the increasing amount of EE.

The observed interactions were strongly intensified by the dipping. The ratio of the associated C=O groups was increased for both EE and EL containing matrices (Figs. S3 and S4, respectively), which is well visible from the increasing intensity of the associated C=O peak at 1555 cm^{-1}, and 1549 cm^{-1} for EE and EL, respectively. Further changes such as the increasing intensity of the peak at 1410 cm^{-1} and a peak shift from 1234 cm^{-1} to 1248 cm^{-1}, associated with the βNH and C-N stretching vibration indicates that under these circumstances the secondary amino group of DIS also involved into the association with EE. In case of EL the corresponding changes may be found at 1409 cm^{-1} 1232 cm^{-1}, and at 1250 cm^{-1}, respectively. Other peak shifts from 1168 cm^{-1} to 1197 cm^{-1}, and from 1190 cm^{-1} to 1198 cm^{-1}, for EE and EL respectively confirms the presence intermolecular associations from the side of the polymers.

In the case of PAR containing compositions exhibit no obvious signs of interactions neither in case of EL (Fig. S5) nor for EE (Fig. S6) containing compositions. The only mentionable change is the slight shift of C-N stretching peak (PAR) from 1221 cm^{-1} to 1224 cm^{-1} or 1226 cm^{-1}, in case of EL and EE containing compositions, respectively. This finding was in accordance with our primary hypothesis, and with the finding of Obediat et al. who also observed no interaction between EE and PAR in compressed matrix systems [26].

Nevertheless, after dipping the tablets into the dissolution medium considerable changes were observed in the FT-IR spectra both the EE and EL containing samples. The shift of the peaks from 1504 cm^{-1} to 1512 cm^{-1} and from 1432 cm^{-1} to 1454 cm^{-1} indicates the participation of the secondary amide group, while the shift of the peak from 1224 cm^{-1} to 1239 cm^{-1} refers on the involvement of the phenolic -OH group, into intermolecular associations (Fig. S7). The shift of the characteristic peak of EE from 1170 cm^{-1} to 1147 cm^{-1} suggest that the drug is connected to tertiary amino groups of the polymer.

The above-mentioned changes may be observed also in case of EL containing samples (peak shifts from 1504 cm^{-1} to 1514 cm^{-1}, from 1434 cm^{-1} to 1424 cm^{-1} and from 1224 cm^{-1} to 1240 cm^{-1}, respectively). While the shift of the characteristic peak of EL from 1169 cm-1 to 1186 cm-1 indicates that here the carbonyl side groups of the polymer are involved into the association (Fig. S8).

Overall, the results confirmed that solid state drug-polymer interactions may be presented after direct compression of the materials which were in accordance with the findings with de Robertis et al. [11]. The weak solid-state H-bonds may further strengthen during the dissolution process and influence the drug release rate [12] or in some cases may even turn into the formation of polyelectrolyte complexes as was observed by Pavli et al. [27].

3.3. Dissolution tests and kinetic study

The drug release kinetics was evaluated with the use of the Korsmeyer-Peppas model (Tables 5 and 6), which is the most regular type of dissolution in case of hydrophilic matrix systems. It can be noticed from the results that the dissolution followed non-Fickian diffusion. Most n values represent non-Fickian kinetics except those below 0.45. In the case of cylindrical shapes Fickian diffusion has a value of 0.45, for spherical shapes this value is 0.43. The reason for having smaller values than the limitations of the model is due to the polydisperse nature of the system [28]. Particle size has a major influence on the release exponent. Also, the geometry of tablets slightly varies from the ideal cylindrical shape.

Table 5. Release rates and release exponents derived from the Korsmeyer-Peppas model (24-h-long test)

Eudragit / PVC ratio (%/%)	Compression pressure (MPa)	Composition	R^2	k	n	Composition	R^2	k	n	Composition	R^2	k	n
25/75	75	PAR-PVC-EL	0.9230	5.7937	0.3858	DIS-PVC-EL	0.9966	0.0419	0.9833	ACE-PVC-EL	0.9945	0.4184	0.7325
	225		0.9840	1.4970	0.5635		0.9997	0.0092	1.1609		0.9979	0.0540	0.9340
	375		0.9870	1.7224	0.5345		0.9999	0.0054	1.2765		0.9976	0.0850	0.8940
50/50	75		0.9410	6.8732	0.3534		0.9867	1.4394	0.4317		0.9994	0.1289	0.8756
	225		0.9845	1.6004	0.5377		0.9979	0.0265	0.9560		0.9691	0.1877	0.8271
	375		0.9712	1.5522	0.5594		0.9942	0.0435	0.9105		0.9899	0.0829	0.8931
75/25	75		0.9920	1.7155	0.5058		0.9789	1.5287	0.5567		0.9906	0.2466	0.7311
	225		0.9974	0.7570	0.6298		0.9902	0.1828	0.7850		0.9990	0.2002	0.7389
	375		0.9928	1.5108	0.5239		0.9976	0.2207	0.6573		0.9991	0.2055	0.7260
25/75	75	PAR-PVC-EE	0.9936	0.9010	0.5693	DIS-PVC-EE	0.9660	1.3715	0.2623	ACE-PVC-EE	0.9998	0.0376	0.5936
	225		0.9977	0.6775	0.5774		0.9609	1.4599	0.2306		0.9933	0.0097	0.7596
	375		0.9755	0.8078	0.5483		0.9286	1.4502	0.2176		0.9820	0.0106	0.7241
50/50	75		0.9915	1.1441	0.5441		0.9974	1.7063	0.2739		0.9877	0.2063	0.4619
	225		0.9973	0.4156	0.6751		0.9846	0.9046	0.3542		0.9972	0.0704	0.5474
	375		0.9978	0.3755	0.6785		0.9823	0.9284	0.3404		0.9969	0.0805	0.4910
75/25	75		0.9920	1.6898	0.5056		0.9867	1.5953	0.3265		0.9839	0.2829	0.6100
	225		0.9983	0.7675	0.5535		0.9659	1.0545	0.3185		0.9933	0.1695	0.5134
	375		0.9918	0.8430	0.5239		0.9641	1.5575	0.2903		0.9670	0.2069	0.4661

The PAR loaded matrices released the most drug from 40 to 90 % within 24 h, the acidic ACE containing ones released between 2 and 80%, while the DIS loaded systems released 6-50%. These differences cannot be explained with the different solubility of the APIs since the applied dissolution environment ensures sink conditions for all tested drugs and therefore the solubility may be no limiting factor.

Nevertheless, the results of statistical analysis (Eq. 5) revealed that the main governing forces of the drug dissolution rate (y_3) are the physicochemical properties, especially the acidic strength of the drug (x_3), and the applied compression force (x_1), which confirm that the release rate is primarily determined by the porosity of the tablets, since PAR loaded matrices have the lowest hardness and highest porosity (Table 3.).

$$y_3=0.937-\mathbf{0.380x_1}-\mathbf{0.284x_1^2}-\mathbf{0.804x_3}+0.185x_4-0.242x_1x_2^2+\mathbf{0.403x_1x_3}+0.116x_1x_3^2+\mathbf{0.289x_1^2x_3}-0.208x_1x_4-0.181x_1^2x_4-0.241x_2x_3-0.135x_2x_3^2+0.197x_2x_4+0.116x_2^2x_4-\mathbf{0.440x_3x_4}-\mathbf{0.427x_3^2x_4} \quad (5)$$

$R^2=0.7669$ adj $R^2=0.6661$ MS Res=0.5176

The amount of excipient (x_2), and excipient used (x_4) exhibited non-significant effect on dissolution rate, but regarding the significant factor interactions, the compressibility of the API and its possible chemical interactions with the polymer also have considerable influence on drug liberation. To confirm this observation, and minimize the effect of the mechanical differences, the dissolution rates of tablets with similar porosities (0.13±0.02) were compared (Fig 6a).

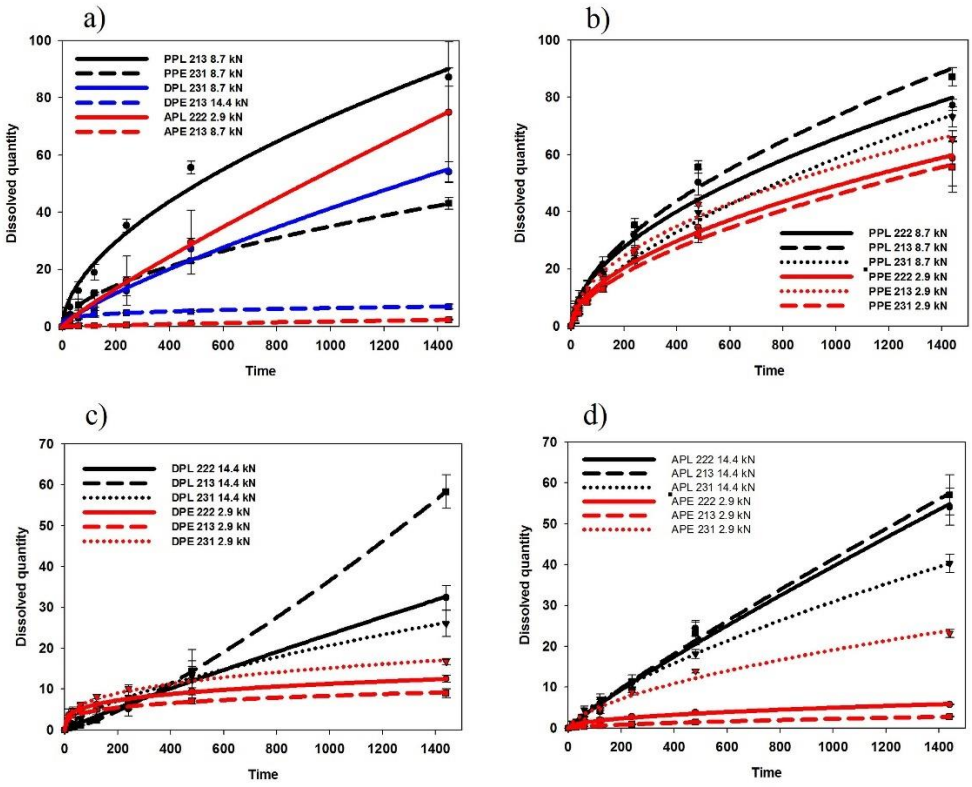

Figure 6. Drug release from various matrices: effect of the drug and polymer properties (a) and effect of the composition and compression force for PAR (b), DIS (c) and ACE (d) containing matrices

The results met with the expectations since EE-based compositions exhibited considerably lower dissolution rates in all cases. Furthermore, in contrast to the observation of Mustafine et al., where in case of acidic APIs a dissolution rate of 100% is expected between 2 to 8 hours with the application of EE and EL [29] slower dissolution was achieved with all tested systems, which also support the importance of drug-matrix interactions on the dissolution rate.

The amount of the released drug decreased to 50.6 % from 78.5 %, to 10.9 % from 45.7 % and to 6.2 % from 58.5 % in the case of PAR, DIS and ACE containing systems, respectively, if EL was switched to EE in the matrix (Fig. 6b-d). This may be partially explained by the bigger hardness and smaller overall porosity of EE containing samples, but the tendency is same if the dissolution rates of samples with similar porosities are compared. In contrast, the observed results are in good accordance with the strength of drug-carrier interactions, since stronger interactions were expected between the acidic drugs and the alkaline EE. This finding supports our previous observation on the role of in situ forming drug-polymer interactions in drug dissolution [12] and were in accordance with the similar findings of Priemel et al. [30], or Mustafine et al. [31].

Finally, to confirm that the interaction-based matrix design is suitable approach for long-term drug delivery one-week long dissolution studies was also performed with some selected compositions. The detailed results can be found in the supplementary material.

3.4. ANN modelling

ANN modelling was performed for a dual purpose: to cross check the DoE-based results on the importance of various descriptors on drug dissolution, and to compare the effectiveness of kinetic-based and point-to-point approaches in the predictability of the dissolution data. The use of various predictor sets may help the further clarification of

which material attributes play crucial role in the dissolution from the developed implantable matrices.

The results revealed that the overall perfection of point-to-point modelling was significantly ($p<0.05$) better as of kinetic parameter-based models (0.92±0.02 and 0.87±0.03, respectively). No significant difference was observed between the prediction performance of retained networks related to the applied hidden neuron number (Table S3), the results were inconsistent and more dependent on network initialization. Similarly, the use of the various predictor sets caused no considerable change in the overall prediction performance, but an interesting difference was observed between the point-to-point and kinetic parameter-based models when the prediction performance was compared on the train, test, and validation subsets. In case of kinetic parameter-based modelling the RMSE of predictions on train (0.22±0.08, 0.15±0.07, 0.09±0.05) and test (0.30±0.04, 0.29±0.05, 0.19±0.05) datasets was significantly improved in order of Approach 1, 2 and 3, respectively, while no significant change was observed on validation dataset. In contrast, for point-to-point modelling the RMSE of predictions on train and test datasets remained unchanged, while it was a significant improvement on the validation dataset (328±19, 235±18, 158±10) in order of Approach 5, 4, and 6, respectively.

Nevertheless, despite of the observed differences it can be stated, that the use of continuous inputs with appropriate descriptors of the tablet texture (hardness, porosity) enable the best prediction performance for both point-to-point and kinetic parameter-based approaches, despite of the fact that texture parameters exhibited relatively low importance in predictivity according to the results of the global sensitivity analysis (Table S4).

The results of the global sensitivity analysis, which show the relative importance of various predictors (inputs) on the prediction outcome, are partly consistent with the results of the experimental design. The greatest effect was observed for drug solubility, but the pKa of the excipients and the peak shift indicating drug-excipient interactions exhibits similar importance, than the compression pressure, tablet texture or the amount of excipient (Table S4).

To ultimately compare the prediction effectiveness of point-to-point and kinetic parameter-based modelling approaches the best performing networks (best overall training perfection and lowest prediction error on validation dataset, with no negative prediction values) was selected for both modelling approaches. The best network for kinetic parameter-based modelling had 9 input, 7 hidden and 2 output neurons, with logistic activation on hidden and exponential on output neurons (training perfection: 0.9103, validation error: 0.0760). The structure of the best point-to-point network was 9 input, 16 hidden and 7 output neurons, with exponential activation on hidden and logistic on output neurons (training perfection: 0.9286, validation error: 83.06). Figure 8 shows the predicted dissolution curves of the best and worst predicted cases.

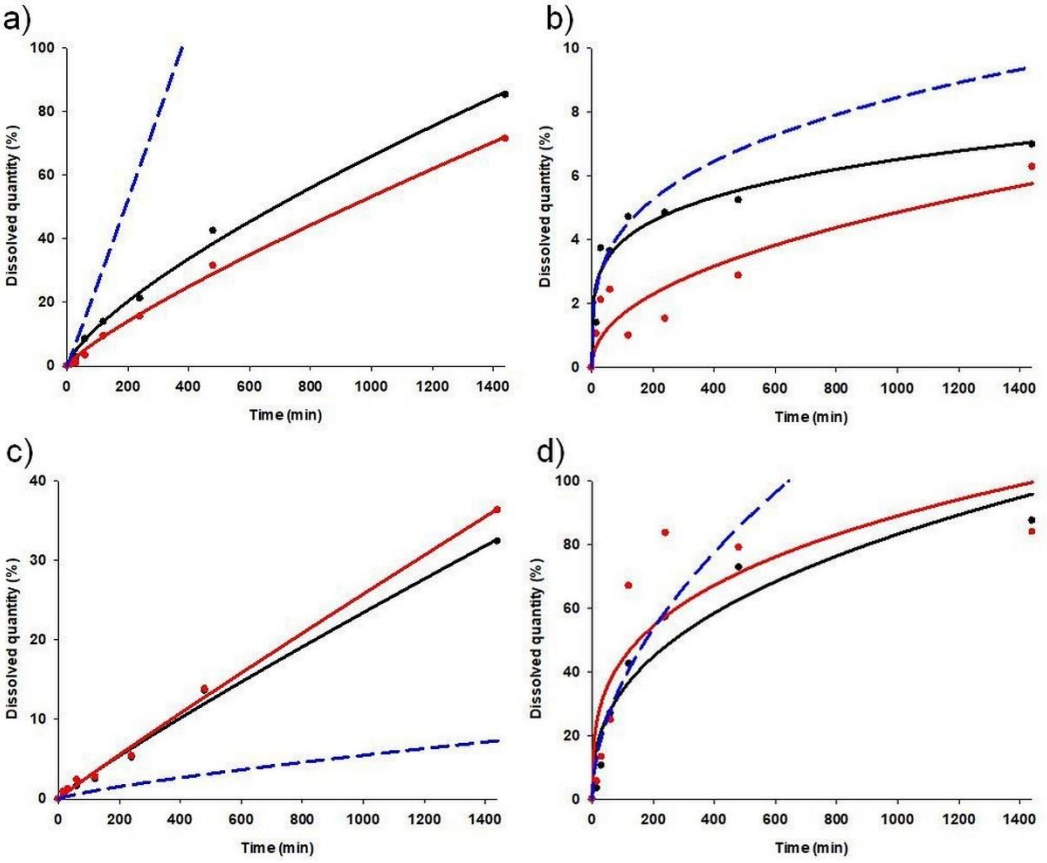

Figure 7. Observed and predicted dissolution curves of case 43 (a), case 36 (b), case 24 (c) and case 7 (d). Black dots: observed data points, black line: fitted model on observed data, red dots: predicted data points, red line: fitted model on predicted data points, blue line: predicted model.

It is clearly visible the point-to-point modeling approach showed more consistent accuracy, especially in cases where drug release was nearly linear (Fig. 7a, c). In other cases, the most considerable inaccuracies were observed at the 2, 4, and 8 h data points. Nevertheless, the predicted results were closer to the observed ones as for kinetic parameter-based models.

The main problem of the kinetic parameter-based approaches that the dissolution data obtained showed large differences, so the corresponding dissolution rates were scattered by two orders of magnitude. This posed a certain limitation on the predictivity, since small inaccuracies in the predicted values of low release rates were resulted in predictions of 3-5-fold faster or slower dissolution (Fig. 7 a, c). The prediction of release exponents, which scattered in a significantly smaller range was more accurate, but the presence of small inaccuracies can also cause large differences between the observed and predicted data at the end of the dissolution curves. It can be stated that the obtained models provide the desired accuracy only in the first 4-8 hours of dissolution (Fig. 7 b, d).

4. Conclusions

The present study introduced a comprehensive systematic approach for the investigation of the role of chemical interactions between APIs and excipients in directly compressed matrices. With help of FT-IR studies it was confirmed that solid-state interactions may be induced also in directly compressed matrix systems. The results also confirmed that the presence of solid-state interactions may not always presented in directly compressed systems, but their presence will definitely predict strong in-situ forming interactions during the drug dissolution process. The interactions are mostly H-bond based, but

the forming of polyelectrolyte complexes cannot be excluded. The results of both the DoE analysis and the ANN modeling supported our primary hypothesis that API-excipient interactions have a considerable effect on drug release by retaining the drug in the matrix.

The secondary hypothesis that kinetic parameters can be effectively used as an output in predicting drug release during ANN modeling has not been substantiated. The simplified structure did not result in a faster generalization of the network, and due to the wide scatter of the output results, small variations in the predicted release rate caused a high degree of uncertainty in the predicted dissolution curves. In contrast, when a point-to-point approach is used, the difference between the observed and predicted data at a given time can be compensated for at other time points. Therefore, applying a point-to-point approach provides greater reliability and more reliable predictions.

Nevertheless, the above-mentioned limitations can be overcome by increasing the number of cases, which makes it possible to fill in the gaps in the training data set. Therefore, the combination of interaction factors and ANN-based modeling may be a promising way to design extended-release products, especially implantable systems with tailored dissolution properties.

Acknowledgments: This topic is respectfully dedicated to Dr Piroska Szabó-Révész Professor Emerita for her scientific support and research motivation in the field of innovative drug formulation. Her scholarly work and intellectual advice play a vital role in the past and current scientific achievements of the Institute of Pharmaceutical Technology and Regulatory Affairs, University of Szeged.

Author Contributions: Conceptualization, T.S and S.S.; Formal Analysis, E.B, K.K. and I.G.I.; Investigation, E.B. and I.G.I..; Methodology, T.S. and K.H; Project Administration, G.R.; Supervision, T.S and S.S.; Validation, S.T.; Visualization, E.B; Writing – Original Draft Preparation, B.E..; Writing – Review & Editing, S.T, R.G., CS.I., S.S.

Funding: The research was supported by CEEPUS MOBILITY: CIII-RS-1113-01-1718-M-113871. Project no. TKP2021-EGA-32 has been implemented with the support provided by the Ministry of Innovation and Technology of Hungary from the National Research, Development, and Innovation Fund, financed under the TKP2021-EGA funding scheme

Conflicts of Interest: The authors declare no conflict of interest.

Data availability: The detailed dataset of ANN predictions in this study are available on request from the corresponding author, due to due to size and file format.

References

1. Crowley MM, Schroeder B, Fredersdorf A, Obara S, Talarico M, Kucera S, et al. Physicochemical properties and mechanism of drug release from ethyl cellulose matrix tablets prepared by direct compression and hot-melt extrusion. International Journal of Pharmaceutics. 2004;269:509–22.
2. Korsmeyer RW, Gurny R, Doelker E, Buri P, Peppas NA. Mechanisms of solute release from porous hydrophilic polymers. International Journal of Pharmaceutics. 1983;15:25–35.
3. Lee PI, Peppas NA. Prediction of polymer dissolution in swellable controlled-release systems. Journal of Controlled Release. 1987;6:207–15.
4. Campos-Aldrete ME, Villafuerte-Robles L. Influence of the viscosity grade and the particle size of HPMC on metronidazole release from matrix tablets. European Journal of Pharmaceutics and Biopharmaceutics. 1997;43:173–8.
5. Huanbutta K, Cheewatanakornkool K, Terada K, Nunthanid J, Sriamornsak P. Impact of salt form and molecular weight of chitosan on swelling and drug release from chitosan matrix tablets. Carbohydrate Polymers. 2013;97:26–33.
6. Thomas NL, Windle AH. A theory of case II diffusion. Polymer. 1982;23:529–42.
7. Kaunisto E, Abrahmsen-Alami S, Borgquist P, Larsson A, Nilsson B, Axelsson A. A mechanistic modelling approach to polymer dissolution using magnetic resonance microimaging. Journal of Controlled Release. 2010;147:232–41.
8. Singh B, Dhiman A, Rajneesh, Kumar A. Slow release of ciprofloxacin from β- cyclodextrin containing drug delivery system through network formation and supramolecular interactions. International Journal of Biological Macromolecules. 2016;92:390–400.
9. Deaconu M, Brezoiu A-M, Mitran R-A, Nicu I, Manolescu B, Matei C, et al. Exploiting the zwitterionic properties of lomefloxacin to tailor its delivery from functionalized MCM-41 silica. Microporous and Mesoporous Materials. 2020;305:110323.

10. Huang J, Jacobsen J, Larsen SW, Genina N, van de Weert M, Müllertz A, et al. Graphene oxide as a functional excipient in buccal films for delivery of clotrimazole: Effect of molecular interactions on drug release and antifungal activity in vitro. International Journal of Pharmaceutics. 2020;589:119811.
11. De Robertis S, Bonferoni MC, Elviri L, Sandri G, Caramella C, Bettini R. Advances in oral controlled drug delivery: the role of drug–polymer and interpolymer non-covalent interactions. Expert Opinion on Drug Delivery. 2015;12:441–53.
12. Sovány T, Csüllög A, Benkő E, Regdon G, Pintye-Hódi K. Comparison of the properties of implantable matrices prepared from degradable and non-degradable polymers for bisphosphonate delivery. International Journal of Pharmaceutics. 2017;533:364–72.
13. Caputo A, Brocca-Cofano E, Castaldello A, De Michele R, Altavilla G, Marchisio M, et al. Novel biocompatible anionic polymeric microspheres for the delivery of the HIV-1 Tat protein for vaccine application. Vaccine. 2004;22:2910–24.
14. Schlocker W, Gschließer S, Bernkop-Schnürch A. Evaluation of the potential of air jet milling of solid protein-poly(acrylate) complexes for microparticle preparation. European Journal of Pharmaceutics and Biopharmaceutics. 2006;62:260–6.
15. Ali ME, Lamprecht A. Polyethylene glycol as an alternative polymer solvent for nanoparticle preparation. International Journal of Pharmaceutics. 2013;456:135–42.
16. Hari BNV, Narayanan N, Dhevendaran K, Ramyadevi D. Engineered nanoparticles of Efavirenz using methacrylate co-polymer (Eudragit-E100) and its biological effects in-vivo. Materials Science and Engineering: C. 2016;67:522–32.
17. Thomas TT, Kohane DS, Wang A, Langer R. Microparticulate Formulations for the Controlled Release of Interleukin-2. Journal of Pharmaceutical Sciences. 2004;93:1100–9.
18. Basarkar A, Singh J. Poly (lactide-co-glycolide)-polymethacrylate nanoparticles for intramuscular delivery of plasmid encoding interleukin-10 to prevent autoimmune diabetes in mice. Pharm Res. 2009;26:72–81.
19. Balaguer-Fernández C, Femenía-Font A, del Rio-Sancho S, Merino V, López-Castellano A. Sumatriptan Succinate Transdermal Delivery Systems for The Treatment of Migraine. Journal of Pharmaceutical Sciences. 2008;97:2102–9.
20. Sovány T., Kása P., Pintye-Hódi K. Modeling of subdivision of scored tablets with the application of artificial neural networks. Journal of Pharmaceutical Sciences. 2010;99:905-15.
21. Sovány T., Papós K., Kása Jr. P., Ilič I., Srčič S., Pintye-Hódi K. Application of physicochemical properties and process parameters in the development of a neural network model for prediction of tablet characteristics AAPS PharmSciTech. 2013;14:511-6.
22. Galata DL, Farkas A, Könyves Z, Mészáros LA, Szabó E, Csontos I, Pálos A, Marosi G, Nagy ZK, Nagy B. Fast, Spectroscopy-Based Prediction of In Vitro Dissolution Profile of Extended Release Tablets Using Artificial Neural Networks. Pharmaceutics 2019;11:400.
23. Jangir DK, Charak S, Mehrotra R, Kundu S. FTIR and circular dichroism spectroscopic study of interaction of 5-fluorouracil with DNA. Journal of Photochemistry and Photobiology B: Biology. 2011;105:143–8.
24. Mihaylov MY, Ivanova EZ, Vayssilov GN, Hadjiivanov KI. Revisiting ceria-NOx interaction: FTIR studies. Catalysis Today. 2019;S0920586119302317.
25. Liu X, Ma X, Kun E, Guo X, Yu Z, Zhang F. Influence of lidocaine forms (salt vs. freebase) on properties of drug–eudragit® L100-55 extrudates prepared by reactive melt extrusion. International Journal of Pharmaceutics. 2018;547:291–302.
26. Obeidat WM, Nokhodchi A, Alkhatib H. Evaluation of Matrix Tablets Based on Eudragit®E100/Carbopol®971P Combinations for Controlled Release and Improved Compaction Properties of Water Soluble Model Drug Paracetamol. AAPS PharmSciTech. 2015;16:1169–79.
27. Pavli M, Baumgartner S, Kos P, Kogej K. Doxazosin–carrageenan interactions: A novel approach for studying drug–polymer interactions and relation to controlled drug release. International Journal of Pharmaceutics. 2011;421:110–9.
28. Ritger PL, Peppas NA. A simple equation for description of solute release I. Fickian and non-fickian release from non-swellable devices in the form of slabs, spheres, cylinders or discs. Journal of Controlled Release. 1987;5:23–36.
29. Moustafine RI, Zaharov IM, Kemenova VA. Physicochemical characterization and drug release properties of Eudragit® E PO/Eudragit® L 100-55 interpolyelectrolyte complexes. European Journal of Pharmaceutics and Biopharmaceutics. 2006;63:26–36.
30. Priemel PA, Laitinen R, Grohganz H, Rades T, Strachan CJ. In situ amorphisation of indomethacin with Eudragit® E during dissolution. European Journal of Pharmaceutics and Biopharmaceutics. 2013;85:1259–65.
31. Moustafine RI, Sitenkov AY, Bukhovets AV, Nasibullin SF, Appeltans B, Kabanova TV, et al. Indomethacin-containing interpolyelectrolyte complexes based on Eudragit ® E PO/S 100 copolymers as a novel drug delivery system. International Journal of Pharmaceutics. 2017;524:121–33.

ANNEX 3

pharmaceutics

Supplementary Material: Predicting Drug Release Rate of Implantable Matrices and Better Understanding of the Underlying Mechanisms through Experimental Design and Artificial Neural Network-Based Modelling

Ernő Benkő, Ilija German Ilič, Katalin Kristó, Géza Regdon Jr., Ildikó Csóka, Klára Pintye-Hódi, Stane Srčič and Tamás Sovány *

Table S1. Dataset of the ANN modelling.

	Subset	Drug	Drug solubility (mg/ml)	Drug pKa	Exci.	Exc. amount*	Excipient solubility (mg/ml)	Excipient pKa	Compression pressure (MPa)	Hardness (N)	Porosity	Peak shift	Release rate	Release exponent	15 min	30 min	60 min	120 min	240 min	480 min	1440 min
1	Train	Par.	19,5	9,46	Eudragit L	22	0,03	4,6	75	15	0,307	3	5,79	0,39	6,06	9,63	12,81	16,80	27,32	43,19	66,47
2	Validation	Par.	19,5	9,46	Eudragit L	22	0,03	4,6	225	114,3	0,136	3	1,50	0,56	3,20	6,58	9,23	14,68	22,88	39,68	73,09
3	Test	Par.	19,5	9,46	Eudragit L	22	0,03	4,6	375	109,1	0,118	3	1,72	0,53	4,71	6,91	10,14	19,76	29,50	39,30	67,22
4	Train	Par.	19,5	9,46	Eudragit L	33	0,03	4,6	75	18,7	0,29	6	6,87	0,35	7,31	12,17	21,78	41,80	63,28	72,20	79,28
5	Test	Par.	19,5	9,46	Eudragit L	33	0,03	4,6	225	95,8	0,122	6	1,60	0,54	4,52	6,22	10,77	21,65	31,56	50,28	77,27
6	Train	Par.	19,5	9,46	Eudragit L	33	0,03	4,6	375	133,6	0,111	6	1,55	0,56	3,34	6,98	10,17	18,91	36,13	59,22	86,65
7	Validation	Par.	19,5	9,46	Eudragit L	44	0,03	4,6	75	28,2	0,306	13	1,72	0,51	3,32	10,55	26,95	42,46	57,16	72,80	87,48
8	Validation	Par.	19,5	9,46	Eudragit L	44	0,03	4,6	225	132,6	0,118	13	0,76	0,63	3,82	6,86	12,57	18,93	35,31	55,68	87,21
9	Train	Par.	19,5	9,46	Eudragit L	44	0,03	4,6	375	153,8	0,091	13	1,51	0,52	5,37	8,14	10,77	21,18	36,54	50,66	81,78
10	Train	Par.	19,5	9,46	Eudragit E	22	0,01	10	75	113,6	0,223	9	0,90	0,57	5,95	9,48	12,63	16,52	26,86	42,48	65,35
11	Validation	Par.	19,5	9,46	Eudragit E	22	0,01	10	225	166,6	0,126	9	0,68	0,58	3,98	3,97	7,68	11,63	15,86	22,90	43,10
12	Train	Par.	19,5	9,46	Eudragit E	22	0,01	10	375	184,5	0,098	9	0,81	0,55	5,85	5,50	7,78	9,38	14,29	20,56	38,63
13	Train	Par.	19,5	9,46	Eudragit E	33	0,01	10	75	50,1	0,191	11	1,14	0,54	2,97	5,52	9,13	14,52	25,64	34,54	58,69
14	Test	Par.	19,5	9,46	Eudragit E	33	0,01	10	225	146,7	0,109	11	0,42	0,68	1,43	4,10	6,74	9,30	16,41	28,71	55,84
15	Train	Par.	19,5	9,46	Eudragit E	33	0,01	10	375	161,8	0,105	11	0,38	0,68	4,15	3,65	5,70	8,61	15,81	24,97	52,17
16	Test	Par.	19,5	9,46	Eudragit E	44	0,01	10	75	128,6	0,282	11	1,69	0,51	2,74	4,38	8,30	12,80	22,73	31,77	55,66
17	Train	Par.	19,5	9,46	Eudragit E	44	0,01	10	225	192,4	0,131	11	0,77	0,55	1,70	4,53	7,21	10,55	17,07	24,09	44,89
18	Train	Par.	19,5	9,46	Eudragit E	44	0,01	10	375	211,2	0,115	11	0,84	0,52	1,66	3,52	6,33	9,59	16,77	28,68	41,73
19	Validation	Dic.	5,15	4	Eudragit L	22	0,03	4,6	75	8	0,423	17	0,04	0,98	2,30	3,95	12,95	23,54	32,46	54,95	84,53
20	Test	Dic.	5,15	4	Eudragit L	22	0,03	4,6	225	118,5	0,125	17	0,01	1,16	0,77	1,37	2,87	6,16	12,53	27,13	54,17

21	Train	Dic.	5,15	4	Eudragit L	22	0,03	4,6	375	140,7	0,082	17	0,01	1,28	1,30	1,62	2,68	5,12	7,98	13,59	26,05
22	Train	Dic.	5,15	4	Eudragit L	33	0,03	4,6	75	34	0,236	17	1,44	0,43	3,79	4,63	10,60	11,68	14,13	21,69	32,92
23	Train	Dic.	5,15	4	Eudragit L	33	0,03	4,6	225	92	0,128	17	0,03	0,96	1,11	1,18	1,34	2,49	4,38	10,00	27,66
24	Validation	Dic.	5,15	4	Eudragit L	33	0,03	4,6	375	134,4	0,058	17	0,04	0,91	0,86	1,14	1,59	2,52	5,18	13,60	32,40
25	Train	Dic.	5,15	4	Eudragit L	44	0,03	4,6	75	27,3	0,026	17	1,53	0,56	0,44	0,82	1,96	3,86	7,52	20,22	53,14
26	Train	Dic.	5,15	4	Eudragit L	44	0,03	4,6	225	97	0,137	17	0,18	0,79	0,42	0,58	1,19	2,47	4,80	12,17	42,56
27	Train	Dic.	5,15	4	Eudragit L	44	0,03	4,6	375	153,8	0,1	17	0,22	0,66	0,50	0,60	1,21	2,38	5,59	14,51	58,30
28	Validation	Dic.	5,15	4	Eudragit E	22	0,01	10	75	94,4	0,092	14	1,37	0,26	2,52	4,70	6,25	8,20	10,13	12,14	16,73
29	Test	Dic.	5,15	4	Eudragit E	22	0,01	10	225	130,7	0,098	14	1,46	0,23	1,18	2,95	4,42	5,67	6,08	7,56	10,45
30	Train	Dic.	5,15	4	Eudragit E	22	0,01	10	375	173,7	0,113	14	1,45	0,22	1,76	4,05	5,44	7,09	8,19	9,55	12,33
31	Train	Dic.	5,15	4	Eudragit E	33	0,01	10	75	57,4	0,21	12	1,71	0,27	3,59	4,45	5,44	6,23	7,24	9,43	12,55
32	Train	Dic.	5,15	4	Eudragit E	33	0,01	10	225	102,6	0,101	12	0,90	0,35	1,37	3,15	4,16	4,92	6,35	8,62	11,55
33	Train	Dic.	5,15	4	Eudragit E	33	0,01	10	375	153,8	0,08	12	0,93	0,34	1,48	2,53	4,24	5,11	6,06	7,94	10,72
34	Test	Dic.	5,15	4	Eudragit E	44	0,01	10	75	102,9	0,147	9	1,60	0,33	1,57	3,55	4,47	5,10	6,07	7,01	8,94
35	Test	Dic.	5,15	4	Eudragit E	44	0,01	10	225	160,6	0,121	9	1,05	0,32	1,70	3,86	4,05	4,50	5,18	6,03	7,72
36	Validation	Dic.	5,15	4	Eudragit E	44	0,01	10	375	201	0,046	9	1,56	0,29	1,40	3,74	3,64	4,72	4,85	5,25	6,99
37	Train	Acec.	8,4	3,44	Eudragit L	22	0,03	4,6	75	13,5	0,279	41	0,42	0,73	1,00	1,26	3,04	6,70	13,98	25,53	49,32
38	Train	Acec.	8,4	3,44	Eudragit L	22	0,03	4,6	225	68,2	0,077	41	0,05	0,93	0,68	1,80	3,79	7,03	11,98	19,34	43,03
39	Test	Acec.	8,4	3,44	Eudragit L	22	0,03	4,6	375	103,6	0,067	41	0,09	0,89	1,02	1,63	4,38	7,10	10,97	18,10	40,34
40	Train	Acec.	8,4	3,44	Eudragit L	33	0,03	4,6	75	22,9	0,232	41	0,13	0,88	1,72	2,20	3,71	7,58	16,05	29,45	74,91
41	Train	Acec.	8,4	3,44	Eudragit L	33	0,03	4,6	225	65,8	0,104	41	0,19	0,83	0,70	1,39	2,87	6,06	12,11	40,87	74,86
42	Validation	Acec.	8,4	3,44	Eudragit L	33	0,03	4,6	375	71,3	0,097	41	0,08	0,89	0,37	1,12	1,56	4,01	9,36	24,38	54,10
43	Validation	Acec.	8,4	3,44	Eudragit L	44	0,03	4,6	75	15,2	0,027	41	0,25	0,73	0,51	2,58	8,49	13,88	21,22	42,42	85,16
44	Train	Acec.	8,4	3,44	Eudragit L	44	0,03	4,6	225	90,7	0,086	41	0,20	0,74	0,19	0,53	1,37	3,86	9,33	18,27	47,89
45	Train	Acec.	8,4	3,44	Eudragit L	44	0,03	4,6	375	116,7	0,06	41	0,21	0,73	0,30	0,83	2,21	5,24	11,42	23,10	57,08
46	Validation	Acec.	8,4	3,44	Eudragit E	22	0,01	10	75	93,4	0,106	46	0,04	0,59	0,90	1,20	2,21	4,65	8,76	13,97	23,18
47	Train	Acec.	8,4	3,44	Eudragit E	22	0,01	10	225	159,1	0,038	46	0,01	0,76	0,55	1,22	1,60	2,09	2,66	3,78	7,21
48	Test	Acec.	8,4	3,44	Eudragit E	22	0,01	10	375	164,7	0,014	46	0,01	0,72	2,66	1,49	1,84	1,82	2,24	3,34	6,37
49	Test	Acec.	8,4	3,44	Eudragit E	33	0,01	10	75	67,6	0,141	47	0,21	0,46	0,48	0,70	1,23	1,99	2,80	3,85	5,76
50	Train	Acec.	8,4	3,44	Eudragit E	33	0,01	10	225	87,5	0,068	47	0,07	0,55	0,20	0,46	0,66	0,90	1,43	2,18	3,73

51	Validation	Acec.	8,4	3,44	Eudragit E	33	0,01	10	375	143,6	0,071	47	0,08	0,49	0,32	0,52	0,65	0,79	1,13	1,65	2,89
52	Test	Acec.	8,4	3,44	Eudragit E	44	0,01	10	75	131,2	0,102	49	0,28	0,61	0,20	0,27	0,42	0,64	0,96	1,49	2,81
53	Train	Acec.	8,4	3,44	Eudragit E	44	0,01	10	225	187,9	0,011	49	0,17	0,51	0,22	0,20	0,24	0,33	0,57	1,05	2,43
54	Train	Acec.	8,4	3,44	Eudragit E	44	0,01	10	375	192,8	0,011	49	0,21	0,47	0,26	0,21	0,24	0,32	0,44	0,93	2,06

*22, 33 and 44 % corresponds with 25:75, 50:50 and 75:25 Eudragit:PVC ratio, respectively.

Full equations:

$$y_1=110.12+\mathbf{47.05x_1}+\mathbf{9.44x_1^2}+\mathbf{19.34x_2}-0.44x_2^2-\mathbf{10.12x_3}+0.36x_3^2-\mathbf{29.48x_4}+2.50x_1x_2-1.64x_1x_2^2+2.42x_1^2x_2+2.31x_1^2x_2^2-\mathbf{6.44x_1x_3}+\mathbf{4.80x_1x_3^2}-4.22x_1^2x_3-3.54x_1^2x_3^2+\mathbf{4.54x_1x_4}+3.20x_1^2x_4+1.33x_2x_3-3.47x_2x_3^2+1.30x_2^2x_3+0.56x_2^2x_3^2-\mathbf{11.48x_2x_4}-2.23x_2^2x_4-2.32x_3x_4+\mathbf{6.83x_3^2x_4} \quad (S1)$$

$R^2=0.9756$ adj $R^2=0.9537$ MS Residual: 141.79

$$y_2=0.132-\mathbf{0.054x_1}-\mathbf{0.022x_1^2}-0.009x_2+0.006x_2^2-\mathbf{0.043x_3}-0.0003x_3^2+\mathbf{0.018x_4}+0.022x_1x_2-0.018x_1x_2^2+0.004x_1^2x^2-0.006x_1^2x_2^2+0.009x_1x_3+0.002x_1x_3^2+0.010x_1^2x_3+0.009x_1^2x_3^2-0.014x_1x_4-0.004x_1^2x_4-\mathbf{0.029x_2x_3}-0.006x_2x_3^2+0.006x_2^2x_3+0.009x_2^2x_3^2-0.009x_2x_4+\mathbf{0.016x_2^2x_4}+0.007x_3x_4-0.0006x_3^2x_4 \quad (S2)$$

$R^2=0.7928$ adj $R^2=0.6079$ MS Res=0.0028

$$y_3=0.936-\mathbf{0.381x_1}-\mathbf{0.283x_1^2}+0.092x_2+0.038x_2^2-\mathbf{0.804x_3}-0.026x_3^2+0.185x_4-0.011x_1x_2-0.241x_1x_2^2-0.033x_1^2x_2-0.042x_1^2x_2^2+\mathbf{0.403x_1x_3}+0.113x_1x_3^2+0.289x_1^2x3+0.046x_1^2x_3^2-0.208x_1x_4-0.181x_1^2x_4-0.242x_2x_3-0.137x_2x_3^2-0.097x_2^2x_3-0.063x_2^2x_3^2+0.197x_2x_4+0.116x_2^2x_4-\mathbf{0.440x_3x_4}-\mathbf{0.427x_3^2x^4} \quad (S3)$$

R2=0.7801 adj R2=0.5838 MS Res=0.6453

Supplementary Figures for FT-IR analysis:

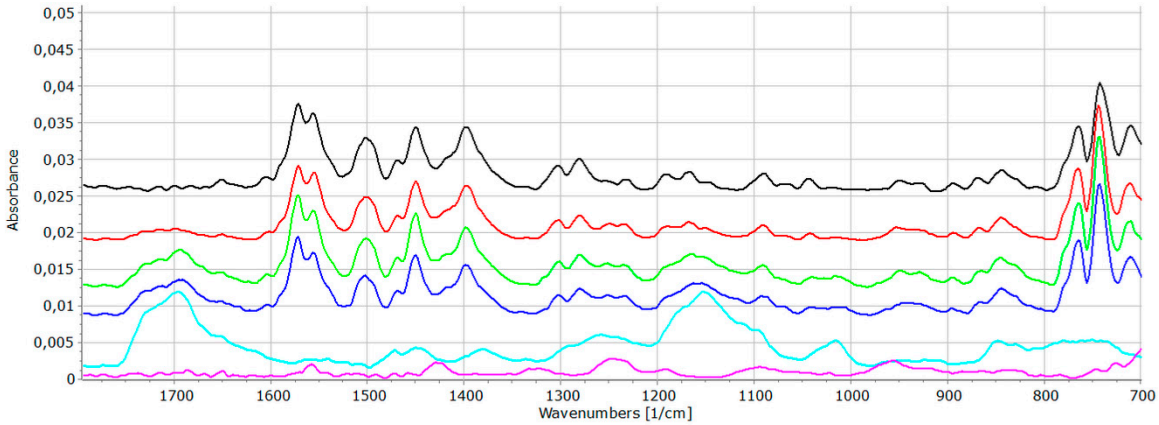

Figure S1. FT-IR spectra (650-1800 cm^{-1} range) of the DIS (black); DIS-PVC:EL 75:25 (red); DIS-PVC:EL 50:50 (green); DIS-PVC:EL 25:75 (deep blue); EL (light blue) and PVC (purple) samples.

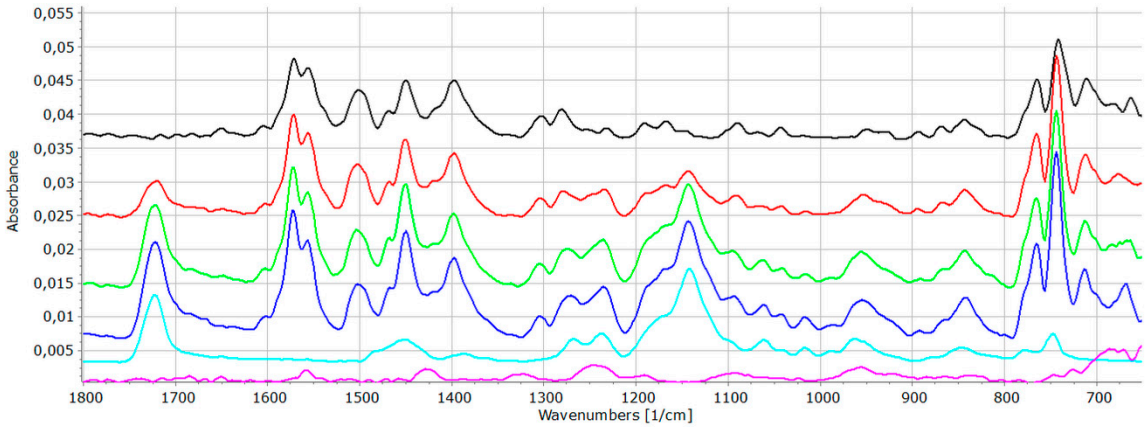

Figure S2. FT-IR spectra (650-1800 cm^{-1} range) of the DIS (black); DIS-PVC:EE 75:25 (red); DIS-PVC:EE 50:50 (green); DIS-PVC:EE 25:75 (deep blue); EE (light blue) and PVC (purple) samples.

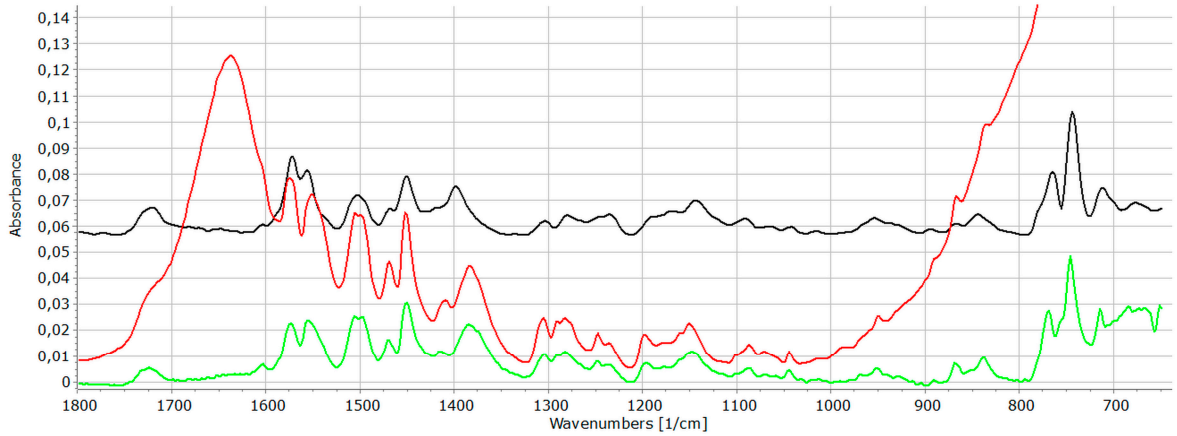

Figure S3. FT-IR spectra of Dis-PVC:EE 75:25 samples: original (black), dipped (red), and dried (green).

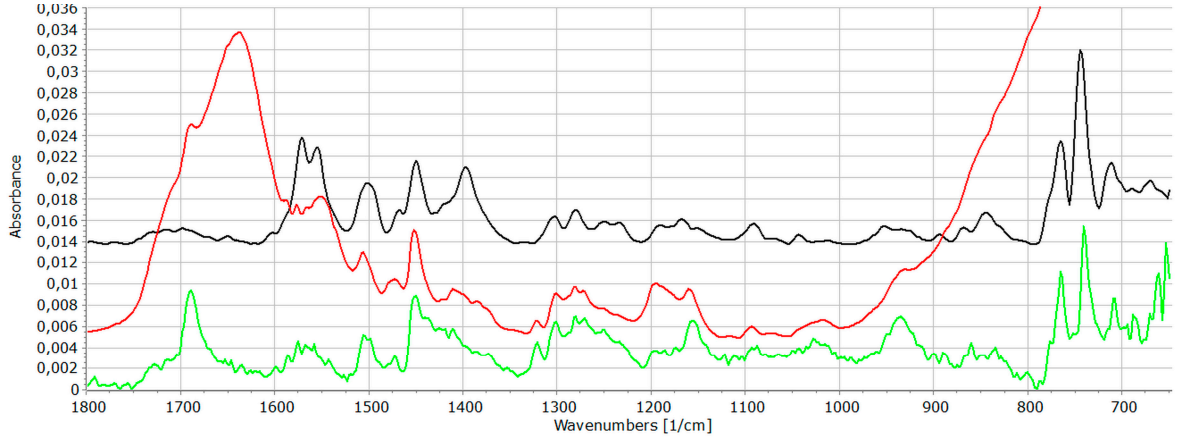

Figure S4. FT-IR spectra of Dis-PVC:EL 75:25 samples: original (black), dipped (red), and dried (green).

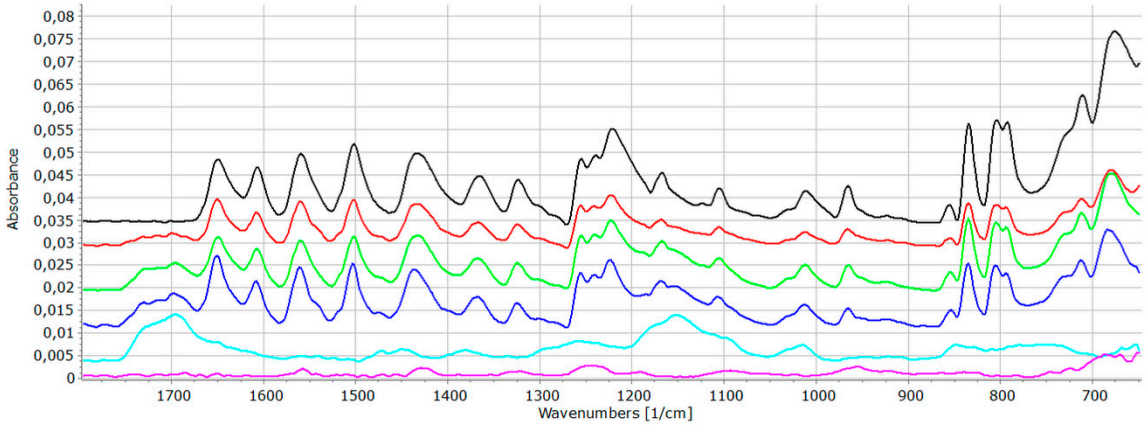

Figure S5. FT-IR spectra (650-1800 cm^{-1} range) of the PAR (black); PAR-PVC:EL 75:25 (red); PAR-PVC:EL 50:50 (green); PAR-PVC:EL 25:75 (deep blue); EL (light blue) and PVC (purple) samples.

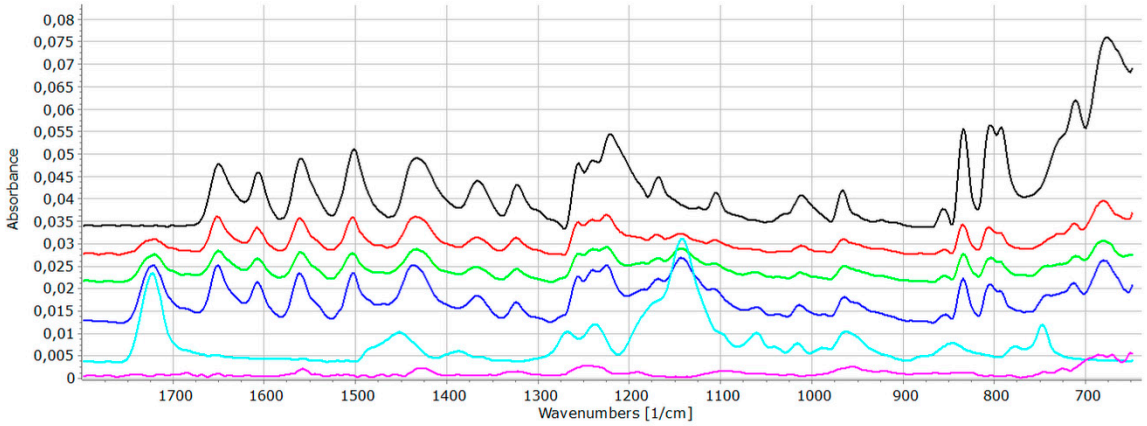

Figure S6. FT-IR spectra (650-1800 cm^{-1} range) of the PAR (black); PAR-PVC:EE 75:25 (red); PAR-PVC:EE 50:50 (green); PAR-PVC:EE 25:75 (deep blue); EE (light blue) and PVC (purple) samples.

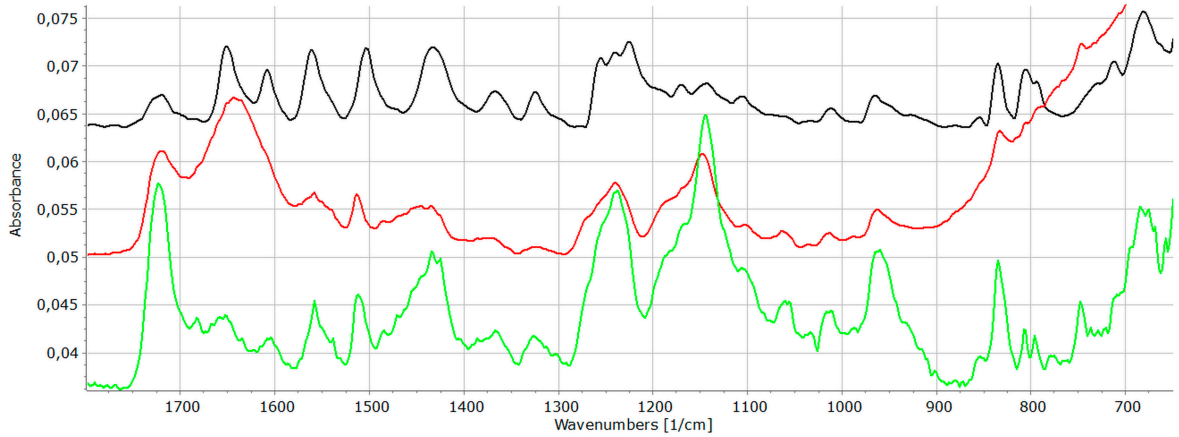

Figure S7. FT-IR spectra of Par-PVC:EE 75:25 samples: original (black), dipped (red), and dried (green).

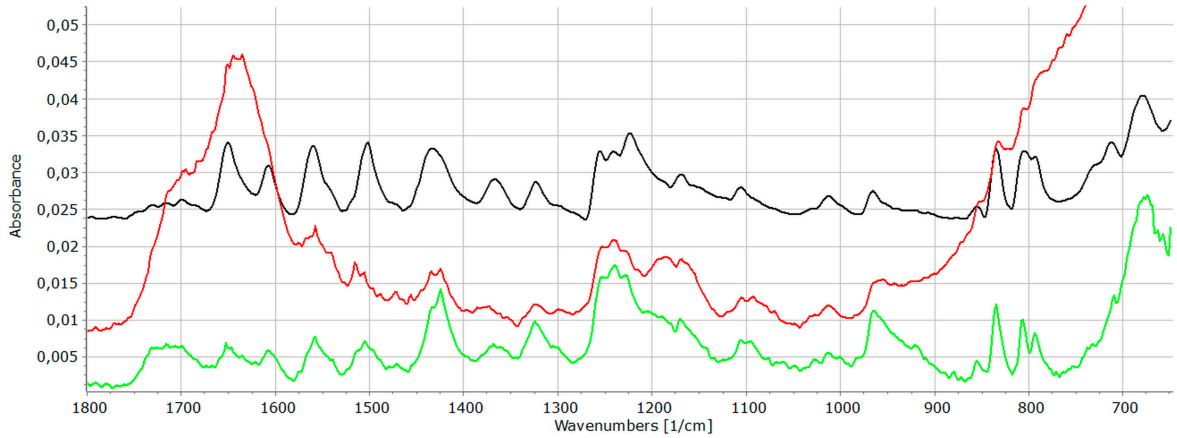

Figure S8. FT-IR spectra of Par-PVC:EL 75:25 samples: original (black), dipped (red), and dried (green).

Supplementary data for 1 week long dissolution study:

Table S2. Release rates and release exponents derived from the Korsmeyer-Peppas model (1-week-long test).

Composition	Eudragit/PVC ratio (%/%)	Pressure (MPa)	R^2	k	n
PAR-PVC-EE	25/75	375	0.9576	4.1992	0.3206
ACE-PVC-EE	75/25	375	0.9918	0.0495	0.532
DIC-PVC-EE	25/75	375	0.8327	3.1193	0.2434
DIC-PVC-EL	50/50	225	0.97	0.2829	0.6428

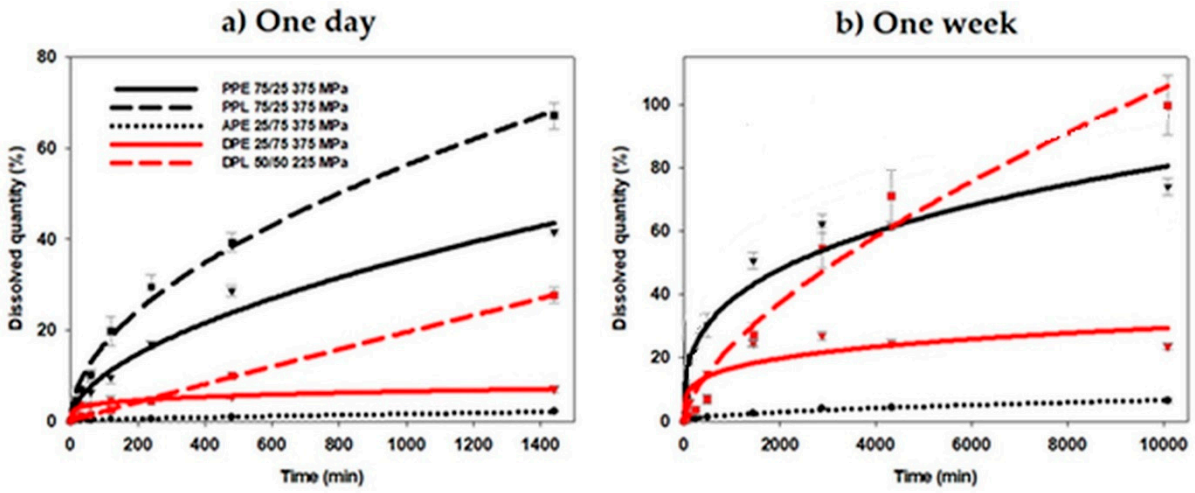

Figure S9. Drug release from various matrices: effect of the drug and polymer properties (a) and effect of the composition and compression force for PAR (b), DIS (c) and ACE (d) containing matrices.

There the results met the expectations, the ACE containing matrix (APE) proved to be the most retentive, liberating around 2% on one day, and reaching 6.5% by the end of a week. As for DIS with EE (DPE), the 24-hour test provided nearly 7% and the one-week test a 23.6% value, while with the EL (DPL) 27.7% was released in one day and 99.85% was reached by the end of the week. PAR with EE (PPE) liberated 42% of the drug during one and 74% in seven days, while if the API was mixed with EL (PPL), the released amount was 67% and 100%, in one day and one week, respectively. Nevertheless, it should be

noted that in this latter case the liberation process reached the maximum 100% till the end of the second day, and after then the drug started to adhere to the silicon tubing of the dissolution device resulting decreasing concentrations, therefore this sample was withdrawn from the one-week dissolution study.

Nevertheless, the results confirm, that strong drug-matrix interactions may help the prolongation of the drug release for several months.

Supplementary Material for ANN modelling:

Table S3. Performance of the neurons.

Number of hidden neurons		Approach 1		Approach 2		Approach 3		Approach 4		Approach 5		Approach 6	
		Perf.	Error	Perf.	Error	Perf.	Error	Perf.	Error	Perf.	Error	Perf.	Error
I+O-3	Mean	0,8777	0,3995	0,8608	0,3103	0,8357	0,3901	0,9304	107,2409	0,9238	162,4238	0,9293	99,3636
	SD	0,0229	0,0250	0,0368	0,0263	0,0852	0,0538	0,0064	20,2784	0,0039	24,6286	0,0058	11,6035
I+O-2	Mean	0,8832	0,3767	0,8808	0,4548	0,8711	0,3875	0,9240	121,0832	0,9186	154,0890	0,9297	91,7769
	SD	0,0071	0,0959	0,0020	0,0630	0,0264	0,0410	0,0083	18,1608	0,0050	15,8342	0,0018	7,4322
I+O-1	Mean	0,8704	0,3086	0,8959	0,3682	0,8826	0,3459	0,9226	101,3835	0,9230	144,6181	0,9294	88,6256
	SD	0,0293	0,0779	0,0214	0,0978	0,0184	0,0464	0,0075	15,5180	0,0020	10,6401	0,0051	5,0336
I+O	Mean	0,8793	0,4695	0,8825	0,3900	0,8885	0,3806	0,9254	116,9167	0,9181	142,9717	0,9273	92,8801
	SD	0,0151	0,0940	0,0144	0,0939	0,0234	0,0711	0,0078	21,1997	0,0028	8,5369	0,0047	10,5143
I+O+1	Mean	0,8562	0,3349	0,8875	0,4569	0,8839	0,3660	0,9314	118,1403	0,9217	152,1861	0,9281	99,1262
	SD	0,0209	0,0620	0,0062	0,1090	0,0202	0,0445	0,0065	25,2726	0,0017	9,1558	0,0026	4,7649

Table S4. Results of the global sensitivity analysis.

	Approach 1		**Approach 2**		**Approach 3**		**Approach 4**		**Approach 5**		Approach 6	
Modelling type	**Kinetic based**		**Kinetic based**		**Kinetic based**		**Point-to-point**		**Point-to-point**		Point-to-point	
Input variable	Mean	SD	Mean	SD	Mean	SD	Mean	SD	Mean	SD	Mean	SD
Drug	5,12	3,06					8,21	1,56				
Drug solubility (mg/ml)			1,99	1,94	2,30	2,91			2,11	0,20	2,45	0,22
Drug pKa			1,81	2,17	2,09	2,89			1,41	0,12	1,37	0,10
Excipient	1,05	0,13					1,00	0,00				
Excipient solubility (mg/ml)			1,21	0,49	5,95	26,47			1,53	0,19	1,30	0,13
Excipient pKa			1,40	0,62	15,39	75,30			2,86	0,37	2,52	0,22
Excipient amount (%)	1,02	0,06	1,01	0,06	1,25	0,92	1,62	0,46	1,05	0,07	1,26	0,07
Compression pressure	1,38	0,22	1,46	0,37	1,37	0,94	1,56	0,27	1,25	0,06	1,00	0,03
Hardness					1,80	2,50					1,54	0,20
Porosity					1,28	0,74					1,23	0,05
Peak Shift	5,26	5,24	1,67	0,88	1,87	1,66	1,20	0,13	1,13	0,08	1,20	0,08

ANNEX 4

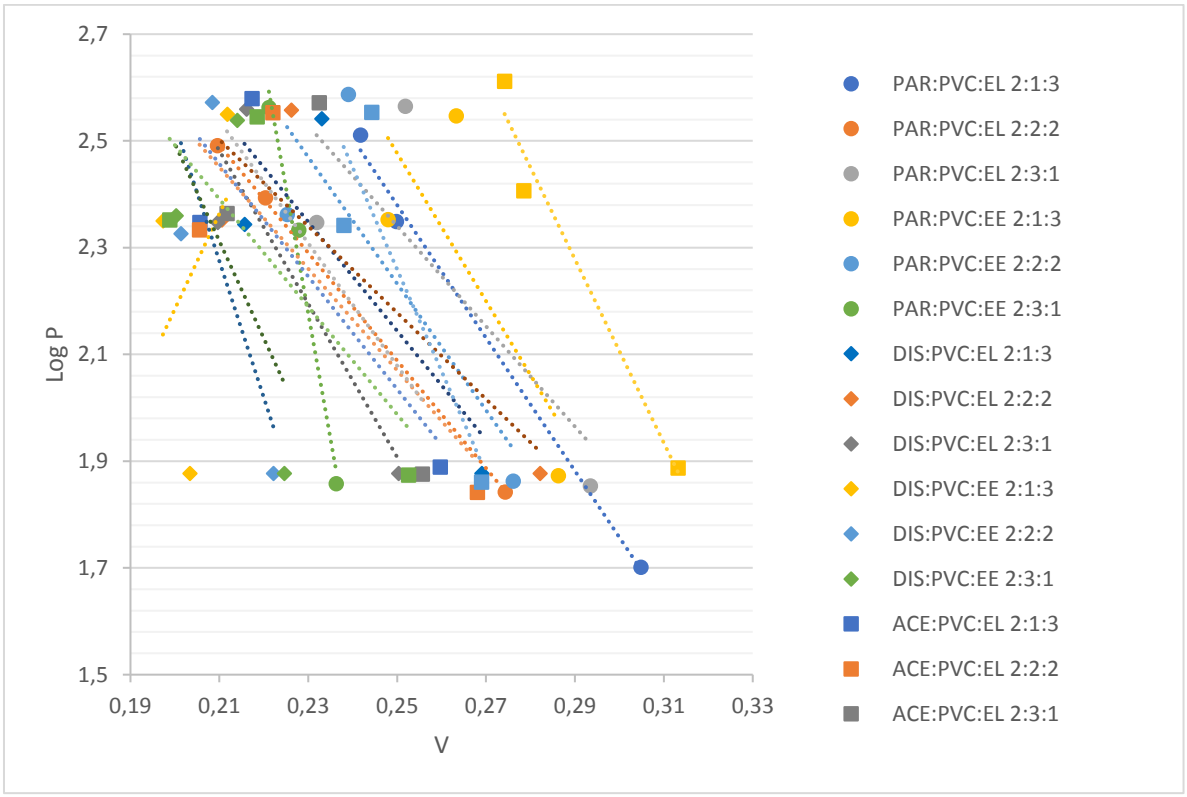

Figure S10 Walker plot based on Eq. 10

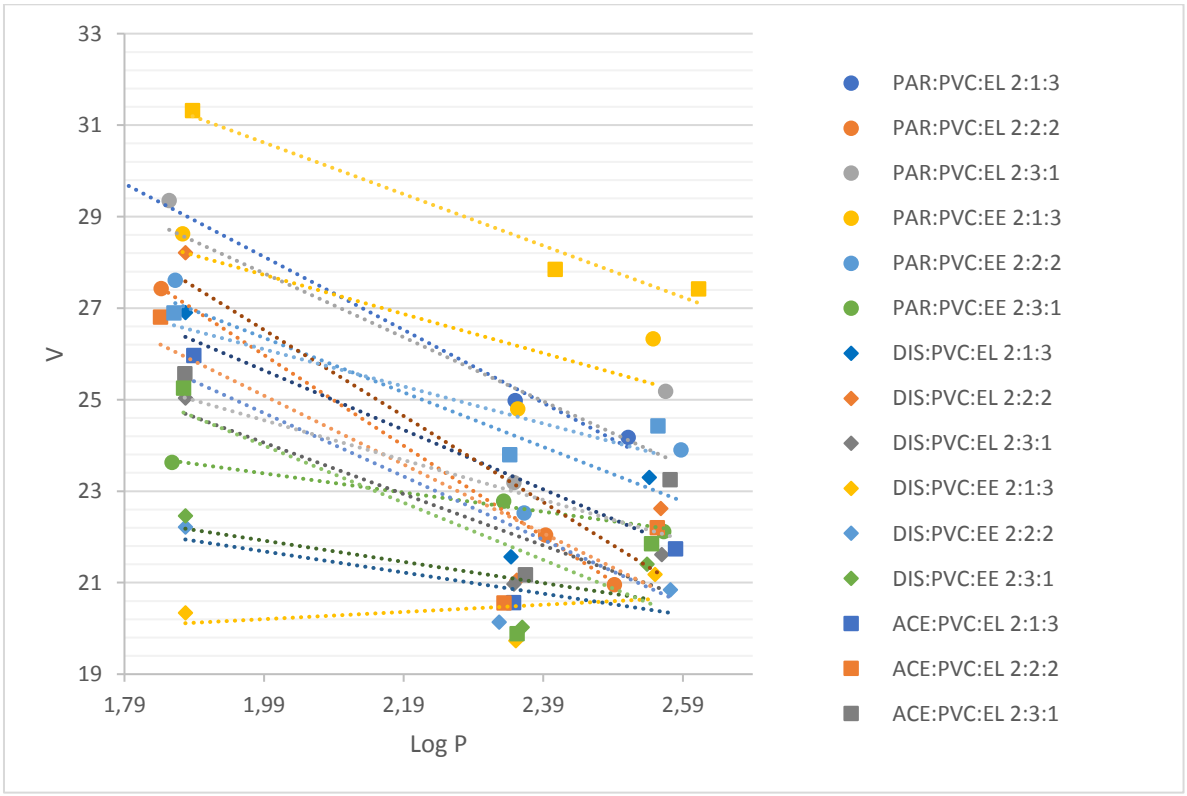

Figure S11. Walker plot based on Eq. 11.